CHAPTER ONE

Heterogeneous Catalysis by Gold

Takashi Takei[*], Tomoki Akita[†], Isao Nakamura[‡], Tadahiro Fujitani[‡], Mitsutaka Okumura[§], Kazuyuki Okazaki[§], Jiahui Huang[¶], Tamao Ishida[||], Masatake Haruta[*]

[*]Department of Applied Chemistry, Faculty of Urban Environmental Sciences, Tokyo Metropolitan University (TMU), Hachioji, Tokyo, Japan
[†]Kansai Center, National Institute of Advanced Industrial Science and Technology (AIST), Ikeda, Osaka, Japan
[‡]Tsukuba Center, AIST, Tsukuba, Ibaraki, Japan
[§]Department of Chemistry, Faculty of Science, Osaka University, Toyonaka, Osaka, Japan
[¶]Dalian Institute of Chemical Physics, Chinese Academy of Science, Dalian, China
[||]Department of Chemistry, Faculty of Sciences, Kyushu University, Hakozaki, Fukuoka, Japan

Contents

Advances in Catalysis, Volume 55
ISSN 0360-0564
http://dx.doi.org/10.1016/B978-0-12-385516-9.00001-6

Abstract

Gold can be deposited as nanoparticles (NPs) with diameters of 2–5 nm and clusters with diameters less than 2 nm on a variety of materials such as oxides, carbides, and sulfides of transition metals, carbons, and organic polymers. Such supported gold NPs and clusters exhibit surprisingly high catalytic activities for many reactions, with both gas- and liquid-phase reactants, in particular, at temperatures below 573 K. Until now, more than 10 techniques have been developed for depositing gold as NPs and clusters. The atomic scale structures of supported NPs and clusters have been extensively and intensively investigated with a high-resolution transmission electron microscopy.

The mechanisms of catalysis by supported gold NPs have recently been elucidated by using real powder catalysts and model single-crystal catalysts for the low-temperature oxidation of CO. Another simple reaction that has recently been investigated is dihydrogen dissociation, for which gold NP catalysts are still poorly active. Both of these reactions have been demonstrated to take place at perimeter interfaces around the gold NPs. This result means that there is a great chance for gold to exhibit high catalytic activity for hydrogenation reactions by an appropriate choice of metal oxide supports and by minimizing the diameters of gold particles. The catalytic nature of gold clusters has also been investigated theoretically in relation to the effect of cluster size and the influence of organic ligands and polymers.

The catalytic performance of gold NPs and clusters has been explored extensively for reactions of both gases and liquids. Supported gold catalysts are useful for air cleaning at room temperature, and they are valuable for green production of bulk and fine chemicals. Supported gold clusters are expected to open new doors for simple chemistry for the selective manufacture of needed products. Size and structure

specificity are expected to present opportunities for selective conversions. It is recommended that researchers explore the magic numbers and structures of gold and suitable support materials for selected target reactions.

LIST OF ABBREVIATIONS, SYMBOLS, AND VARIABLES

ABF-STEM annular bright field scanning transmission electron microscopy
AC activated carbon
BOMD Born–Oppenheimer *ab initio* molecular dynamic
CAPD cathodic arc plasma deposition
CP coprecipitation
DFT density functional theory
DHA dihydroxyacetone
DP deposition precipitation
DPA diphenylacetylene
DR deposition reduction
E_{app} apparent activation energy
E_d**(CO)** activation energy for CO desorption
E_{LH} Langmuir–Hinshelwood activation energy defined as $E_{LH} = E_{app} + E_d(CO)$
FDA 2,5-difurandicarboxylic acid
GG gas-phase grafting
GLA glyceric acid
GLAD glyceraldehyde
GLYCA glycolic acid
GTO Gaussian-type-orbital
GVL γ-valeroactone
HAADF-STEM high-angle annular dark-field scanning transmission electron microscopy
HF Hartree–Fock
HMF 5-hydroxymethylfurfural
HRTEM high-resolution transmission electron microscopy
HT hydrotalcite, $Mg_6Al_2(OH)_{16}CO_3{\cdot}nH_2O$
IMP impregnation
K/A oil mixture of cyclohexanone and cyclohexanol
L Langmuir
LA lactic acid
LVA levulinic acid
ML monolayer
MOF metal organic framework
MOF-5 metal organic framework composed of nanoporous zinc(III) telephthalate, $Zn_4O(OOCC_6H_4COO)_3$
MOXA mesoxalic acid
MTP multiply-twinned particle
MTY metal time yield
NP nanoparticle
PBC periodic boundary condition
PMMA poly(methyl methacrylate)
PO propylene oxide
PVC polyvinyl chloride

PVD physical vapor deposition
PVP polyvinyl pyrrolidone
PW plane wave
QM/MM quantum mechanics/molecular mechanics
SG solid grinding
SI sol immobilization
TARAC tartanic acid
TEM transmission electron microscopy
TOF turnover frequency, reaction rate per catalytically active site
TOF-P reaction rate calculated by normalizing to the total number of Au atoms at the perimeter interfaces
TOF-S reaction rate calculated by normalizing to the total number of exposed Au atoms
TPD temperature-programmed desorption
TPR temperature-programmed reduction
TS-1 titanosilicalite-1 (with ZSM-5 structure)
UHV ultra high vacuum
VASP Vienna *ab initio* simulation package
VOC volatile organic compound
XPS X-ray photoelectron spectroscopy
XRD X-ray diffraction
1D one dimensional
2D two dimensional
3D three dimensional

1. INTRODUCTION

About 7000 years ago, human beings recognized the existence of gold on earth. Gold is the only element that can be present as metallic species in nature, because, thermodynamically, spontaneous oxide formation is prevented. The melting point of gold is 1336 K, noticeably lower than those of palladium (1825 K) and platinum (2045 K). Gold could be melted even in a primitive rock furnace, allowing the production of large ingots. Its softness enabled hand crafting to make jewelry and decorative objects used for religious ceremonies and festivals. During the course of its long history, gold has been regarded as the most precious metal because it shines brilliantly and eternally. This feature attracted the governors of human communities, who regarded gold as a symbol of eternal youth, beauty, and power—so that they desired to produce it artificially from cheap elements such as lead, tin, copper, iron, mercury, and sulfur *(1)*.

Alchemy was born in Egypt, then grew in Greece, and was continued in the Islamic world in around the tenth century. The alchemists' attempts to create gold from other elements were continued and intensified in Western Europe until the dawn of modern science. Although the efforts of alchemists were in vain, they brought about modern chemistry—and thereby the production of a wide variety of valuable materials such as organic polymers, food additives, medicines, pesticides, and semiconductors.

In classical chemistry, gold was treated as an inert material. The only industrial use was very thin wires for electrical connections, taking advantage of gold's high electrical conductivity and chemical inertness. The sole chemistry of gold might be considered to have been that associated with the wine-red color of colloids in stained glass windows of cathedrals and churches. It was Michael Faraday who initiated scientific approaches to the investigation of small colloidal gold particles, which represented a fourth state of matter in addition to gas, liquid, and solid phases.

Now a new gold rush is expanding as a leading edge of nanoscience and nanotechnology research. A typical example is catalysis by gold. For more than a century, bulk gold had been considered to be too noble to work as a catalyst. However, it was found in 1989 *(2)* that gold exhibited surprisingly high catalytic activity for CO oxidation when deposited as NPs on some selected base metal oxides. On the other hand, Hutchings reported *(3)* that cationic gold could theoretically be the most active metal for the hydrochlorination of ethylene, which was later confirmed experimentally *(4)*.

These findings have motivated many scientists to work on catalysis by gold. Although the number of published papers dealing with gold catalysis and catalysts was only a few tens in the middle of the 1980s, in 2009 it reached 1000, showing a rapid growth of gold research. In the area of heterogeneous catalysis, the discovery of CO oxidation at 200 K ignited the first wave of catalysis research at the beginning of 1990. The second wave around 2000 was driven by selective oxidation, typically, propylene epoxidation *(5)* and glucose oxidation to gluconic acid *(6)*. The latest keyword in catalysis by gold appears to be hydrogenation by gold clusters, which may constitute the most important target reactions for gold catalysts since 2010.

This chapter is a review of recent advances in heterogeneous catalysis by gold, focusing on the advances in the latest 10 years. For details of the past work, refer to the books *(7–12)* and review articles *(13–18)* already published.

2. PREPARATION OF SUPPORTED GOLD CATALYSTS

To prepare highly active gold catalysts, it is crucial to minimize the size of the gold particles to diameters less than 10 nm and to deposit them as hemispherical particles, which maximize the perimeter lengths *(19)*. The significant influence of the support on the catalytic performance is a characteristic feature of supported gold catalysts. Accordingly, preparation methods and conditions are essential to the creation of high-performance gold catalysts.

Historically, deposition of gold NPs on metal oxides (in principle, basic oxides) and metal hydroxides was among the first successes *(19)*. Then, carbon materials such as activated carbon (AC) and carbon black were used as supports in combination with sol immobilization techniques. Recently, new carbon materials such as carbon nanotubes, carbon nanohorns, fullerenes, graphene, and nano-diamonds are emerging or expected to emerge as new supports. Furthermore, organic polymers are interesting supports for gold catalysts. Deposition of gold NPs on conventional polymers, such as polyethylene, poly(methyl methacrylate) (PMMA), and polyvinyl chloride (PVC), and on dendrimers and metal organic frameworks (MOFs) has recently been studied. In this chapter, nine major deposition methods, which are shown schematically in Figure 1.1, are briefly described with an emphasis on innovative approaches.

2.1. Impregnation

The most traditional method for preparing supported metal catalysts is impregnation (IMP), which can be used to form NPs of palladium and of platinum. In this method, the support materials are first immersed in an aqueous solution of metal salts (typically, nitrates or chlorides) and then dried after water is removed by evaporation. Second, the precursors of the catalytic metal dispersed on the solid support surfaces are calcined in air to produce catalytic metal oxides, and finally the metal oxide precursors are reduced to metallic particles in a stream containing H_2. This method is not applicable to gold catalysts. When $HAuCl_4$, which is one of the most popular sources for preparation of gold catalysts, is used as a starting reagent, gold particles grow rapidly as a consequence of chlorine

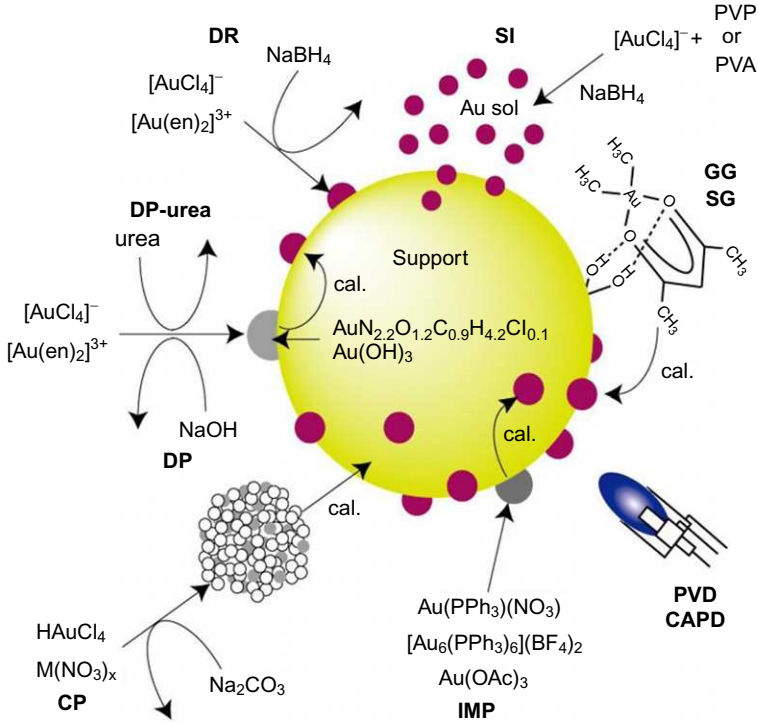

Figure 1.1 Illustration of various preparation methods for supported gold catalysts. cal., calcination.

contamination. When the gold loading is very low, <0.1 wt%, these gold particles often remain smaller than 5 nm in diameter. When $HAuCl_4$ is used as a gold source, washing with ammonia *(20)* or treatment in an NH_3 steam *(21)*, addition of Na_2CO_3 *(22)* after IMP, and the selection of HCl as an aqueous medium *(23)* lead to good dispersion of gold NPs on metal oxide surfaces.

The IMP method is sometimes effective, if a suitable gold source is selected, for example, $Au(PPh_3)(NO_3)$ *(24,25)*, $[Au_9(PPh_3)_8](NO_3)_3$ *(24,25)*, $[Au_6(PPh_3)_6](BF_4)_2$ *(26)*, $(CH_3)_2Au(CH_3COCHCOCH_3)$ *(27,28)*, $Au(S_2O_3)_2^{3-}$ *(29)*, and $[NEt_4][AuFe_4(CO)_{16}]$ *(30)*. Recently, Sakurai *et al.* *(31)* reported that $Au(CH_3COO)_3$ enables the formation of gold NPs on a variety of materials including zeolites, clays, carbons, and ion-exchange resins.

2.2. Coprecipitation

The coprecipitation (CP) method *(2,32,33)* is the first that led to the attainment of good dispersions of gold NPs on metal oxide particles. In this method, the precursor is a mixture of metal hydroxides or carbonates of support materials with $Au(OH)_3$, which is prepared by neutralization of metal salts with alkali. During calcination in air, hydroxides or carbonates of metal components of the supports are converted to metal oxides, and $Au(OH)_3$ is reduced to give metallic gold without H_2 reduction. Owing to the copresence of gold complex ions, the specific surface area of the gold catalysts becomes larger than that of simple metal oxides. The CP method can be applied to the 3-d metal oxides, such as MnO_x, Fe_2O_3, Co_3O_4, NiO, ZnO, and to many other metal oxides (ZrO_2, CeO_2, and La_2O_3). By choice of the calcination temperature, the size of the gold NPs can be controlled to a certain extent. Herzing *et al. (34)* reported that in the case of Au/Fe_2O_3 dried at 393 K, two-atom layer gold patches were formed and were the most active species for CO oxidation catalysis at room temperature. In general, the coprecipitated precursors are calcined in air at 573 K or higher temperatures to produce crystalline metal oxide supports.

The atmosphere of pretreatment at low temperature (373 K) is critical in the preparation of active gold catalysts. The catalytic activity of gold supported on $La(OH)_3$ for CO oxidation depends strongly on the pretreatment atmosphere *(35)*. Pretreatment of a hydroxide complex ($AuLa_2(OH)_9$) prepared by the CP method in air or N_2 resulted in low catalytic activity, whereas the sample pretreated in 10 vol.% CO in helium or 10 vol% H_2 in N_2 showed high catalytic activity. Transmission electron microscopy (TEM) observations led to the inference that it is likely that gold clusters <2 nm in diameter can be stabilized when the $AuLa_2(OH)_9$ precursors are pretreated in reducing gases.

2.3. Deposition–precipitation

The deposition–precipitation (DP) method *(36–39)* is especially useful for the basic metal oxide supports. $[Au(OH)_4]^-$ or $[AuCl(OH)_3]^-$ ions formed by ligand exchange of $[AuCl_4]^-$ ions in the high pH range (adjusted by addition of NaOH) interact with positively charged oxide surfaces or hydroxyl groups *(40)* on the surfaces, and then $Au(OH)_3$ species precipitate on the support oxide surfaces. It is difficult to deposit gold nanoparticles (NPs) on SiO_2 and WO_3 by the DP method because the surfaces of these oxides over a wide range of pH values of aqueous solutions bear negative charge.

There is repulsion between $[Au(OH)_4]^-$ ions and the negatively charged surfaces. The positively charged ethylenediamine–gold complex is a useful gold precursor for these negatively charged solid surfaces. In the case of SiO_2, deposition of gold NPs with diameters of 3–5 nm was attained on fumed silica NPs *(41,42)* and on mesoporous silica *(43,44)*. The DP method with NH_3 solutions which form positively charged gold amine complexes is also effective for the preparation of gold NPs on silica supports *(45,46)*.

In the DP method, NaOH is usually used as a reagent for pH control. Zanella *et al.* *(47,48)* employed urea instead of NaOH to deposit gold NPs on TiO_2. By use of the DP method with urea, all of the starting gold source can be deposited as ammonia complexes, and thus high gold loadings ($\sim$8 wt%) can be achieved. Heating time and temperature can be used to tune the size of the gold NPs. In the case of NaOH solution, gold hydroxide species ($[Au(OH)_4]^-$ or $[AuCl(OH)_3]^-$) are formed at a constant pH and precipitate on the support surface as $Au(OH)_3$. In the case of the urea solution, the pH of the solution gradually changes from acidic to basic during decomposition of the urea by heating:

$$CO(NH_2)_2 + 3H_2O \rightarrow CO_2 + 2NH_4^+ + 2OH^- \qquad [1.1]$$

An amorphous compound containing nitrogen, oxygen, and carbon, which formed by the reaction between gold precursors and the products of urea decomposition, is precipitated on the support. The composition of the precipitated gold precursors affects the dispersion and size of the gold particles. This method has been applied to the following supports: $Mg(OH)_2$ *(49)*, Al_2O_3 *(50)*, Mn_2O_3 *(51)*, MnO_2 *(52)*, MnO_x *(53)*, Fe_2O_3 *(54)*, CeO_2 *(55)*, $CeZrO_2$ *(56)*, and hydroxyapatite *(57)*.

2.4. Deposition–reduction

In the deposition–reduction (DR) method, gold complex ions are directly reduced near the support surfaces. This method is effective for depositing gold NPs on carbons and polymer supports. It is important to confine the reduction so that it takes place only on the support surface without reduction in the liquid phase. To obtain good dispersion of gold NPs on the support surfaces, the electrostatic interactions between gold precursors and the support surfaces should be strong. As carbon materials generally show negative electrical charge in water, positively charged ethylenediamine–gold complexes strongly interact with the carbon surfaces. Ethylenediamine–gold complex ions are reduced only on the carbon surfaces when $NaBH_4$ is added as a reductant at room temperature. Gold NPs can be deposited on PMMA, polystyrene, and PVC surfaces by this

method *(58,59)*. Functional amino groups on the polymer surfaces, for example, ion-exchange resins, play the role of a reductant for gold precursors, and gold NPs are directly deposited on the polymer surfaces *(60,61)*.

In the case of metal oxide supports, the DR method has rarely been reported for preparing gold catalysts. Sunagawa *et al.* *(62)* succeeded in depositing gold NPs (1–5 nm in diameter) on metal oxides (Fe_2O_3, ZrO_2, and TiO_2) or hydroxide (FeOOH) using the reduction of Au^{3+} ions by electron transfer from coordinated OH^- in liquid phase.

2.5. Sol immobilization

The sol immobilization (SI) method *(63–65)* is one of the liquid-phase methods to directly deposit gold NPs on solid surfaces. First, a sol of gold NPs is prepared with appropriate protecting agents (PVP, polyvinyl pyrrolidone; polyvinyl alcohol; etc.) which prevent the aggregation of gold NPs. Second, the sol of gold NPs is mixed with the support material and deposited on the support. Finally, the protecting agents are removed by washing or calcination. In this method, the combination of the protecting agents and the type of support is important for obtaining good dispersion of gold NPs on the support without aggregation. This method is applicable to metal oxides: TiO_2 *(66,67)*, Fe_2O_3 *(68)*, TS-1 *(69)*, and CeO_2 *(70)*, and carbon materials: AC *(71)*, graphite *(72,73)*, and carbon nanotubes *(74,75)*.

2.6. Gas-phase grafting

The gas-phase grafting (GG) method *(76–80)* is one of the chemical vapor deposition methods. Typically, an organogold complex, $(CH_3)_2Au(CH_3COCHCOCH_3)$, which has a very low vapor pressure of 1.1 Pa at room temperature, is vaporized in a vacuum line and adsorbed on the support. Then the solid precursor is calcined in air at 573 K or a higher temperature to remove organic ligands. Gold NPs can be deposited not only on metal oxides but also on other materials such as carbon and organic polymers. When organic polymers are used as supports, the solid precursors are treated at 393 K in a gas stream containing H_2. Because it is difficult for the gold complex to adsorb uniformly on all the exposed surfaces when the support materials are not agitated, the size distribution of gold particles is relatively broad.

Hermes *et al.* *(81)* attempted to deposit gold on MOF-5 by using the complex $(CH_3)_2Au(PMe_3)$. Polydisperse gold particles in the range of 5–20 nm in diameter were observed. As a consequence of aggregation of the mobile Au atoms or clusters, large gold particles (about 20 nm in diameter) were found outside the pores.

2.7. Solid grinding

Direct mixing of a solid gold complex and a support material is simple and effective for the preparation of gold NPs dispersed on support surfaces *(82–85)*. The solid grinding (SG) is carried out by using an agate mortar or a ball mill. Sometimes, the gold complex is mixed with organic solvents such as acetone or ethanol. The gold complex vaporizes during grinding and may move over the surfaces of the support and adsorb. Especially in the case of metal oxide supports, the gold complexes interact with the surface hydroxyl groups on the oxide surfaces. The SG method is applicable to almost all kinds of support materials including metal oxides, carbon, and organic polymers. Furthermore, gold NPs in the range of 1.5–4 nm in diameter can often be obtained.

2.8. Physical vapor deposition

Physical vapor deposition (PVD) is a clean, fast method compared with other chemical preparation methods. As this method does not require solvents or reducing agents, washing with water, or calcination for decomposition of gold precursors, post-preparation treatments of wastewater and exhaust gases are not necessary. The 3M company has commercially produced very active gold catalysts by the PVD method *(86,87)*. It takes only 2–3 h to make 400 mL of catalyst *(88)*. This gold catalyst is commercially available as "NanAucat^{TM}."

Gold catalysts on various supports including TiO_2 *(89,90)*, SiO_2 *(91,92)*, Al_2O_3 *(93)*, WO_3 *(94)*, AC *(94)*, C_3N_4 *(95)*, and steel fiber *(96)* have been prepared by a sputtering method. The activities of the catalysts prepared by the PVD method show activities equivalent to those of the catalysts prepared by wet chemical methods (e.g., the DP method).

2.9. Cathodic arc plasma deposition

Fujitani *et al.* *(97,98)* prepared gold NPs on single-crystal $TiO_2(110)$ surfaces with precise control of the size distribution (e.g., 4.2 ± 0.3 nm) by applying cathodic arc plasma deposition (CAPD), which is a kind of PVD. Such precise size control of the sizes of the gold NPs while maintaining the same gold loading, for example, one monolayer, is important in investigations of the size dependency of the catalytic properties. The characteristic features of arc plasma deposition contrasted with the conventional PVD method are as follows: (a) it is possible to control both the particle size and surface gold coverage, (b) gold particles are free from contamination, and (c) the adhesion of gold particles to the support is strong.

Table 1.1 Characteristics of various preparation methods for supported gold catalysts

Method	Suitable support[a]	Gold loading (wt%)	Gold NP shape[b]	Gold NP diameter (nm)	Wet or dry[c]	Notes	References
IMP	M, C	0.1–10	S	3–100	W	Selection of gold source and suitable treatment needed for preparing NPs	*(20–31)*
CP	M	1–20	H	1–5	W	Sophisticated mixture of various gold species	*(32–35)*
DP	M, C	0.1–10	H	3–10	W	SiO_2, WO_3: $Au(en)_2Cl_3$ DP-urea method: ~10 wt%	*(36–57)*
DR	M, P, C	1–5	S	1–10	W	Useful for polymers and carbon	*(58–62)*
SI	M, P, C	1–5	S	2–50	W	Useful particularly for carbon	*(63–75)*
GG	M, P, C	15	H	2–5	D	Vacuum line required	*(76–81)*
SG	M, P, C	0.5–3	H	2–5	W, D	Applicable to all supports, simple and easy	*(82–85)*
PVD	M, P, C	0.5–10	H	2–10	D	Fast and clean	*(86,87,89–96)*
CAPD	M, P, C	0.5–	H	0.5–5	D	Narrow size distribution of NPs	*(97,98)*

[a]M, metal oxide; P, polymer; C, carbon.
[b]S, sphere; H, hemisphere.
[c]W, wet; D, dry.

2.10. Summary

A variety of preparation methods have been developed for gold catalysts to obtain small gold NPs (<5 nm in diameter) with homogeneous dispersions on supports. The selection of the preparation method is crucially important and depends on the type of support material. The characteristic features of various preparation methods described in this section are summarized in Table 1.1. For a good understanding of the effects of gold particle size on catalytic properties, samples with monodisperse size distributions are desired. Extension to new kinds of support materials might be most exciting when the samples are prepared by the deposition of gold clusters with defined numbers of atoms because such samples would offer the opportunity to determine the size specificity of gold clusters for many green reactions. Work with new supports such as nano-carbon, polymers, and metal organic frameworks is also warranted.

3. FINE STRUCTURES OF SUPPORTED GOLD CATALYSTS

3.1. Electron microscopy as an efficient tool

Electron microscopy is indispensable for estimating the fine structure of small gold particles at the nano- and atomic scales. It is usually used for the measurement of size distributions of metal particles. Even single atoms can be observed by TEM under appropriate imaging conditions *(99)*. TEM can be applied to real powder catalysts as received without making special specimens, which are necessary for usual bulk materials. For precise structure analyses, model catalysts prepared by using well-defined supports are adopted for TEM observations. It is easy to control the direction of the incident electron beam along the zone axes of support crystals in high-resolution TEM (HRTEM) experiments, whereas it is difficult for small particles in powder supports in real catalysts. HRTEM images can easily be obtained when single crystals or polycrystals having large crystalline grains are used as supports. Although the imaging conditions are controlled to Bragg conditions for HRTEM observation, off-Bragg conditions for the support are also useful for high-contrast observations of gold NPs in plan-view TEM images to allow measurement of size distribution.

Figure 1.2 shows a typical TEM image of gold NPs on TiO_2 (P-25) and on Fe_2O_3, which were prepared by the DP and CP methods, respectively. Gold NPs are observed as dark areas in low-magnification TEM images, which allow estimation of the dispersion of the gold particles. The lattice fringes of gold, TiO_2, and Fe_2O_3 crystals are clearly evident in HRTEM.

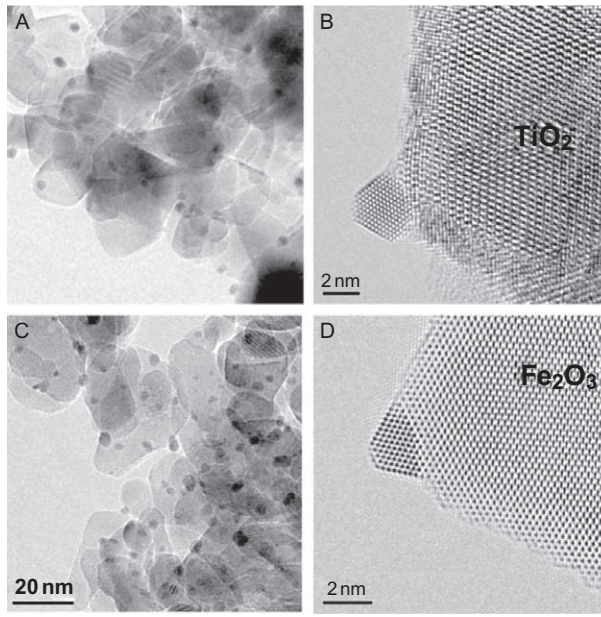

Figure 1.2 Typical low- and high-resolution TEM images of gold NPs supported on TiO_2 prepared by the deposition–precipitation (DP) method (A) and (B), and gold NPs supported on Fe_2O_3 prepared by the coprecipitation method (C) and (D).

As shown in Figure 1.2B and D, the crystal orientations between gold and the support can be estimated from such images *(100)*.

Recently, high-angle annular dark-field scanning transmission electron microscopy (HAADF-STEM) has begun to find wide use for the characterization of very small metal NPs in catalysts as well as the atomic structure of interfaces. The HAADF-STEM method is powerful for detecting small metal clusters composed of heavy atoms because the image intensity of HAADF-STEM is almost proportional to the square of the atomic number *Z*. Figure 1.3 shows a conventional TEM image and a HAADF-STEM image of Au/CeO_2 prepared by the DP method *(101)*. Although it is difficult to distinguish small gold NPs on CeO_2 in the TEM image shown in Figure 1.3A, the NPs are clearly evident with a high contrast in the HAADF-STEM image, even when the NPs are less than 2 nm in diameter, as shown by the black arrows in Figure 1.3B. In the TEM image, the diffraction contrast caused by small CeO_2 crystals and the complicated phase contrast caused by the uneven crystalline support thickness disturb the contrast of the small gold NPs. HAADF-STEM is more sensitive to the atomic number (*Z*) and thickness without diffraction contrast and phase contrast.

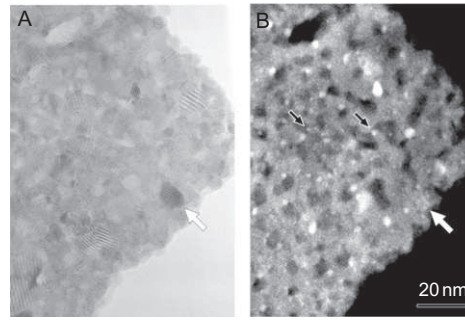

Figure 1.3 TEM (A) and HAADF-STEM (B) images of a Au/CeO_2 catalyst prepared by the deposition–precipitation method.

A key feature is evident in Figure 1.3. The dark area indicated by the white arrow in Figure 1.3A did not appear as a bright area in the HAADF-STEM image in Figure 1.3B. This comparison implies that the dark area in the former TEM image is not indicative of gold NPs, but is instead a diffraction contrast of the CeO_2 crystal, indicating that it is difficult to detect the small gold NPs by TEM imaging alone.

Aberration-corrected TEM and STEM are also available to image single Au atoms on the various metal oxide supports with high contrast *(34,102)*, as shown in Figure 1.4. HAADF-STEM can even detect the motion of single atoms *(103)* of heavy elements like gold. This technique will be indispensable for precise measurements of the size distributions of gold clusters less than 2 nm in diameter, which can hardly be detected by conventional TEM. Determinations of size effects in catalysis by gold NPs will become more reliable when precise size distribution measurements are carried out with aberration-corrected STEM. Moreover, aberration-corrected STEM will contribute to the counting of atoms in metal clusters *(104,105)*.

3.2. Growth of gold particles on metal oxide supports

To control the sizes of gold NPs and obtain stable catalytic performance, the calcination of catalyst precursors is an important process in catalyst preparation. TEM images of Au/TiO_2 (P-25) catalysts prepared by the DP method followed by calcination at various temperatures are shown in Figure 1.5. The images were taken from the same area, by repeating alternately the TEM observation and calcination in a conventional furnace. The small gold clusters and NPs are observed as dark areas in the as-received sample as indicated by arrows in Figure 1.5A. The growth of gold NPs is apparent with the increment of calcination temperature, and larger gold NPs were observed at

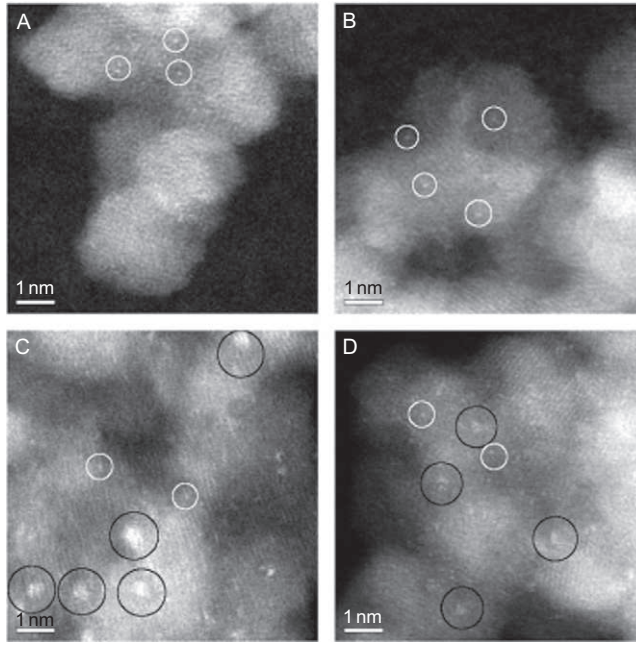

Figure 1.4 Aberration-corrected HAADF-STEM images of Au atoms and gold clusters in (A and B) the inactive and (C and D) the active Au/FeO_x catalysts; the images were acquired by aberration-corrected STEM. *Published with permission from Ref.* (34).

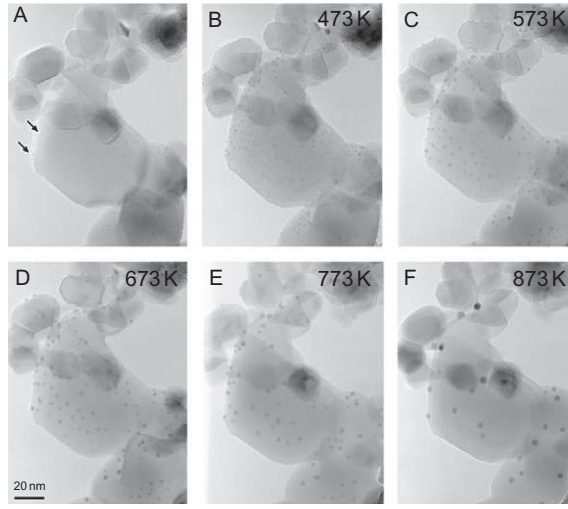

Figure 1.5 TEM images of a Au/TiO_2 catalyst prepared by DP method; without calcination (A), calcined at 473 (B), 573 (C), 673 (D), 773 (E), and 873 K (F).

the boundaries between TiO_2 particles after calcination at 873 K. This observation means that Au atoms can diffuse over the smooth surfaces of TiO_2 and gold particles are stuck in the boundaries between TiO_2 particles, which are the large geometrical defects. Gold catalysts are usually prepared by calcination at 573–673 K, because the gold NPs grow rapidly at temperatures exceeding 673 K *(106)*, resulting in an appreciable decrease in the catalytic activity for CO oxidation.

Figure 1.6 shows HAADF-STEM images of gold NPs on a rutile TiO_2(110) single-crystal support heated in air for 4 h at temperatures of 473, 573, 673, and 873 K, respectively. Gold particles were deposited by vacuum deposition. The HAADF-STEM images were obtained sequentially from the same area after each heat treatment to clarify the growth process of the gold NPs.

Gold NPs grow as a result of sample calcination at elevated temperatures, with the mean diameter increasing from 2.7 to 4.7 nm. Larger gold NPs are mostly observed in the same positions, whereas small gold NPs disappear as a result of heating, as indicated by the black arrows. In treatments at temperatures from 573 to 673 K, gold NPs indicated by white arrows became smaller and then disappeared at 873 K. This growth process indicates Ostwald ripening, which is characterized by the formation of larger gold NPs at the expense of smaller gold NPs.

The Au/TiO_2 samples were also heated in a stream of 10 vol% H_2 in argon. In contrast to the gold particles heated in air, these did not increase in size. Oxygen vacancies seem to be created on the TiO_2 surfaces in the H_2 atmosphere, preventing the diffusion of Au atoms on the TiO_2 surfaces *(107)*. The growth of gold NPs on TiO_2 was also investigated for the

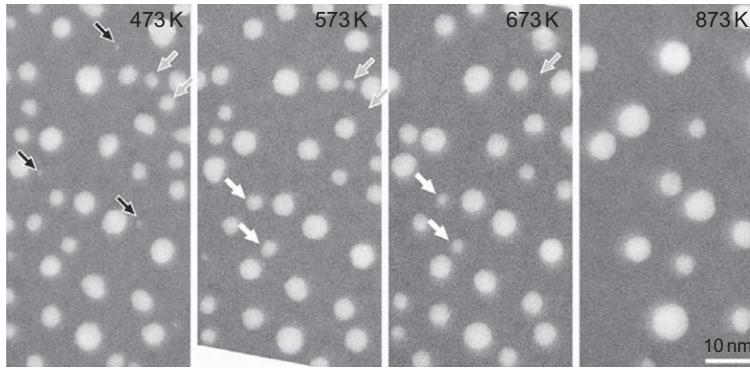

Figure 1.6 HAADF-STEM images of gold NPs deposited on single-crystal rutile TiO_2(110) substrate by vacuum deposition followed by calcination at 473, 573, 673, and 873 K.

powder catalysts by heating under various conditions. The growth of gold particles is appreciably suppressed in the H_2 atmosphere *(108)* owing to the relatively strong interaction between an Au atom and a surface O vacancy *(109)*. Smaller gold NPs can be deposited by calcination in H_2-containing stream. Then heating in O_2 or air at a lower temperature results in high catalytic activity. A similar tendency was also observed for gold on CeO_2 *(110)*.

A series of TEM images of gold NPs deposited on CeO_2 were taken during heating of the sample in an electron microscope by a specimen holder equipped with a tungsten coil heater *(111)*. The Ostwald ripening process was also confirmed in these *in situ* TEM observations, and the movement and aggregation of each gold NP were not observed during the heating process, owing to strong interactions of gold with CeO_2. The growth process of gold NPs on FeO_x was also observed by *in situ* aberration-corrected STEM *(112,113)*, as was the dispersion of small clusters and single Au atoms in Au/FeO_x catalysts.

3.3. Fine structure of gold particles on metal oxide supports

Pioneering HRTEM work concerning the fine structures of gold NPs was carried out in the 1980s *(114–118)*. Gold particles take the form of various structures at the nanoscale, including, for example, fcc single crystals (a Wulff construction shape), decahedral multiply-twinned particles (MTPs), and icosahedral MTPs *(119–121)* when the gold particles are free (in vacuum) or deposited on supports that interact weakly with the gold. The structure of gold is, in principle, appreciably influenced by the type of metal oxide used to support it. Gold NPs often consist of particles with the low-index faces {111} and {100} based on the Wulff construction. Single crystals with truncated shapes are frequently observed on metal oxide supports because of the adhesion energy between gold and the supports. When gold NPs become larger, MTP or twinned particles are often observed. The strength of the interaction with the support decreases with increasing gold particle size, and the shapes of the particles shift to stable shapes of bulk gold as a result.

The structures of gold–metal oxide interfaces and the perimeters of gold NPs are important for clarifying the mechanisms of catalysis by supported gold, because the perimeter is considered to act as the active site for various catalytic reactions, as discussed below *(13,97,122)*. HRTEM has been used to observe the interface structure of gold NPs and metal oxides at the atomic scale *(123–125)*. The interface structure between gold particles and TiO_2 was also observed by profile-view HAADF-STEM at the atomic scale *(126)*. Gold NPs were deposited on single-crystal rutile $TiO_2(110)$ surfaces by vacuum deposition. The gold particle is supported with the orientation

relationship Au(111)⟨110⟩//TiO_2(110)⟨001⟩. The distance between Au and Ti atomic layers was measured by HAADF-STEM to be 0.33 ± 0.01 nm. On the basis of theoretical calculations for Au atoms on stoichiometric and oxygen-defective TiO_2(110) surfaces *(109)*, the distance between Au and Ti atomic layers observed by HAADF-STEM was inferred to indicate that the gold particles were supported on the stoichiometric TiO_2(110) surface. The detailed structure of gold NPs on TiO_2 has also been assessed on the basis of HAADF-STEM observations *(127)*.

Profile-view HAADF-STEM observations were also made of the interface structures between gold and CeO_2 in a poly-crystalline CeO_2 model structure, which was prepared by vacuum deposition *(128)*. As shown in Figure 1.7, the orientation relationship of gold NPs and the CeO_2 support is Au(111)⟨1−10⟩//CeO_2(111)[−110] and Au(111)[1−10]//CeO_2(111)[−110] for TEM (Figure 1.7A) and HAADF-STEM (Figure 1.7B), respectively, as observed in TEM of Au/CeO_2 powder catalysts prepared by the DP method. The interface is formed with flat faces of gold NP and CeO_2 without apparent disordering of atoms, as shown schematically in Figure 1.7C. Although the value of the lattice mismatch is 28% for gold NPs (lattice constant: 0.40786 nm, JCPDS No. 04-0784) on CeO_2 crystals (lattice constant: 0.541134 nm, JCPDS No. 34-0394), four times the spacing of the gold lattice plane corresponds to three times the spacing of the CeO_2 lattice plane, giving the preferential orientation relationship. The distance between gold NP and Ce atomic layers at the interface was estimated to be 0.28 ± 0.01 nm on the basis of the HAADF-STEM image intensity profile. It is difficult to estimate whether the oxygen atoms exist on or in the interface on the basis of the conventional TEM and HAADF-STEM images. This issue can be resolved by comparison with first-principles calculations. The distance of 0.28 nm suggests that the gold particle is deposited on the oxygen-defective CeO_2(111) surface *(129)*.

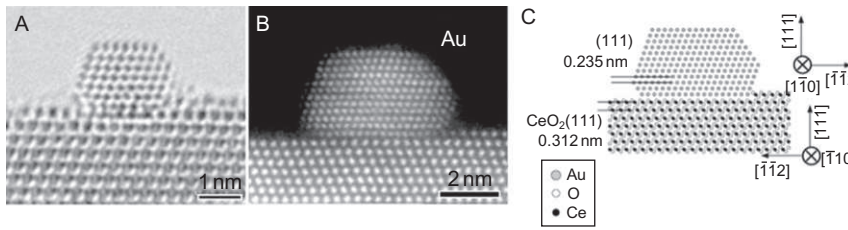

Figure 1.7 Profile-view HRTEM (A) and HAADF-STEM (B) images of a gold NP deposited on CeO_2 by vacuum deposition and a schematic drawing of the corresponding model structure (C).

Figure 1.8 is a HAADF-STEM image of a gold NP on poly-crystalline CeO_2 during the structure change, resulting from electron beam irradiation *(129)*. The gold NP becomes smaller during the HAADF-STEM observations. Similar structure changes were also observed by TEM for gold on CeO_2 powder *(128,130,131)*. Raft-like gold in two-atom layers was observed on the CeO_2(111) surface (Figure 1.8B). The small contact angle implies a relatively large adhesion energy between Au atoms and the CeO_2(111) surface. The stoichiometry of the CeO_2(111) surface can influence the shape of the gold NPs. The adhesion energy between gold and the oxygen-defective surface may be greater than that with the stoichiometric surface. As indicated by arrows in Figure 1.8, the Au atoms at the perimeter are disordered from the bulk structure of fcc gold NPs. Not a single Au atom, but instead approximately five atoms, exist along the beam direction as indicated by the HAADF-STEM image intensity. It is inferred that the oxygen defects of the CeO_2(111) surface might have been created around the gold NPs because the images were taken during electron beam irradiation. The reduction of the CeO_2 support by the electron beam was confirmed by electron energy loss spectroscopy analyses *(132)*.

Figure 1.9 shows the HAADF-STEM image of a gold NP on the CeO_2(111) surface. The gold particle is a structure characterized by low-index planes. The displacement of Au atomic columns was often observed on the (100) surfaces of the gold NPs. The surface of reconstructed Au(100)

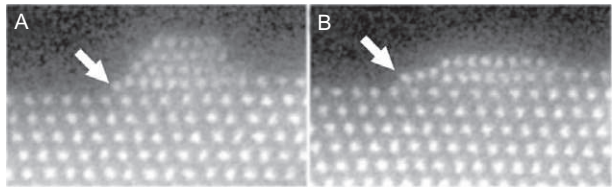

Figure 1.8 Profile-view HAADF-STEM images recorded during electron beam irradiation of a gold NP deposited on CeO_2(111) by vacuum deposition.

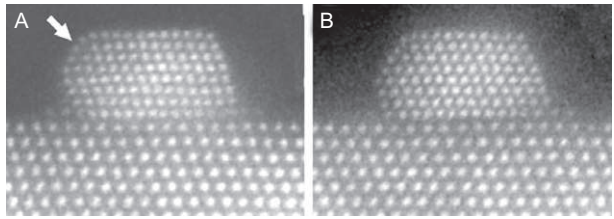

Figure 1.9 HAADF-STEM images of a gold NP deposited on CeO_2(111) by vacuum deposition showing surface reconstruction of the Au(100) surface.

(133,134) was observed as in well-defined clean Au(100) surfaces. Although the clean reconstructed structure of Au(100) is usually observed after cleaning under ultra-high-vacuum (UHV) conditions and the adsorption of residual gases destroys the reconstructed structure, the clean surface can be observed even under poor vacuum conditions by strong electron beam irradiation to remove adsorbed gases. It is likely that the area of the (100) surface is very small on the NPs. However, the reconstructed surface of gold NPs was not stable during TEM observations, and the structure was changing with time as indicated in Figure 1.9A and B, which were observed at different times.

3.4. Recent topics and future prospects

Recently, aberration-corrected TEM and STEM have become widely available for the observations of various materials with high spatial resolution. Aberration-corrected STEM has been used to observe gold catalysts. Single Au atoms are detected in Au/Fe_2O_3 catalysts *(34)*. The process of heating Au/Fe_2O_3 catalysts was also observed by *in situ* STEM *(112,113)*. The modification of the crystal lattice of small gold NPs by the support crystal was observed for a sample supported on rutile $TiO_2(110)$ *(135)*. Environmental TEM *(136–138)* was also applied for the dynamic observation of a gold catalyst in a reactive gas atmosphere *(139–144)*. These advanced techniques will bring valuable knowledge about the relationships between the fine structures of gold NPs and the catalytic properties.

It has also been reported that annular bright field STEM (ABF-STEM) combined with aberration-corrected STEM is powerful for direct observation of the light atoms such as oxygen and hydrogen in crystal lattices *(145–147)*. It is also expected that it will be possible to observe the structure of the gold–metal oxide interface by ABF-STEM to help clarify the possible existence of oxygen atoms at the contact interfaces or gold perimeters. Electron tomography is another advanced technique for the determination of the three-dimensional structures of gold NPs and support materials *(148,149)*, as shown in Figure 1.10. If the spatial resolution is improved to less than 1 nm *(150)* and it can be used easily, this technique will become powerful for estimating the distribution of gold clusters on planar and porous supports.

Electron holography provides another interesting approach to investigating the three-dimensional shapes of gold NPs and detecting local potentials *(151,152)*, which are important for understanding charge transfer at interfaces.

Bimetallic NPs including gold have also been widely investigated as new catalysts. The fine structures of bimetallic NPs have been investigated by

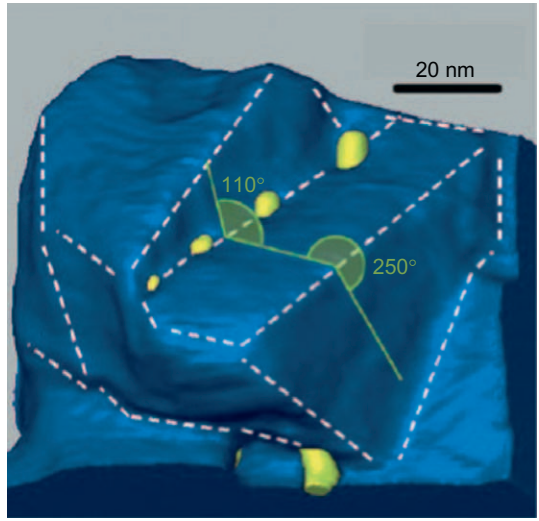

Figure 1.10 Reconstructed three-dimensional structure of gold NP on $Ce_{0.50}Tb_{0.12}Zr_{0.38}O_{2-x}$ support determined by electron tomography. *Published with permission from Ref.* (148).

HRTEM and STEM *(153,154)*, leading to significant results characterizing the local structures in core–shell NPs at the atomic scale. In view of the recent progress in the understanding of nano-structured catalysts, we infer that advanced electron microscopic techniques will become more useful, and even indispensable, for the study of the catalysis at the nanoscale and atomic scale.

4. SURFACE SCIENCE OF CO OXIDATION CATALYZED BY GOLD

Gold NPs supported on base metal oxides exhibit high catalytic activity for reactions including low-temperature CO oxidation, the water-gas shift reaction, and selective oxidation. Numerous investigations have addressed how the structure and electronic properties of gold surfaces and particles correlate with the catalytic activity. However, the reaction mechanisms and the nature of the active sites of gold NP catalysts are still not well understood because the size distributions, shapes, and the contact (interfacial) structures of gold NPs supported on base metal oxides are not uniform. In contrast, fundamental studies of the reaction chemistry of gold single crystal and model supported gold catalysts can provide significant insights into the mechanistic details of catalysis by gold because it is possible to control

carefully the surface structures and reaction parameters. This section is a review of the current understanding of low-temperature CO oxidation catalyzed by gold developed mainly on the basis of surface science studies.

4.1. Gold single crystals

4.1.1 Low-index (flat) gold surfaces

The oxidation of CO catalyzed by low-index gold single-crystal surfaces such as Au(111) *(17,155–157)* and Au(110) *(158,159)* was investigated by Friend *et al. (17,155)*, who prepared oxygen layers by ozone decomposition on the Au(111) surface and examined the effect of oxygen coverage and the preparation temperature of atomic oxygen on the rate of CO_2 production at 200 K (Figure 1.11). This rate increased linearly with increasing oxygen coverage up to 0.5 ML (monlayer) when oxygen was deposited at 200 K. The rate of CO oxidation is dropped by an order of magnitude at coverages between 0.5 and 1.2 ML. In contrast, the rate of CO_2 production was found to be independent of oxygen coverage when the oxygen layer was prepared at 400 K. At an oxygen coverage of 0.5 ML, the rate of

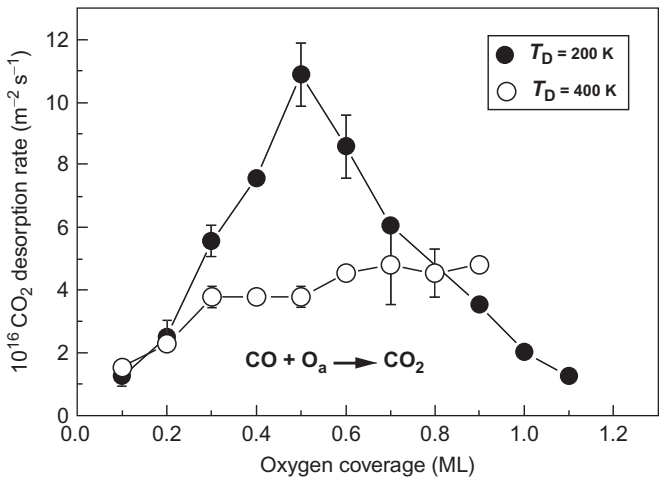

Figure 1.11 Initial rate of CO_2 production on a Au(111) surface as a function of oxygen coverage at 200 (filled circles) and 400 K (open circles). The initial reaction rate was determined by the initial increase of CO_2 desorption resulting from the CO oxidation; the data were obtained with a mass spectrometer and normalized by the total area of the CO_2 desorption profile collected on a period of 300 s. The data were converted to the absolute number of CO_2 molecules per area per unit time (atoms/m^2/s), assuming that 1 ML of CO_2 corresponds to the number of Au atoms on the Au(111) surface (1.3×10^{15} atoms/cm^2). *Published with permission from Ref.* (155).

CO_2 production with an oxygen layer deposited at 200 K was approximately three times greater than that with an oxygen layer formed at 400 K. These results were explained by the formation of three different types of oxygen-containing structures, depending on the preparation temperature of atomic oxygen and the oxygen coverage. The reactivity of atomic oxygen in CO oxidation decreased in the following order: chemisorbed oxygen > oxygen in a surface oxide > oxygen in a bulk gold oxide. Moreover, Lazaga *et al.* *(157)* reported that the CO oxidation occurs readily at low temperatures on O/Au(111) surfaces prepared by ozone decomposition at 300 K. They observed negative apparent activation energies ($E_{app} = -10.5$ kJ mol^{-1}) with no strong dependence on oxygen coverage.

Outka and Madix *(158)* observed that CO reacts with oxygen adatoms on the Au(110) surface with an apparent activation energy of 8.4 ± 4.2 kJ mol^{-1}. Neither CO nor CO_2 could be stabilized on the clean Au(110) surface at temperatures as low as 125 K. On the basis of isotopic labeling experiments with $C^{18}O$, the authors found that CO did not dissociate on the surface. Gottfried and Christmann *(159)* examined CO oxidation on an oxygen-precovered Au(110)-(1×2) surface, showing that the reaction rate on Au(110) with an initial oxygen atom coverage of 0.45 ML increased with temperature until the temperature reached about 170 K. At temperatures above 175 K, the surface reaction was no longer the rate-limiting step, as the adsorption of CO then controlled CO_2 production. At low oxygen coverages, the reaction was found to be first order in the oxygen coverage with an apparent activation energy of -1.8 kJ mol^{-1}. Assuming a Langmuir–Hinshelwood mechanism, the authors calculated the true activation energy to be 57 kJ mol^{-1} and showed a complete reaction energy diagram of the CO oxidation on Au(110) (Figure 1.12).

4.1.2 High-index (stepped) gold surfaces

The adsorption and oxidation of CO have been investigated on stepped gold single-crystal surfaces *(160,161)*. Kim *et al.* *(160)* examined CO adsorption on a Au(211) stepped single-crystal surface using temperature-programmed desorption (TPD) and infrared reflection/absorption spectroscopy. TPD experiments were performed after CO exposures ranging from 0.0025 to 50 Langumuirs (L) at 85 K. TPD curves exhibited a peak at 190 K (α) and a broad feature from 100 to 150 K ($\beta_1 = 150$ K, $\beta_2 = 127$ K, $\beta_3 = 109$ K). The α peak shifted from 197 to 190 K with increasing CO exposure. This peak was attributed to desorption of CO from step sites on the Au(211) surface. The CO desorption energy E_d for this peak was estimated to be roughly

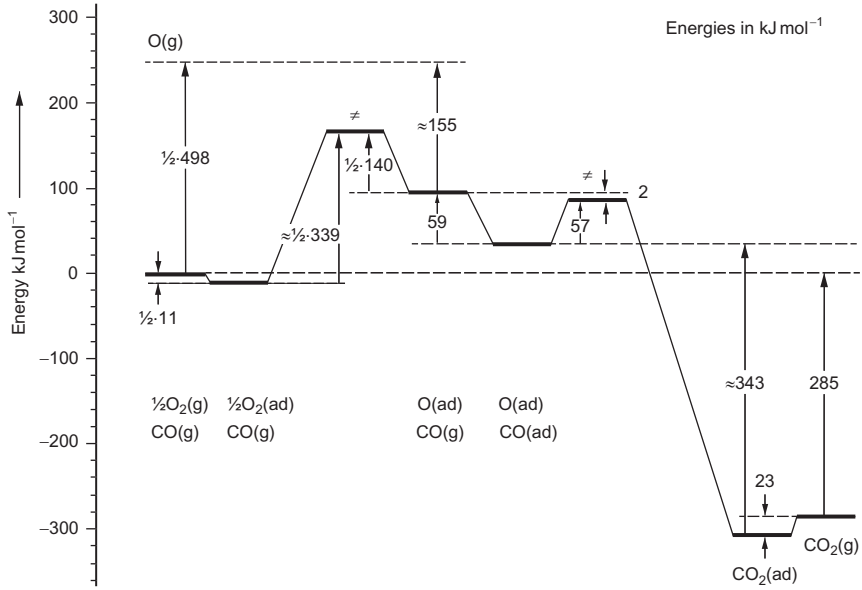

Figure 1.12 Quantitative energy diagram of the CO oxidation on Au(110)-(1 × 2). All values concerning dioxygen adsorption are multiplied by ½ to account for the stoichiometry of the reaction, which requires only ½O_2 for the oxidation of one CO molecule. All values (apart from the standard gas-phase reaction energy of 285 kJ mol^{-1} and the O_2 dissociation energy of 498 kJ mol^{-1}) were taken from this and our recent publications. *Published with permission from Ref.* (159).

50 kJ mol^{-1}. On the other hand, the broad feature at lower temperatures was attributed to CO desorption from terrace sites. Values of E_d for CO desorption in these peaks were estimated to be roughly 27 (β_3), 34 (β_2), and 38 kJ mol^{-1} (β_1). Thus, CO was more strongly bound at step sites than at terrace sites. The sticking coefficient of CO on the Au(211) surface was also higher during occupation of step sites than that at populating terrace sites at higher coverages. The authors concluded that the presence of these particular step sites on the Au (211) surface leads to stronger CO bonding and a higher reactivity than that on the flat Au(111) surface, but these changes are not remarkable in comparison with the chemistry on other more reactive crystal planes or on other stepped gold surfaces. Thus, it is unlikely that the presence or absence of this particular crystal plane alone on supported gold NPs can be correlated with the remarkable properties of highly active gold catalysts.

Samano *et al. (161)* performed transient kinetic experiments, characterizing CO oxidation on a stepped Au(211) single-crystal surface precovered with atomic oxygen created by ozone decomposition. They showed that the rate of

CO oxidation was strongly dependent on the initial oxygen coverage, and the maximum initial rate of CO_2 production occurred at an oxygen coverage of $\sim$0.5 ML. Furthermore, they determined an apparent activation energy (E_{app}) for CO oxidation of -7.0 kJ mol^{-1} for $\Theta_O = 0.9$ ML. This negative value is close to those reported for reaction on Au(111) *(157)* and Au(110) surfaces *(159)*. Within the Langmuir–Hinshelwood reaction scheme, the activation energy (E_{LH}) for CO oxidation on the Au(211) surface was estimated to be 20–43 kJ mol^{-1}, on the basis of the following equation:

$$E_{LH} = E_{app} + E_d(CO) \quad [1.2]$$

where E_d(CO) is the activation energy for CO desorption (27–50 kJ mol^{-1}).

The authors concluded that the activation energy for CO oxidation on the stepped Au(211) surface is not much different from that for the reaction on the flat Au(111) *(157)* or Au(110) *(159)* surfaces, suggesting that there is no evidence for any special reactivity of CO oxidation associated with stepped gold surfaces.

4.2. Model supported gold catalysts

4.2.1 Preparation of model catalyst surfaces

Investigations of model catalytic systems composed of metal particles supported on single crystals of base metal oxides or thin-film substrates under well-controlled conditions can provide fundamental knowledge on the nature of gold catalysis.

The Au/TiO_2(110) system is the most intensively studied among the model gold catalysts because both components are catalytically inactive when isolated. The TiO_2(110) surface consists of alternating rows of Ti and O atoms with half of the Ti atoms covered by bridging oxygen. This arrangement leads to both six- and fivefold coordinated Ti as well as three- and twofold coordinated oxygen *(162,163)*. As a consequence of the deeper coordinative under-saturation, the bridge-bonded O atoms can be easily removed to form point defects or color centers. Surface defects can be created by Ar^+ sputtering or annealing in UHV. The nature of the surface defects, which depend on the preparation conditions of the TiO_2(110) sample, influences the adsorption energy and the shape and electronic structure of the deposited gold NPs, and thus the catalytic activity *(125,164)*.

The growth of gold on the TiO_2(110) surface has been examined by means of surface science techniques *(165–168)*. Santra *et al.* *(169)* showed that the growth rate of gold particles on TiO_2(110) surfaces with relatively low defect

densities was much higher on step edges than on terraces, resulting in a bimodal cluster size distribution. Furthermore, Goodman *et al.* *(163,170)* showed an STM image of 0.25 ML of gold deposited on TiO_2(110) at 300 K followed by annealing at 850 K for 2 min, as well as schematics of the 1D (one-dimensional), 2D (two-dimensional), and 3D (three-dimensional) gold structures with one-, two-, and three-atomic layer thicknesses (Figure 1.13). The atomically resolved TiO_2(110) surface consists of flat terraces with rows of atoms separated by $\sim$0.65 nm. Gold NPs with a relatively narrow size distribution and specific morphologies are imaged as bright protrusions.

Zhang *et al.* *(171)* observed the growth of thin gold films (0.2–12 nm in thickness) and the surface morphology of 3D gold islands on the TiO_2(110) surface by using HRSEM. At 300 K, the gold film morphology evolved with an increasing average gold thickness h, from hemispherical islands present initially ($h < 1.0$ nm), to partially coalesced worm-like island structures ($h > 1.5$ nm), to percolation at $h \sim 8$ nm, and finally to a continuous and rough film at $h \sim 12$ nm. Cosandey *et al.* *(172)* examined the effects of substrate temperature on the epitaxial growth of gold on TiO_2(110) by HRSEM and electron backscatter diffraction. After room-temperature

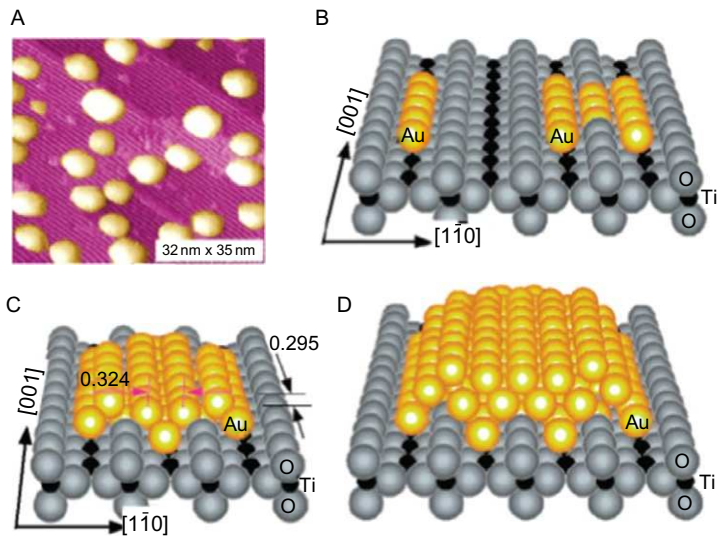

Figure 1.13 (A) STM image of Au/TiO_2(110)-(1 $\times$ 1) with a gold coverage of 0.25 ML and (B–D) schematic structural models for 1D, 2D, and 3D structures with one-atomic-, two-atomic-, and three-atomic-layers thick gold particles on the TiO_2(110). *Published with permission from Ref.* (163).

deposition of gold followed by annealing at 775 K, the epitaxial orientation relationship is (111)Au//(110)TiO_2 with ⟨110⟩Au//[001]TiO_2. When the sample was prepared by direct deposition at 775 K, the epitaxial orientation relationship was found to be (112)Au//(110)TiO_2 with ⟨110⟩Au//(001) TiO_2. These results are consistent with those reported by Lazzari *et al.* *(173)*. Matthey *et al.* *(174)* investigated the adhesion of gold clusters on the reduced and oxidized TiO_2 supports. They showed that covalent bonds form between gold clusters and TiO_2 on a reduced TiO_2(110) surface, whereas the bonding of gold clusters on an oxidized TiO_2(110) surface is partially ionic, to make the gold clusters cationic.

4.2.2 Active sites for CO oxidation

The discovery by Haruta that gold NPs supported on base metal oxides are highly active catalysts for low-temperature CO oxidation has spurred extensive research directed toward understanding the nature of gold catalysts. Haruta *(175)* reported that the performance of gold NPs is defined by three major factors: the contact structure to the oxide support, the nature of the support, and the particle size, with the contact structure being the most important. Recently, some investigators *(98,176,177)* have reported that the Au–TiO_2 perimeter interface is the active site for CO oxidation on Au/TiO_2 catalysts. Theoretical investigations *(178–180)* have also highlighted the importance of the periphery around gold particles (this point is addressed below).

In contrast to the perimeter model, Goodman *et al.* *(181,182)* claimed that the TiO_x support acts mainly as a dispersant and a promoter, and a bilayer of gold which blocks the direct access of the reactants to the support is responsible for CO oxidation. Therefore, although extensive experimental and theoretical studies have been carried out to elucidate the origin of the unique activity of supported gold NPs, arguments continue concerning the nature of the active gold species, their structures, and the catalytic sites. In principle, the origins of the catalytic activity of gold were considered to stem from more than one of the four contributions: (1) quantum size effects; (2) the presence of low-coordination gold sites; (3) charge transfer between the support and gold; and (4) the perimeter interface between gold and the oxide support. These points are addressed in the following paragraphs.

4.2.2.1 Quantum size effects

It is known that the activity of gold NPs supported on base metal oxide surfaces for CO oxidation is strongly correlated with the particle size of gold *(2,3,10,13,16–18,163,170,180–198)*. Chen and Goodman *(181)* reported

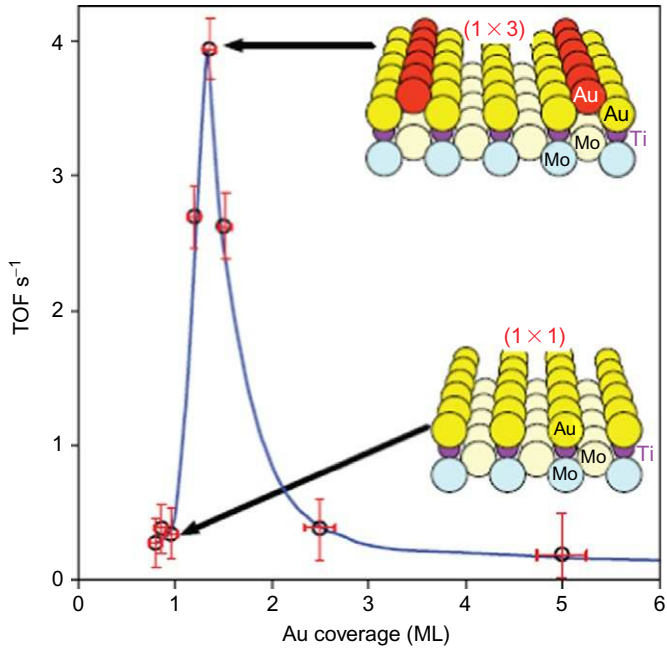

Figure 1.14 Rates of CO oxidation at room temperature as a function of gold coverage on Mo(112)-(8 × 2)–TiO_x. The CO:O_2 molar ratio was 2:1 and the total pressure was 6.7 mbar. The data represent initial rates derived by extrapolating the rate data to zero time. The TOF for the (1 × 1) gold structure was calculated from the total number of Au atoms in the structure. The TOF for the (1 × 3) structure was calculated by dividing the overall rate minus two-thirds the (1 × 1) rate (those reactive atom sites blocked by the second layer of gold) by the number of Au atoms in the second layer of the structure; for gold coverages >2.0 ML, the TOFs are based on total gold because 3D clusters formed. Insets: Schematic models of the (1 × 1) and (1 × 3)-Au/TiO_x surfaces. *Published with permission from Ref.* (181).

that gold bilayers were significantly more active (by more than an order of magnitude) than gold monolayers (Figure 1.14). Bondzie *et al. (194)* also examined the influence of gold island thickness on TiO_2(110) on the CO oxidation. The rate of CO oxidation at room temperature was found to be slightly lower on the thinnest gold (2D) islands than on thick gold (3D) islands. Valden *et al. (186)* proposed that the pronounced structure sensitivity of CO oxidation on metal oxide-supported gold NPs arises mainly from the changes of the electronic properties of the gold clusters as a function of their size, with gold clusters that are two atomic layers thick being optimum. The gold cluster size giving the highest heat of CO adsorption ($-\Delta H_{ads}$) is very close to that exhibiting the maximum catalytic activity for CO oxidation

(190). The size of gold particles might be also crucial to the activation of molecular oxygen because the CO oxidation activity in the reaction catalyzed by $Au/TiO_2(110)$ is only weakly dependent on the gold particle size when the surface is populated with atomic oxygen *(194–197)*.

The shapes, adsorption sites, and size distributions of size-selected Au_n cluster cations ($n = 1–8$) on $TiO_2(110)$ were investigated *(191)*. Lee *et al.* *(189)* showed that the activity is strongly dependent on the deposited cluster size, with substantial activity for Au_n clusters as small as three-atom clusters. Arenz *et al.* *(180)* reported that at least eight Au atoms are necessary for the genesis of catalytic activity of gold clusters on a single-crystal MgO support. Boyen *et al.* *(198)* showed that a maximum oxidation resistance appeared for "magic-number" clusters containing 55 Au atoms, suggesting that Au_{55} clusters may act as especially effective oxidation catalysts, such as for oxidizing CO at low temperature and for the selective oxidation of hydrocarbons.

4.2.2.2 Low-coordinated gold sites

It has been proposed that the origin of the catalytic activity of small gold particles is the presence of low-coordinated Au atoms at sites such as corner and edge sites *(17,183,185,199–207)*. Mavrikakis *et al.* *(200)* found that steps bind molecules considerably more strongly than the (111) terraces and that an expansive strain has the same effect. On this basis, they suggested that the unusually high catalytic activity of highly dispersed gold NPs may in part be a consequence of high step densities on the small particles and/or strain effects attributed to the mismatch at the gold–support interface. Lopez *et al.* *(185)* also proposed that the most important effect contributing to the high catalytic activity of supported gold NPs was related to the availability of many low-coordinated Au atoms on the small particles.

Lemire *et al.* *(201)* clearly showed a particle size effect, indicating that small gold deposits adsorb CO more strongly than larger ones. They proposed that the adsorption of CO involves only low-coordinated atoms and is consequently independent of the particle dimensions except as they affect the number of uncoordinated atoms. The particle size effects were therefore attributed not to quantum size effects but rather to the presence of highly uncoordinated Au atoms in very small particles. The importance of coordinatively unsaturated gold sites was also addressed by experimental observations with nanoporous unsupported gold *(206, 207)*. Nanoporous unsupported gold is highly active for CO oxidation and contains a high density of low-coordinated surface sites such as step and kink atoms. The samples were produced by leaching silver from Au–Ag alloy and accordingly were modified by Ag_2O.

4.2.2.3 Charge transfer between gold and metal oxide support

The interaction between gold NPs and the oxide support modifies the electronic structure of gold and may play an important role in low-temperature CO oxidation *(16,17,19,28,162–164,170,181,183,184,208–235)*. Campbell *(218)* indicated that the active species were metallic gold particles. Goodman *et al. (170,181)* also found that metallic gold was indispensable for the genesis of catalytic activity on $Au/TiO_2(110)$ model catalysts. Carrettin *et al. (219)* reported that cationic gold on $Au/FeO_x/TiO_2$ was rapidly reduced to zerovalent gold during CO oxidation. Schwartz *et al. (220)* concluded that oxidized gold is not necessary for high activity on Au/TiO_2 catalysts. The necessity of metallic gold NPs for high CO oxidation rates on Au/TiO_2 was also confirmed by Yang *et al. (221)*. Calla *et al. (222)* concluded that active Au/TiO_2 and Au/Al_2O_3 catalysts contain predominantly metallic gold.

Notwithstanding the results cited in the preceding paragraph, it seems that the most crucial phase in gold catalysts is AuO_x or AuO(OH) species or more specifically cationic species *(28,183,230–234)*. Bond and Thompson *(209)* suggested that the Au atoms at the interface of the gold particles and the oxide support could be cationic and are responsible for the activation of dioxygen in the catalytic process. Kobayashi *et al. (230)* found that Au^+ ions in $Au/Mg(OH)_2$ catalysts play an important role in catalytic activity at 200 K. Guzman and Gates *(28, 231)* demonstrated that the rate of CO_2 formation from CO and O_2 catalyzed by Au/MgO increased with the concentration of Au^+. Furthermore, Guzman *et al. (235)* showed that the catalytic activity for CO oxidation catalyzed by Au/CeO_2 correlates with the concentration of Au^{3+}. Boyd *et al. (233)* showed that only the Au(I) on Au/TiO_2 and $Au/TiO_2/ZrO_2$ correlates directly with the CO oxidation activity. Hutchings *et al. (234)* demonstrated that bilayer gold plays a crucial role in catalyzing CO oxidation on co-precipatated $Au/\alpha\text{-}Fe_2O_3$.

On the other hand, electron-rich Au ($Au^{\delta-}$) NPs have been suggested to play an important role in the catalytic activity for CO oxidation *(163,185)*. Stiehl *et al. (227)* demonstrated the presence of adsorbed molecular oxygen on electron-rich gold clusters supported on a $TiO_2(110)$ surface. Chemisorbed molecular oxygen can participate directly in CO oxidation *(228)*. Minato *et al. (226)* also concluded that negatively charged gold clusters supported on $TiO_2(110)$ show high catalytic activity. Defect sites on the oxide support may play an important role in charge transfer to gold clusters, resulting in the formation of negatively charged gold clusters. Yoon *et al. (216)* reported that gold octamers bound to oxygen-vacancy F-centers on MgO(001) are the smallest clusters to catalyze the low-temperature

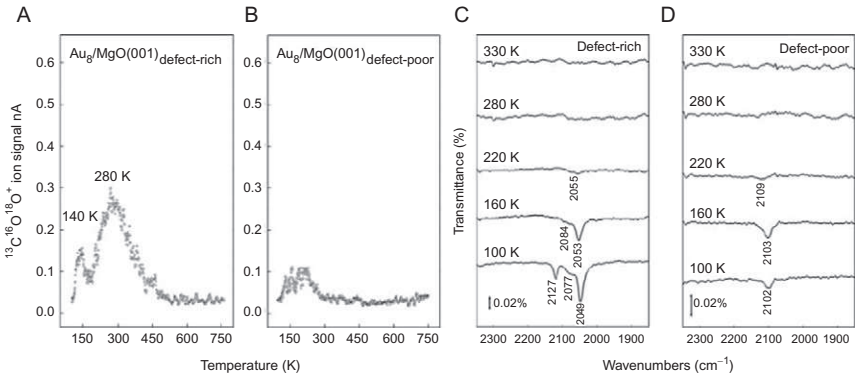

Figure 1.15 Mass spectrometric signals pertaining to the formation of CO_2 on Au_8 deposited on (A) F-center-rich and (B) F-center-free MgO(001) thin films. To unambiguously show that both CO and O_2 are involved in the reaction, isotopically labeled ^{13}CO and $^{18}O_2$ were used. (C) and (D), Fourier-transform IR spectra were obtained for the same surfaces (defect-rich and defect-poor) and with the same CO and O_2 exposures as in (A) and (B), respectively, at various annealing temperatures. The indicated temperatures cannot be compared directly with the ones in the temperature-programmed reaction spectrum but instead are lower limits. An IR absorption band was also observed at 1300 cm^{-1}, which is attributed to superoxo/peroxo-type O_2. To better disentangle the vibrational band of ^{13}CO adsorbed on Au_8 deposited on defect-poor films (B) from that of the CO weakly bound to the support material, the sample was annealed at 120 K. In this way, the ^{13}CO frequency characterizing MgO-adsorbed CO disappeared, which otherwise was observed at 2127 cm^{-1}. *Published with permission from Ref.* (216).

oxidation of CO to CO_2, whereas clusters deposited on close-to-perfect magnesia surfaces remain chemically inert (Figure 1.15). It has also been shown that the surface F-centers on MgO play a critical role in the activation of gold on Au/MgO catalysts *(223,224)*.

A definitive study has not yet been published concerning the active oxidation state or states of gold in NPs for CO oxidation. It is an area that may attract more attention by surface scientists.

4.2.2.4 Formation of reactive gold–metal oxide perimeter interfaces

The perimeter interface sites between gold NPs and oxide supports have recently been regarded as reaction sites for CO oxidation *(19,98,122, 176–180,236–244)*. This hypothesis was proposed for the first time by Haruta *(19,122,236)* for high-surface-area gold catalysts. The unique catalytic properties of supported gold can be explained by assuming that the gold–metal oxide perimeter interface acts as a site for activating at least one of the reactants, for example, oxygen. The dominant reaction pathway presumably involves adsorption of a mobile, molecular oxygen species on the support, and reaction

on the gold particles and/or at the periphery with CO adsorbed on the gold. Schubert *et al.* *(237,238)* reported that the dissociation of molecular oxygen occurs on a Au/Fe_2O_3 catalyst at the interface before reacting with CO.

Grunwaldt and Baiker *(239)* investigated the role of the Au/TiO_2 interface in the low-temperature oxidation of CO and the chemisorption of the reactants CO and O_2 using structurally different Au/TiO_2 model catalysts. The observed chemisorptive properties of the structurally different Au/TiO_2 interfaces support a mechanistic model for CO oxidation which is based on oxygen adsorption on vacancy sites of titania and CO adsorption on gold. Recently, Green *et al.* *(176)* reported that the mechanism of low-temperature CO oxidation (120 K) on a Au/TiO_2 catalyst takes place at a perimeter zone or the support surfaces (Figure 1.16). Widmann and Behm *(177)* showed the pathway for CO oxidation on Au/TiO_2 catalysts at temperatures >353 K. The authors concluded that the active oxygen species for CO oxidation is surface lattice oxygen at the gold–TiO_2 perimeter sites.

Fujitani and Nakamura *(98)* investigated the reaction mechanism and active sites for CO oxidation using $Au/TiO_2(110)$ model catalysts. The Arrhenius plot for CO_2 formation in the presence of H_2O clearly shows a sudden change in the slope at approximately 320 K (Figure 1.17B). The apparent

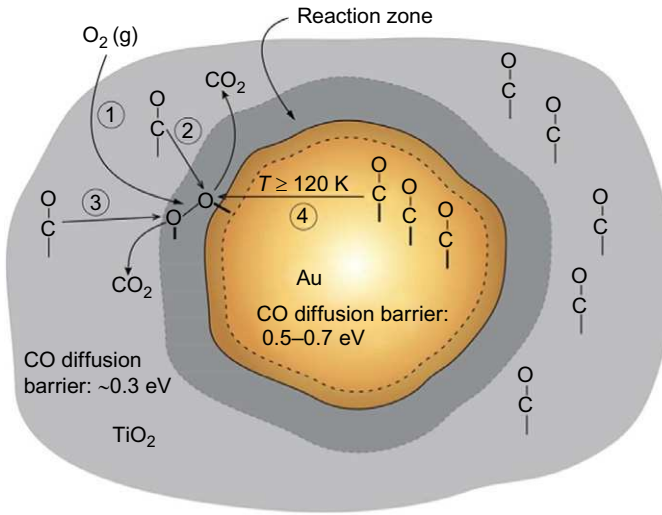

Figure 1.16 Schematic representation of the mechanism of low-temperature CO oxidation on a Au/TiO_2 catalyst at a perimeter zone of reactivity. Experiments directly observing CO/TiO_2 and CO/Au surface species show that processes 2 and 3 are fast compared with process 4. *Published with permission from Ref.* (176).

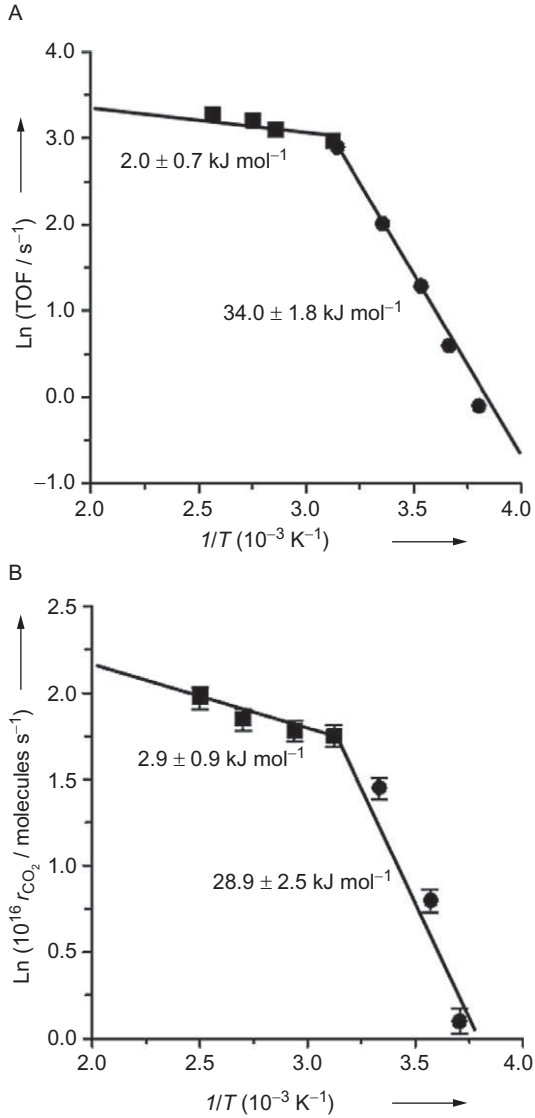

Figure 1.17 Arrhenius plots for the formation of CO_2 on (A) a powder Au/TiO_2 catalyst *(236)* and (B) one MLE of $Au/TiO_2(110)$. The oxidation of CO was performed in batch mode under 33 mbar of CO, 833 mbar of O_2, and 0.13 mbar of H_2O. *Published with permission from Ref.* (98).

activation energies at temperatures above and below 320 K were estimated to be 2.9 ± 0.9 and 28.9 ± 2.5 kJ mol^{-1}, respectively. These values and the overall dependence of the rate on the temperature agree well with results obtained for a powder Au/TiO_2 catalyst (Figure 1.17A) *(236)*, indicating that $Au/TiO_2(110)$ is a good model surface to represent powder Au/

TiO_2 and that the active sites and the reaction mechanism on the Au/TiO_2(110) surface might change at 320 K. Furthermore, Fujitani and Nakamura *(98)* examined the turnover frequency (TOF) for the formation of CO_2 at the two reaction temperatures as a function of the mean gold particle diameter (Figure 1.18). At 300 K, TOF-S (the TOF value calculated by

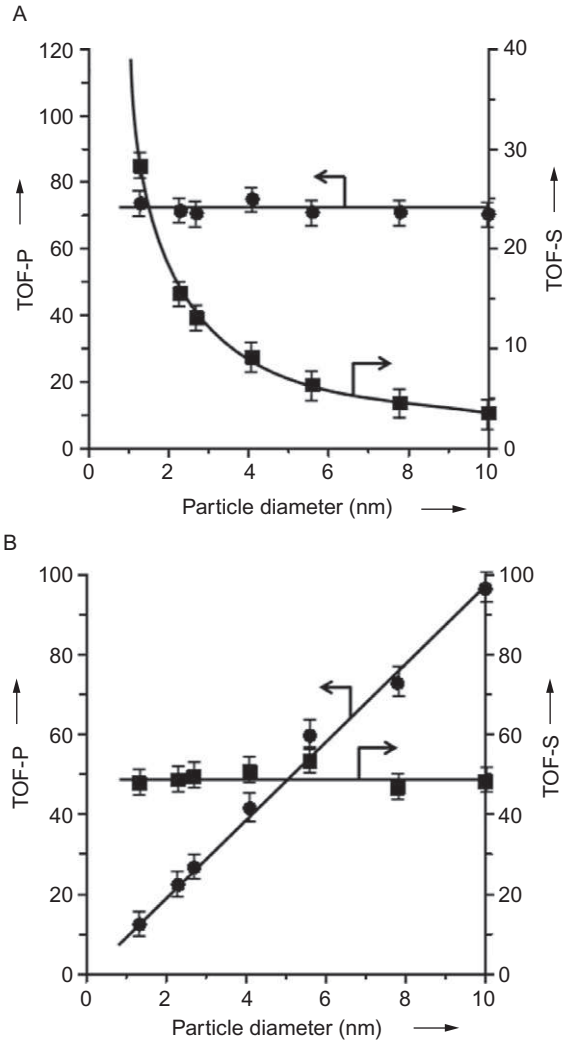

Figure 1.18 Values of TOF characterizing the formation of CO_2 on one MLE of Au/TiO_2-(110) as a function of the mean diameter of the gold particles at (A) 300 and (B) 400 K, (●) by normalizing the number of CO_2 molecules formed per second to the total number of Au atoms at the perimeter interfaces (TOF-P) and (■) by normalizing the number of CO_2 molecules formed per second to the total number of exposed Au atoms at the gold particles (TOF-S). *Published with permission from Ref.* (98).

normalizing to the total number of exposed Au atoms on the gold particles) decreased with increasing mean gold particle diameter, whereas TOF-P (calculated by normalizing to the total number of Au atoms at the perimeter interfaces) remained nearly constant regardless of the particle diameter (Figure 1.18A). These results suggest that the active sites for CO oxidation are the gold atoms located at the periphery of the gold particles attached to TiO_2. In contrast, TOF-S at 400 K remained nearly constant regardless of the mean gold particle diameter (Figure 1.18B), suggesting that the active sites for CO oxidation were newly created on the gold–metal surface at high temperature. The authors concluded that both the reaction mechanisms and the active sites differed between the low- (<320 K) and the high-temperature reaction regimes (>320 K).

4.3. Role of moisture

Fujitani and Nakamura *(98)* reported the promotional effect of moisture on the oxidation of CO in experiments done with an $Au/TiO_2(110)$ model catalyst. The rate of CO_2 formation at 300 K increased significantly with increasing H_2O partial pressure (Figure 1.19). In contrast, at 400 K, the oxidation of CO proceeded without moisture, and the rate of CO_2 formation did not

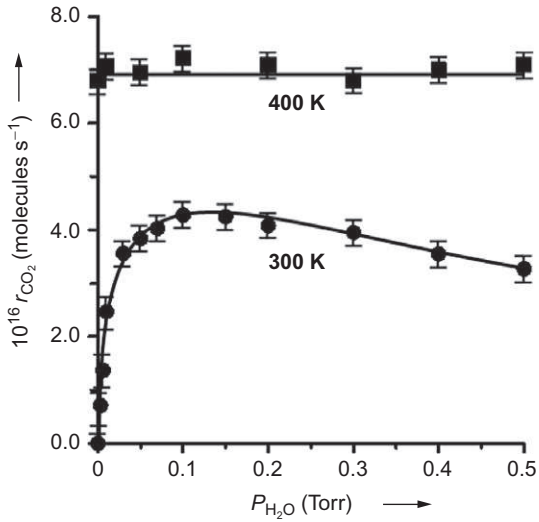

Figure 1.19 Rate of CO_2 formation (r_{CO_2}) on one MLE of $Au/TiO_2(110)$ as a function of the H_2O partial pressure at 300 (●) and 400 K (■). The oxidation of CO was performed in batch mode under 33 mbar of CO and 833 mbar of O_2. *Published with permission from Ref.* (98).

depend on the H_2O partial pressure. These results indicate that moisture promoted the oxidation of CO on the $Au/TiO_2(110)$ surface only at low temperatures, suggesting that how O_2 molecules are activated depends strongly on the reaction temperature. That is, O_2 molecules were activated directly on the $Au/TiO_2(110)$ surface at high temperatures, whereas moisture took part in the activation at low temperatures. The authors speculated that molecular oxygen is activated by the formation of hydroperoxide species, which can be produced directly from the reaction of O_2 with H_2O.

Daté and Haruta *(245)* investigated the effect of moisture in the reactant gas on CO oxidation on Au/TiO_2 at room temperature in the range of concentrations from 0.1 to 6000 ppm. Moisture enhanced the reaction rate by more than 10 times at concentrations up to 200 ppm H_2O, whereas further increases in the moisture content suppressed the reaction. The apparent activation energy was, however, found to be independent of the concentration of moisture. The amount of moisture adsorbed on the catalyst rather than the moisture content in the gas phase influences the catalytic activity, which suggests that the low-temperature CO oxidation on gold catalysts involves water-derived species on the catalyst surface. Furthermore, Daté *et al. (246)* showed that the effect of moisture depends on the type of metal oxide (TiO_2, Al_2O_3, and SiO_2). The authors proposed that moisture plays two roles in the CO oxidation reaction: the activation of oxygen molecules and the enhancement of decomposition of carbonates.

It has been reported that water reacts with oxygen atoms to form transient hydroxyls, which are directly involved in the reaction of CO oxidation on Au(111) *(156, 247)*. Kim *et al. (247)* demonstrated how CO could react with water when oxygen adatoms were present on Au(111) at 77 K. When a beam of $C^{16}O$ impinged on a 0.18 ML atomic oxygen [^{16}O]-covered surface, only mass 44 $C^{16}O_2$ was observed during the CO impingement. No formation of CO_2 was observed on Au(111) covered by 0.1 ML of isotopically labeled $H_2{}^{18}O$. When the surface was Au(111) covered with both atomic oxygen ($^{16}O_a$) and isotopically labeled water ($H_2{}^{18}O$), in addition to mass 44 $C^{16}O_2$, a small amount of mass 46 $C^{16}O^{18}O$ was observed, indicating that oxygen originating from water was directly involved in CO oxidation at 77 K on Au(111) when atomic oxygen was preadsorbed on the surface. With the same amount of preadsorbed ^{16}O on the surface, 77% more CO_2 production was observed with water added to the surface. Thus, the authors speculated that activated water or OH groups formed from water interacting with atomic oxygen on Au(111) react directly with CO to produce CO_2 on the surface. Costello *et al. (248)* proposed a model of

the active site consisting of an ensemble of metallic Au atoms and Au–OH groups for CO oxidation on Au/Al_2O_3. Tanaka *(249,250)* recently proposed that the CO reacted with the OH^- ion produced from H_2O forming the HCOO intermediate, which further reacted with OH_a to produce CO_2 at low temperature. Haruta *(122)* also claimed that OH^- species are responsible for the low-temperature CO oxidation reaction.

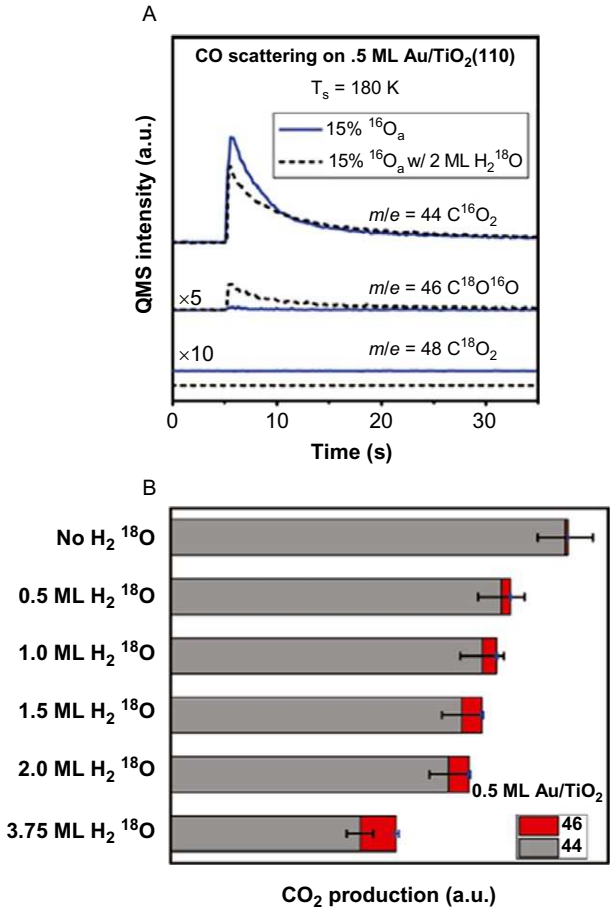

Figure 1.20 (A) Production of CO_2 in CO scattering measurements on the 0.5ML Au/TiO_2(110) surfaces at 180 K. The solid blue lines represent the reaction on the surface precovered with 15% $^{16}O_a$ only, whereas the dotted black lines show the one with 15% $^{16}O_a$ and 2.0 ML $H_2{}^{18}O$. The surface was annealed at 170 K between the oxygen and water doses. At time = 5 s, a beam of $C^{16}O$ was dosed onto the surface. (B) The bar charts represent the amount of CO_2 produced in a series of reactive scattering measurements on the 0.5 ML Au/TiO_2(110) surfaces at 180 K, precovered with (1) 15% $^{16}O_a$ only, (2) 15% $^{16}O_a$ and 0.5 ML $H_2{}^{18}O$, (3) 15% $^{16}O_a$ and 1.0 ML $H_2{}^{18}O$, (4) 15% $^{16}O_a$ and 1.5 ML $H_2{}^{18}O$, (5) 15% $^{16}O_a$ and 2.0 ML $H_2{}^{18}O$, and (6) 15% $^{16}O_a$ and 3.75 ML $H_2{}^{18}O$. *Published with permission from Ref.* (252).

In contrast, Gao *et al.* *(251)* investigated the effects of water on CO oxidation catalyzed by $Au/TiO_2/Mo(110)$ using polarization modulation infrared reflection/absorption spectroscopy. They showed that the introduction of water into the reactant mixture caused two effects: (1) a decrease in the CO coverage and (2) the appearance of a carbonate species. Since both effects inhibit CO oxidation, the promotional role of water found by previous researchers can be rationalized only by its effects on molecular oxygen adsorption and activation. It is further inferred that carbonate species first form on TiO_2 sites and then migrate to gold sites. Yan *et al.* *(252)* examined the effect of moisture on CO oxidation on $Au/TiO_2(110)$ model catalysts using TPD and molecular beam reactive scattering under UHV conditions. They observed oxygen exchange between adsorbed atomic oxygen and isotopically labeled water. Isotope experiments showed that $C^{16}O$ can be oxidized to give $C^{18}O^{16}O$ when O_a and $H_2{}^{18}O$ are coadsorbed on the $Au/TiO_2(110)$ surface (Figure 1.20A). The amount of $C^{16}O^{18}O$ produced increases with increasing water coverage; however, the total amount of CO_2 produced decreases (Figure 1.20B).

5. THEORETICAL INTERPRETATIONS AND PREDICTIONS OF CATALYSIS BY GOLD

5.1. Introduction

Various calculational methods based on theory have been applied to model gold cluster catalysts. The most frequently used methods are first-principles calculations, which are divided into density functional theory (DFT) and post-Hartree–Fock (HF) methods. Gaussian-type-orbital (GTO) and plane-wave (PW) basis sets are frequently used for these calculation methods. The various types of basis sets were selected depending on the type of the gold cluster catalyst model. Generally speaking, GTO was used for the isolated cluster model calculations and PW for the surface model calculations with a periodic boundary condition (PBC), respectively. The selection of the calculation methods is limited depending on the type of the model gold cluster catalysts. For example, hybrid DFT methods, such as B3LYP, etc. are not applicable to the surface models of gold catalysts because of the difficulty of the exact exchange integrals for these systems. Therefore, both the selection of the calculation methods and models to be investigated should be chosen to satisfy both the accuracy of the calculations and reasonableness of the computational costs.

In the following sections, topics are divided into two parts that are related to the results for the isolated models with GTO and the surface models with PBC, respectively. By the application of theoretical calculations, the origin

of the catalytic activities of gold clusters has been gradually revealed, although the models investigated are still simpler or smaller than the real systems. Because several reviews *(178,253–255)* have already appeared regarding the theoretical work on gold catalysts, this section is focused mainly on recent achievements.

5.2. Structures of isolated gold clusters

Numerous experimental and theoretical investigations of gold clusters and alloys including gold have been carried out. Schwerdtfeger *et al. (256)* estimated the minimum energy structures of small Au_n clusters ($n = 2$–20) and their electronic properties. Energetically degenerated local minimum structures of low-spin $Au_{4–20}$ clusters were elucidated by using a DFT-based genetic algorithm, as summarized in Figure 1.21. We emphasize that the 2D–3D crossover of the Au_n cluster structure occurs at $n = 11$. Truhlar *et al. (257)* investigated the

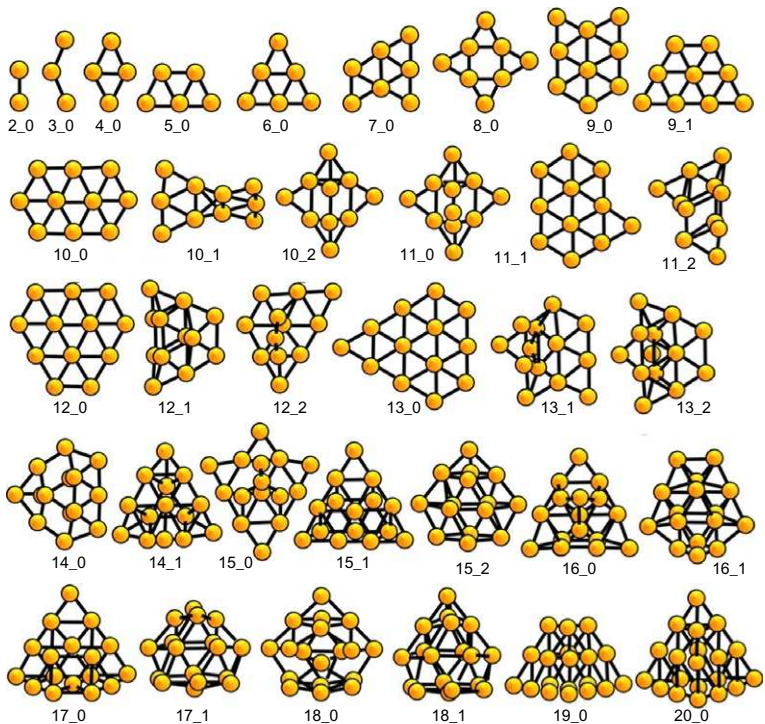

Figure 1.21 Predicted global minima and a few lowest-energy isomers of $Au_{2–20}$. The cluster *n_m* denotes the *m*th energetic isomer with *n* atoms.

validity of DFT methods such as M05, M06-L, M06, and SOGGA to predict the planar to three-dimensional structural transition in anionic gold clusters. The DFT calculations also led to the prediction that the 2D–3D transition of anionic Au_n clusters takes place between $n=11$ and $n=12$.

For the particular sizes of small clusters considered, detailed theoretical investigations were also carried out because the characteristics of these small gold clusters drastically change depending on their size. Fielicke *et al.* *(258)* investigated the structures of neutral Au_7, Au_{19}, and Au_{20} clusters and determined a two-dimensional structure for neutral Au_7 and a pyramidal structure for neutral Au_{20} by using DFT and the results of several experiments. Pal *et al.* *(259)* examined the relativistic effects on the structure and reactivity of tetrahedral Au_{19} and Au_{20} clusters by using DFT. The charge density distributions of Au_{19} and Au_{20} clusters were changed by the relativistic effect. Especially, the negative charges on site "B" Au atoms shown in Figure 1.22 are markedly increased. This effect is attributed to the geometry effect induced by the relativistic effect. In the case of the vibrational frequencies of gold clusters, it was clearly observed that the nonrelativistic calculations are not in good agreement with the experimental results, whereas the relativistic calculations coincided well with the experimental trends. Therefore, it was concluded that the properties of gold clusters are significantly affected by relativistic effects, but that the relativistic effects have no influence on the catalytic activity of the gold clusters. It was also suggested that vertex atoms were the most reactive ones in Au_{20} for a nucleophilic attack, whereas atoms connecting the missing vertex edge with the pyramid base along with the vertex atom are the most reactive ones for nucleophilic attack in Au_{19}.

The fluxionality of gold clusters is becoming an interesting topic of research owing to the energy differences among gold cluster isomers. This issue was investigated by Baiker *et al.* *(260)* by using Born–Oppenheimer

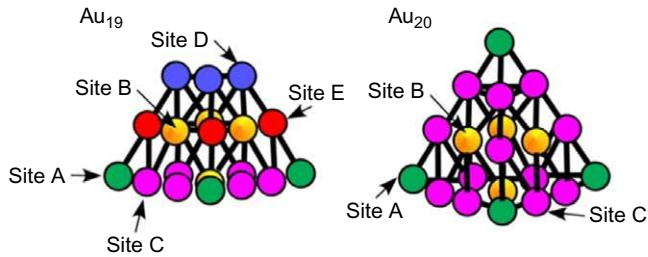

Figure 1.22 Projection views of the most stable structures of Au_{19} and Au_{20} clusters (Site A), vertex atoms (Site B), center atoms of each face (Site C), edge atoms of the pyramid base (Site D), atoms with missing vertex on the top.

ab initio molecular dynamic (BOMD) simulations. Gaussian and the plane-wave formalism were used for the BOMD simulations and for geometry optimizations. Moreover, a zero-order regular approximation relativistic calculation was used for geometry optimizations and for a study of relativistic effects on cohesion. The results of the calculations show that the dynamic behavior at 300 K of Au_n clusters is complex. In particular, Au_{12}, Au_{13}, Au_{14}, and Au_{15} clusters have marked fluxional behavior. In contrast, Au_{20} was found to be especially stable and exhibited no fluxional behavior on the time scale of the simulation.

Bimetallic clusters including gold are also interesting to investigate because, for example, AuPd alloy clusters exhibit high catalytic activities for several reactions, such as H_2O_2 synthesis from a mixture of H_2 and O_2 *(261–264)*, diesel exhaust gas treatment *(265)*, and aromatic hydrogenations *(266)*. To investigate the characteristics of bimetallic NP catalysts, their surface morphology and segregation behavior must be elucidated. Because it is too difficult to apply first-principles calculations to solve all their structures, an accurate embedded atom method potential was applied in the model calculations by Cho *et al. (267)*. The potential was parameterized on the basis of an extensive set of DFT calculations of metal clusters in addition to bulk-alloy properties. The calculations indicate almost full segregation of gold to the surface in small NPs.

5.3. Interaction between gold clusters and molecules

Different from bulk gold, nano-size gold clusters exhibit high catalytic activities. Therefore, the investigation of the interactions between molecules and gold clusters is essential for understanding the catalytic behavior of gold clusters. Kim *(268)* reported the interaction between adsorbates such as H and O_2 and anionic gold clusters. The experimental work suggested that non-dissociative adsorption of oxygen molecules on anionic gold clusters occurs, and the adsorption energies of H atoms on anionic odd-numbered Au_n clusters ($n = 3, 5, 7$) showed larger values than those of anionic even-numbered Au_n clusters ($n = 2, 4, 6, 8$). This is a typical feature of the size effect of small gold clusters that is related to the number of electrons in the clusters. A theoretical investigation characterizing this effect was reported by Taketsugu *et al. (258–267,269–272)*. The adsorption energies of O_2 on gold clusters indicated a zigzag pattern similar to that shown in Figure 1.23.

Jacob *et al. (269)* examined the adsorption of CO on charged and neutral Au and Au_2 by using both post-HF and DFT methods. The results of the

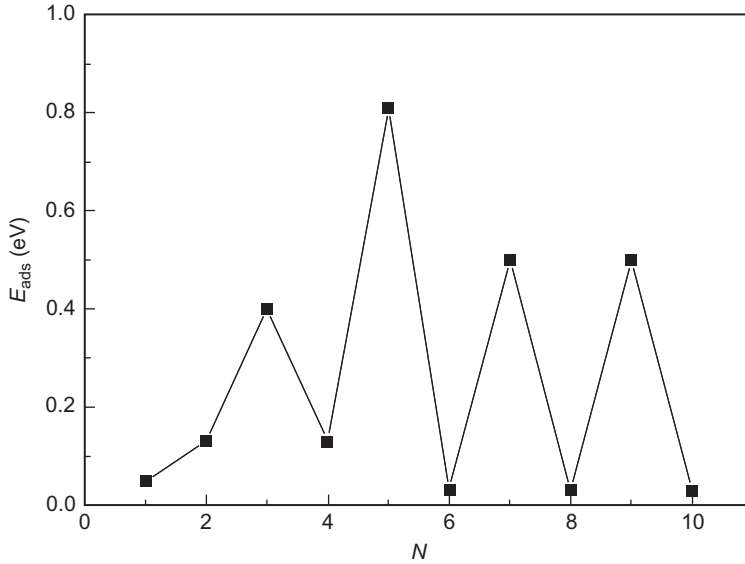

Figure 1.23 Molecular adsorption energy, $E_{ads,}$ of O_2 on the neutral Au_n clusters with $1 \leq n \leq 10$.

calculations showed that the dissociation energies decreased in the series Au^+–CO, Au–CO, and Au^-–CO as well as in the series $Au_2{}^+$–CO, Au_2–CO, and $Au_2{}^-$–CO. Furthermore, although the performance of the various density functionals applied varies widely, the B3LYP functional which includes exact exchange integrals performed reasonably well.

It is known that gold catalysts exhibit high activities for the oxidation of formaldehyde and the hydrogenation of α,β-unsaturated aldehydes *(273,274)*. These reactions involve the interactions of C—C and C—O bonds with Au atoms, the investigation of which were carried out by the Li and Kanhere groups *(270,271)*. Li *et al.* investigated the adsorption of C_2H_4 and CH_2O on Au_n clusters ($n = 1$–5) using DFT, and Kanhere *et al.* examined the interaction between acetone and Au_n clusters ($n = 2$, 3, 5, 7, 9, 13). The typical structures of Au_n–C_2H_4 and Au_n–CH_2O models ($n = 2$, 4, 5) are shown in Figure 1.24. The calculated results indicate that C_2H_4 interacts more strongly with gold clusters than CH_2O does. Ethylene and CH_2O prefer π-type interactions in which the two C atoms of C_2H_4 or the C and O atoms of CH_2O bind to a single Au atom of small gold clusters. Consequently, the population analyses indicate that the donor–acceptor interaction between reactants and gold clusters plays an important role in making both Au_n–C_2H_4 and Au_n–CH_2O complexes. Taketsugu *(272)* also

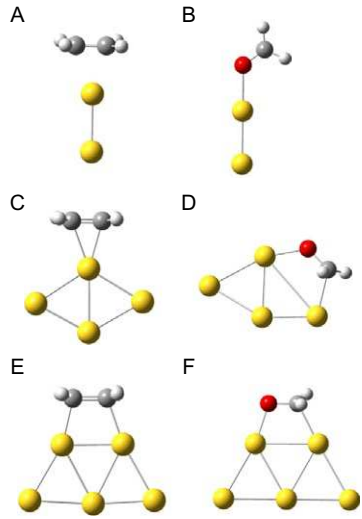

Figure 1.24 The most stable adsorption geometries of C_2H_4 and HCHO on gold clusters Au_n ($n = 2, 4, 5$) optimized at the PW91/cep-122 level.

investigated the interaction between C_2H_4 and small gold clusters and found that the interaction of C_2H_4 with Au_n clusters ($n = 1$–10) resulted in considerable weakening of the C—C double bond, and the coadsorption of O_2 and C_2H_4 on gold clusters with an odd number of atoms led to the further stabilization of the adsorbates. These results further suggested that the coadsorption of O_2 and C_2H_4 on gold clusters promoted the oxidation process via a Langmuir–Hinshelwood mechanism. These results also suggested that the donor–acceptor interaction (the charge transfer interaction) between adsorbates and gold clusters plays an important role.

This charge transfer interaction is significant in the activation of O_2 molecules on gold/PVP catalysts. Landman and Okumura *(275,276)* reported that anionic gold clusters play an important role in the activation of O_2. Okumura *(277)* also investigated the Au_{13}/PVP_n and Au_{13}–O_2/PVP_n ($n = 1, 2, 4$) models. The calculations show that the charge transfer from the adsorbed PVP to Au_{13} produces negatively charged Au_{13} clusters, and these clusters induce the generation of active O_2 on Au_{13}/PVP_4.

The quantum mechanics/molecular mechanics (QM/MM) method combines QM calculation for the active site and reactants with MM calculations for the remaining area. Therefore, a QM/MM calculation is frequently used for large-scale model systems in the GTO-based calculations. Thus, a metal cluster catalyst supported on a zeolite is a suitable system for the QM/MM

calculation. Choudury *et al.* *(278)* examined the interaction of CO with Au atoms in three different oxidation states, 0, +1, and +3, on a faujasite. The calculated results show that the gas-phase structures of Au—CO were retained on the zeolite with a slight variation in the O—C—Au angle. The CO vibrational frequency in this model exhibited a blue shift with increasing gold oxidation state. Thomson *et al.* *(279)* reported H_2 dissociation and hydrogen–deuterium exchange on four potentially active sites in TS-1 by using a QM/MM method. They found that the support effect in an Eley–Rideal mechanism (H_2 dissociation and H/D exchange reaction) was significant. In particular, the long-range interactions markedly enhanced the stability of the H—Au_3—H species formed inside the TS-1 pores.

The hydrogen dissociation on neutral and negatively charged Au_n clusters ($n = 1$–3) was investigated by using coupled cluster with single and double and perturbative triple excitations (CCSD(T)) *(280)*. The activation energies characterizing the dissociation of H_2 adsorbed on neutral Au_2 and Au_3 were found to be 1.10 and 0.59 eV, respectively. In contrast, molecular hydrogen did not form stable complexes with negatively charged Au_2 and Au_3 clusters, and the dissociation barriers for reaction of H_2 were found to be 0.93 and 1.39 eV, respectively. It is suggested that the charge density on small gold clusters plays an important role in hydrogenation reactions.

Hydrogen peroxide is a green oxidant, and its direct production from H_2 and O_2 is an important challenge in catalysis research. Theoretical investigations of the formation of hydrogen peroxide from H_2 and O_2 on small cationic, neutral, and anionic gold clusters were reported by Ding *(281)* and Thomson *(282)*. These workers found that the gold clusters were active in the peroxide formation reaction and that a hydroperoxy intermediate was the precursor in the catalytic cycle for H_2O_2 formation. These results are in good agreement with Goodman's experimental results *(283)*. Because appreciably higher catalytic performance has been reported for bimetallic (PdAu) catalysts *(264,284)*, the synergetic effect between palladium and gold should also be elucidated with theory.

5.4. Interactions between gold surfaces and molecules

To elucidate possible mechanisms of catalytic reactions, some investigations of the interactions between catalyst surfaces and oxygen atoms or molecules have been carried out by use of PW basis sets with PBC. Norskov and Mavrikakis *(285–287)* examined the adsorption and dissociation of O_2 on Au(111) and Au(211) surfaces by use of DACAPO program package and showed that steps and tensile strain substantially facilitate O_2 activation on the gold surfaces. Results, summarized in Table 1.2, indicate that the surface

Table 1.2 Energetic properties of key states along the O_2 dissociation coordinate on several static gold surfaces in Ref. *(253)*

	Calculation by PW91				Calculation by RPBE			
Gold surface	E_b^O	E_b^{IS}	E_b^{TS}	E_a	E_b^O	E_b^{IS}	E_b^{TS}	E_a
(111) unstretched	−2.54	n/a	n/a	n/a	−1.99	n/a	n/a	n/a
(111) 10% stretched	3.14	−0.08	1.29	1.37	−2.54	0.29	1.90	1.62
(211) unstretched	−2.77	−0.15	0.97	1.12	−2.27	0.20	1.65	1.44
(211) 10% stretched	−3.07	−0.26	0.37	0.63	−0.24	0.12	1.08	0.96

E_b^O, E_b^{IS}, and E_b^{TS} are the binding energies of the stable atomic oxygen state, the initial (molecular) state, and the transition state, respectively. E_a is the activation energy of O_2 dissociation. E_b and E_a have units of eV.

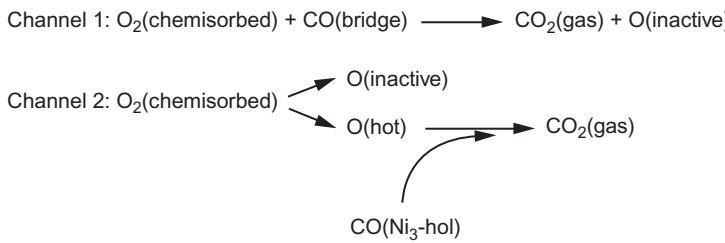

Figure 1.25 Oxidation pathways for CO_2 formation on $AuNi_3(111)$.

with stretched cell constants is characterized by higher adsorption energies of oxygen and a lower activation barrier for O_2 dissociation than the normal surface. Landmann *et al. (288)* and Mehmood *et al. (289)* also showed the importance of the kinks and steps on gold surfaces in the adsorption of O or CO. Shi and Stampfl *(290)* examined surface oxide formation on Au(111) using Vienna *ab initio* simulation package (VASP) *(291)* and advocated the possibility that a very thin surface-oxide-like structure might be present and play a role in the heterogeneous oxidation reaction on supported gold NPs. Okazaki and Kohyama *(292–294)*, using STATE program package, examined the energies and configurations of the oxygen atom adsorption on Au(100) and Au(111) as a function of coverage and found that atomic oxygen was stably adsorbed on both the (111) and the (100) surfaces at low coverages and that an oxide-like layer was formed on the (100) surface at high coverages.

Surfaces of alloy-like structures such as Au–Ni *(279)* and Au–Pd *(280,281)* have also been investigated. Wang *et al. (295)* examined CO oxidation on $AuNi_3(111)$ using STATE and found two oxidation channels, as shown in Figure 1.25. In the first channel, the adsorption of CO markedly

changes the reaction barrier. On the other hand, in the second oxidation channel, the metastable adsorption of O is more important. Yuan *et al.* *(296)* used VASP to examine CO adsorption on PdAu(111), and Ham *et al.* *(297)* examined H_2O_2 formation from H_2 and O_2 on a AuPd alloy.

The effect of water on CO oxidation is scientifically challenging and practically important. Water effects were investigated in detail by use of a specially designed ultraclean fixed-bed flow reactor *(246)*. In a complement to this experimental work, CO coadsorption with OH *(298)* and the adsorption of CO and O_2 with H_2O *(299)* were examined theoretically. In the coadsorption of CO with OH, the species COOH, HCOO, and HOCO were found to play important roles as reaction intermediates *(298)*. In the adsorption of CO and O_2 with H_2O, the adsorption states of CO, O_2, and O on the gold surfaces are stabilized by the electron transfer from H_2O to the gold surfaces *(299)*. Qian *et al.* *(300)* reported the hydroxyl-induced oxygen activation on "inert" gold NPs during low-temperature CO oxidation, assessed both experimentally and theoretically; they proposed the catalytic cycles shown in Figure 1.26.

The adsorption of molecules and atoms other than CO and O_2 has also been investigated, for example, including N *(301)*, NO *(302,303)*, and Cl *(304,305)*. Moreover, the computations were done not only for a slab but also for clusters, for example, accounting for the adsorption of acetone on gold clusters *(270)*; CO oxidation on Au_{55}, Ag_{55}, and $Au_{25}Ag_{35}$ *(306)*; CO and O_2 adsorption on Au_{32} and Au_{55} *(307)*; and selective alcohol oxidation to give aldehydes on Au(111), Au(511), Au-rods, and Au_{38} *(308)*. It is difficult to investigate the adsorption of a large molecule on gold surfaces

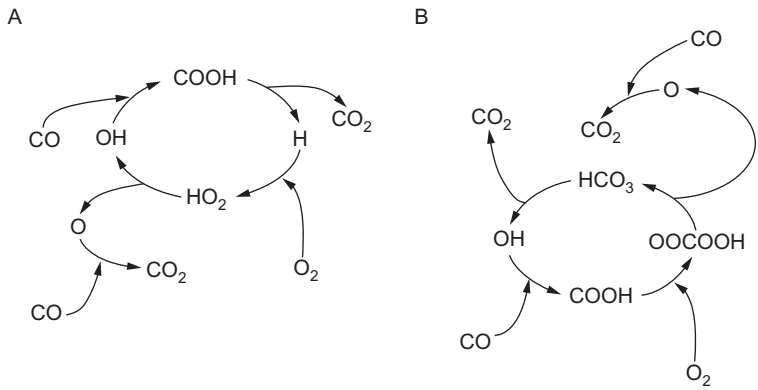

Figure 1.26 Schematic illustrations of two different surface reaction cycles: (A) dissociation of COOH (A) and (B) reaction of COOH (A) with O_2.

because it is necessary to consider long-range interactions such as those involving van der Waals forces. Raul *et al.* *(309,310)* examined the adsorption of 4,4′-diamino-*p*-terphenyl and 3,4,9,10-perylenetetracarboxylic-dianhydride on Au(111) surfaces using a semiempirical, so-called DFT-D, scheme based on the London dispersion formula to approximately account for dispersion interactions *(311)*.

5.5. Supported gold clusters

Interfacial interactions between gold NPs and supports are among the critical properties that define the catalytic activity of supported gold catalysts. Okazaki *et al.* *(60,109)* examined the dependence of the interaction between a Au atom and the stoichiometric surface of rutile TiO_2(110). The charge transfer between the Au adatom and the support was found to be negligible for the stoichiometric surface, in accordance with its smaller adhesive energy. The electron transfer occurs from the sixfold-coordinated Ti atom to the Au atom on the Ti-rich surfaces, whereas it occurs from the Au atom to the in-plane and inner oxygen atoms on the O-rich surfaces. This was the first investigation of the O-rich TiO_2(110) surface. Recently, Camellone *et al.* *(312)* examined the interaction between gold and TiO_2(110) using a Perdew–Burke–Ernzerhof+U (PBE+U) scheme. Pabisiak and Kiejna *(313–315)* examined the interaction between a gold cluster and defective rutile TiO_2(110), and Shi *et al.* *(316)* examined interactions with gold rods and rutile TiO_2(110), using VASP. Both investigations showed that the defect sites were important in the interactions between gold and TiO_2 surfaces.

Investigations of the interaction between gold and other supports *(66–68,91,317,318)* and of the interactions between other noble metals and supports *(319,320)* have also been made by a number of research groups.

Possible mechanisms of catalytic reactions on supported gold have been investigated by researchers focusing on CO oxidation on the Au/TiO_2 *(321–325)*, Au/graphene *(326,327)*, and Au/CeO_2 systems *(328)*. Borant *et al.* *(324)* examined the adsorption of CO on Au_{13}/TiO_2(110) considering various conditions of the TiO_2(110) surface and found that the adsorption energy of CO on Au_{13}/TiO_2(110) without oxygen vacancies was smallest among all the models and that on Au_{13}/TiO_2(110) with oxygen vacancies and oxygen adatoms was the largest. Zhou *et al.* *(326,327)* examined CO oxidation on metal clusters (gold or platinum) supported on grapheme. They showed that the adsorption energies of reactants and the activation energy depend on the condition of graphene, such as strain and defects. Landman *et al.* *(216)* examined the mechanisms of CO oxidation on the Au_8/MgO(001)

system, finding partial electron transfer from F-centers of MgO to the adsorbed gold clusters and inferring that such interactions affect the chemical and physical properties of the gold clusters. These results show that catalytic activities of supported gold depend strongly on the condition of the Au/support interface.

Green *et al.* *(176)* used *in situ* FTIR spectroscopy to examine the catalytically active sites for CO oxidation at temperatures as low as 100 K on the gold-rod/TiO_2(110) system. They found the following processes: (1) O_2 is captured at the perimeter site. (2) CO molecules adsorbed on TiO_2 sites are delivered to the active perimeter sites via diffusion on the TiO_2 surface. (3) CO molecules assist O—O bond dissociation and react with oxygen at perimeter sites. The authors also found that the CO molecules on the gold sites cannot approach the active perimeter sites at such a low temperature as 100 K but become more mobile and can start to actively participate in catalytic CO oxidation at room temperature.

Landman *et al.* *(299,329)* examined the effects of water on CO oxidation on free and supported gold nanoclusters. They found a significant enhancement of the binding and activation of O_2 via coadsorption of O_2 and water on small gold clusters supported on defect-free MgO(100). The binding of O_2 molecules to the Au(111) surface was also found to be enhanced by the coadsorption of O_2 and H_2O, and the reaction $H_2O + O_2 \rightarrow OOH + OH$ was found not to occur. The results illustrate a difference between the bulk gold surface and the gold cluster/support systems.

5.6. Summary

By applications of theoretical calculations, the characteristic features of supported gold catalysts have been widely investigated and the essential features of gold cluster catalysts have been gradually revealed. Specifically, the characteristics of gold clusters, O_2 activation, and H_2 dissociation on model gold clusters were investigated in detail by first-principles calculations. The theoretical work characterizing the catalytic reactions on gold surfaces and on the surfaces of models of the hetero-junction between gold clusters and metal oxide supports indicates the importance of the charge transfer between gold clusters and the support and between gold surfaces and adsorbed molecules. In particular, the charge transfer between gold clusters and supports depends on the surface conditions of the metal oxide support.

In the future, increased computing power and more reliable DFT and post-HF methods are expected to enable researchers to elucidate the reactivities and other properties of much more realistic gold cluster catalysts than have been investigated so far.

6. CATALYSIS BY GOLD WITH REACTANTS IN THE GAS PHASE

Gold catalysts have been shown to catalyze many types of reactions, including oxidation, hydrogenation, the water-gas shift, coupling reactions, etc. *(3,5,6,32,170,330–337)*. These reactions are catalyzed by gold with reactants in the liquid phase and/or in the gas phase. In this section, we focus on gas-phase reactions including selective hydrogenation of unsaturated organic compounds (alkynes, alkadienes, and unsaturated aldehydes), selective oxidation of hydrocarbons (alkanes and alkenes) and alcohols, and complete oxidation of volatile organic compounds (VOCs).

6.1. Selective hydrogenation

Selective hydrogenation of unsaturated organic compounds is important in the chemical industry, with examples including selective hydrogenation of α,β-unsaturated aldehydes to α,β-unsaturated alcohols. Conventionally, VIII–X group metals such as ruthenium, palladium, and platinum are used to catalyze this type of reaction, but only poor selectivities are obtained. In the 1970s, Bond *et al. (338)* reported that Au/boehmite catalyzes selective hydrogenation of 1,3-butadiene and of 2-butyne with a butene selectivity of 100%. However, a much lower catalytic activity was observed for Au/boehmite than for palladium and platinum catalysts, and the work failed to attract further attention. In the 1980s, gold NPs (2.0–5.0 nm in diameter) supported on metal oxides were reported to be highly active for low-temperature CO oxidation *(32,330)*. This milestone discovery ignited extensive investigations of gold catalysts for selective hydrogenation of alkynes, alkadienes, α,β-unsaturated aldehydes, CO, CO_2, etc.

6.1.1 Hydrogen dissociation

In the selective hydrogenation of unsaturated organic compounds on gold catalysts, a key step is the activation of H_2. Until now, supported gold catalysts have shown the capability to catalyze many kinds of selective hydrogenation reactions at relatively high temperatures, suggesting that supported gold catalysts can dissociate H_2. So far, three types of active sites of gold have been proposed, low-coordinated Au atoms such as those at corners and edges *(339–342)*, perimeter interfaces between gold particles and metal oxides *(97,343)*, and isolated Au cations *(28,344,345)*. Unfortunately, it is not clear yet which type of gold site is the most active.

Bus *et al.* *(339)* speculated that H_2 could be dissociatively adsorbed on gold particles supported on γ-Al_2O_3 after analyzing the data from *in situ* X-ray absorption spectroscopy, H_2 chemisorption, and H_2–D_2 exchange reaction experiments. Further analyses indicated that low-coordinated Au atoms on corners and edges of gold particles might be the active sites for H_2 dissociation. Later, theoretical calculations by Corma *et al.* *(340,341)* and Barrio *et al.* *(342)* supported this hypothesis.

On the other hand, Fujitani *et al.* *(97)* found that the H_2–D_2 exchange reaction did not take place on the single-crystal surfaces Au(111), Au(311), and TiO_2(110). However, when gold was deposited on TiO_2(110) or TiO_2 was deposited on Au(111), the H_2–D_2 exchange reaction proceeded smoothly *(97,343)*. Figure 1.27 shows that the HD formation rate on Au/TiO_2(110) increased rapidly with a decrease in the diameter of the gold particles. This result means that smaller gold particles have more active sites for H_2 dissociation than larger ones. TOF values based on the length of the perimeter interfaces between gold and TiO_2(110) were found to be independent of the gold particle size (Figure 1.27). Fujitani *et al.* *(97)* proposed that perimeter interfaces should be the active sites for H_2 dissociation.

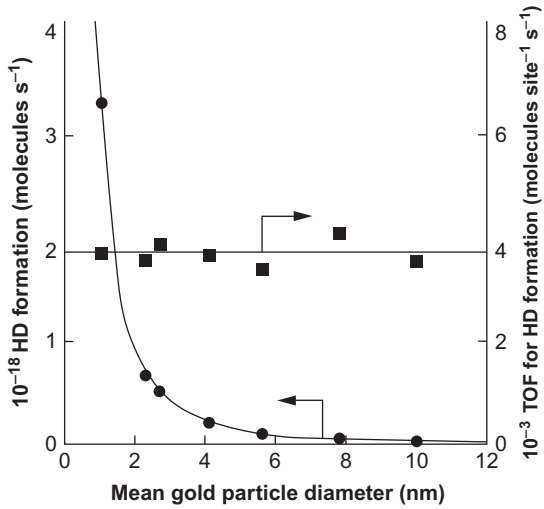

Figure 1.27 Effect of the diameter of gold particles on the rate of HD formation per a catalyst specimen and turnover frequencies (TOF) based on the length of perimeter interfaces. H_2–D_2 exchange reaction was carried out on Au/TiO_2(110) in a batch mode using a mixture of 8.0 Torr H_2 and 8.0 Torr D_2 at 425 K *(97)*.

Guzman *et al.* *(28)* observed that isolated Au^{3+} ions supported on MgO catalyzed the hydrogenation of ethylene to ethane and that the ethylene conversion decreased when isolated Au^{3+} ions aggregated to form tiny gold clusters. They proposed that isolated Au^{3+} ions were active sites for ethylene hydrogenation and for H_2 dissociation.

6.1.2 Selective hydrogenation of alkynes and alkadienes

In the polymerization of alkenes, small amounts of alkynes (or alkadienes) poison the polymerization catalysts. Therefore, selective hydrogenation of alkynes (or alkadienes) to give alkenes is important in the polymer industry. In commercial practice, supported palladium or palladium-gold catalysts are used to catalyze this reaction, but the selectivity to alkenes is not high enough. Gold catalyzes this reaction with high selectivities to alkenes, even 100%. Gold catalysts have been widely investigated for selective hydrogenation of alkynes (ethyne, propyne, and butyne) and 1,3-butdiene, etc. *(338,344–355)*.

In 2000, Jia *et al.* *(346)* reported that Au/Al_2O_3 catalyzes selective hydrogenation of ethyne to ethylene with 100% selectivity in the temperature range of 413–523 K, and 3.0-nm gold NPs were found to be the most active. In this case, the reaction temperature was critical to ethylene selectivity. When the temperature was higher than 573 K, the consecutive hydrogenation of ethylene to form to ethane took place *(346)*. Later, Choudhary *et al.* *(347)* found that the addition of a small amount of palladium to Au/TiO_2 greatly enhanced the catalytic stability in selective hydrogenation of ethyne, while maintaining the high selectivity to ethylene.

Lopez-Sanchez and Lennon *(348)* investigated Au/TiO_2 and Au/Fe_2O_3 for selective hydrogenation of propyne; 100% selectivity to propylene was achieved on Au/TiO_2, but this catalyst gradually deactivated. In the reaction with Au/Fe_2O_3, propylene selectivity and deactivation patterns were determined by catalyst pretreatment and the reaction temperature. Segura *et al.* *(349)* investigated the selective hydrogenation of propyne in the presence of propylene and found that Au/CeO_2 catalyzed this hydrogenation with a high selectivity (95%). In the 1970s, Bond *et al.* *(338)* reported that Au/boehmite catalyzed selective hydrogenation of 2-butyne to butene with 100% selectivity.

Segura *et al.* *(349)* carried out theoretical calculations to explain why gold catalysts were highly active in selective hydrogenation of alkynes to alkenes. The results showed that the adsorption of C≡C at edges and corners of gold NPs was much stronger than that of C═C. Because activation energies for

hydrogenation of C≡C and C═C are comparable to each other, this characteristic of gold favors preferential hydrogenation of alkynes to alkenes and then the desorption of the alkenes that are formed.

In the selective hydrogenation of 1,3-butadiene to butene, all three isomers are formed, 1-butene, *cis*-2-butene, and *trans*-2-butene. Gold catalysts have been widely investigated for this reaction *(338,344,345,350–355)*. Okumura *et al*. *(350)* reported that Au/Al_2O_3, Au/TiO_2, and Au/SiO_2 prepared by DP, liquid-phase grafting (LG), GG, and IMP methods catalyzed this reaction. Among these gold catalysts, Au/TiO_2 prepared by DP was the most active, characterized by a 1,3-butadiene conversion of 68.7% with a butene selectivity of 100% at 415 K and a 1,3-butadiene conversion of 98.0% with a butene selectivity of 99.7% at 456 K *(350)*. Later, Zhang *et al*. *(344)* prepared Au/ZrO_2 samples with low gold loadings (<0.1 wt%) by the DP method and investigated their catalytic activities. The results showed that 1,3-butadiene was selectively hydrogenated to butene, and no butane was produced. Further characterizations with temperature-programmed reaction (TPR) and X-ray photoelectron spectroscopy (XPS) demonstrated that the most active sites were isolated Au^{3+} ions. Recently, Zhang *et al*. *(345)* also found that isolated Au^{3+} ions immobilized on a MOF (IRMOF-3) were highly selective for hydrogenation of 1,3-butadiene to give butenes (Figure 1.28).

6.1.3 Selective hydrogenation of α,β-unsaturated aldehydes

Selective hydrogenation of α,β-unsaturated aldehydes to α,β-unsaturated alcohols is usually difficult because two requirements need to be met, preferential hydrogenation of C═O to C═C and efficient suppression of the subsequent hydrogenation of the unsaturated alcohols that are formed. Traditional catalysts such as ruthenium, palladium, and platinum favor the preferential hydrogenation of the C═C bond, and thus novel catalysts should be explored.

Significantly, gold catalysts displayed unique properties in this type of reaction *(350,356–363)*. Bailie *et al*. *(356)* found that Au/ZnO and Au/ZrO_2 prepared by CP catalyzed selective hydrogenation of crotonaldehyde to crotyl alcohol with selectivities of 54% and 51%, respectively. Modification of Au/ZnO with thiophene enhanced the crotyl alcohol selectivity from 54% to 65% *(356)*. Bailie *et al*. *(357)* found that Au/ZnO catalyzed selective hydrogenation of but-2-enal to but-2-en-1-ol. The highest selectivity to but-2-en-1-ol that was achieved was 80% with 5.0 wt% Au/ZnO, which was reduced at 673 K before reaction. Large gold NPs (10–20 nm in

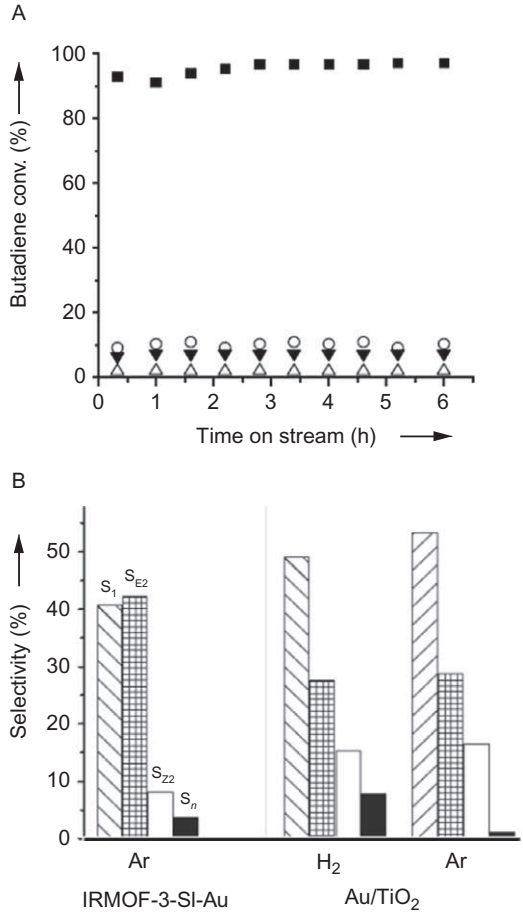

Figure 1.28 (A) 1, 3-Butadiene conversion in a flow reactor changing with time on stream and (B) product selectivity for reaction on IRMOF-3-SI (Δ), IRMOF-3-SI-Au (■), and Au/TiO_2 pretreated in flowing H_2 at 523 K (○) and argon 403 K(▼) at the reaction temperature of 403 K. S_1, S_{E2}, S_{Z2}, and S_n represent the selectivities for formation of 1-butene, *trans*-2-butene, *cis*-2-butene, and *n*-butane, respectively. *Published with permission from Ref.* (345).

diameter) were speculated to be responsible for the high selectivity for formation of but-2-en-1-ol.

Okumura *et al.* *(350)* investigated the performances of Au/Al_2O_3, Au/TiO_2, and Au/SiO_2 for selective hydrogenation of crotonaldehyde. The selective hydrogenation of the C═O group was found to be slightly sensitive to the support, and TiO_2 was found to be the most suitable one. Zanella *et al.* *(358)* investigated the effect of gold particle diameter (1.3–8.7 nm) on the catalytic performance of Au/TiO_2. The selectivity to crotyl alcohol was

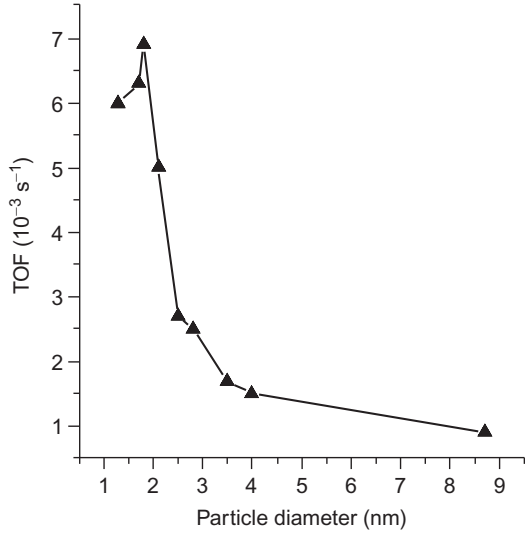

Figure 1.29 Dependence of TOF on average gold particle size in selective hydrogenation of crotonaldehyde catalyzed by Au/TiO_2 prepared by the DP method. *Published with permission from Ref.* (358).

60–70%, almost independent of the gold particle size. However, the TOF was found to depend on the gold particle size and drastically increased with a decrease in this particle size to ~2.0 nm (Figure 1.29). The authors proposed that H_2 dissociation was the rate-determining step, which took place on low-coordinated Au atoms *(358)*.

Campo *et al. (359–361)* investigated the effect of surface area of CeO_2 supports (80, 150, and 240 m^2 g^{-1}) on the catalytic performance of Au/CeO_2 in selective hydrogenation of crotonaldehyde to crotyl alcohol. Au/CeO_2-80 and Au/CeO_2-150 displayed only low selectivities to crotyl alcohol, 20–32%, whereas Au/CeO_2-240 displayed a much higher selectivity to crotyl alcohol, ~75%. Characterizations with TPR, XPS, TEM, and X-ray diffraction confirmed that the gold particles formed on CeO_2-80 and CeO_2-150 were larger than those on CeO_2-240. This comparison suggests that small gold particles favor high selectivity to crotyl alcohol.

Mohr *et al. (362,363)* investigated the performance of gold catalysts in selective hydrogenation of acrolein to allyl alcohol. They first investigated the effect of the shape of the gold particles, MTPs, and spherical particles, finding that MTPs gave a lower selectivity to allyl alcohol and a lower TOF *(362)*. Later, Mohr *et al. (16,363)* found that indium could be selectively deposited on the faces of gold NPs, with the edges and corners remaining uncovered (Figure 1.30). In the selective hydrogenation of

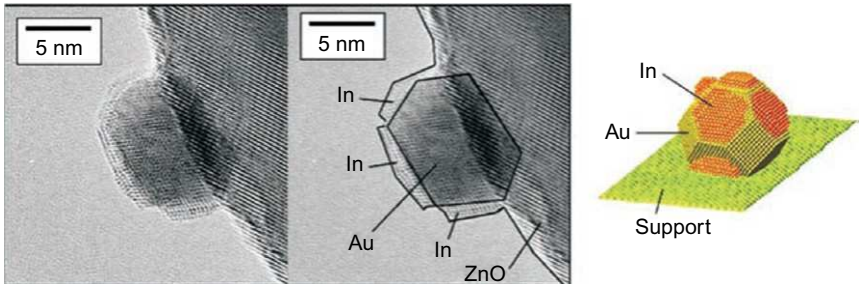

Figure 1.30 HRTEM image of Au–In/ZnO (left) and surface model (right), which was used as the catalyst for the selective hydrogenation of acrolein in the presence of gas-phase reactants *(16,363)*. Indium was preferentially deposited on faces of gold NPs and corners and edges were uncovered. *Published with permission from Ref.* (363).

acrolein Au–In/ZnO displayed a maximum selectivity to allyl alcohol exceeding 60%, whereas Au/ZnO gave a low selectivity to allyl alcohol of 34%. Because the activity as well as selectivity to allyl alcohol on monometallic indium is much lower than that on monometallic gold, it can be inferred that Au atoms on Au(111) and Au(100) faces of gold NPs were active in C═C hydrogenation to propanal, whereas Au atoms at edges and corners favored preferential hydrogenation of C═O to allyl alcohol.

6.1.4 Selective hydrogenation of CO and of CO_2

The hydrogenation of CO and of CO_2 to methanol is an important industrial process and is currently carried out with $Cu/ZnO/Al_2O_3$ catalysts. Some supported gold catalysts also catalyze this reaction *(364–369)*. Sakurai *et al. (364–366)* first reported that gold particles supported on various metal oxides, including TiO_2, Fe_2O_3, ZnO, $ZnFe_2O_4$, and $ZnO–TiO_2$, catalyze hydrogenation of CO and CO_2 to methanol. CO_2 was more easily hydrogenated to methanol than CO, and the selectivity was found to depend appreciably on the type of support. ZnO and $ZnFe_2O_4$ gave the highest selectivity (68%) to methanol, and acidic oxides such as TiO_2 gave lower selectivity (10%). The ZnO component appeared to be indispensable for methanol synthesis.

On the other hand, Vilchis-Nestor *et al. (370)* reported that gold catalysts are active for CO hydrogenation to methane. This characteristic of gold catalysts might be applied to the purification of hydrogen streams from refineries to reduce CO concentrations to extremely low levels (<50 ppm), as these are required in polyelectrolyte membrane fuel cell systems *(371,372)*.

6.2. Selective oxidation

The selective oxidation of hydrocarbons and alcohols is a profitable business owing in part to the substantial increase in the weight of the products. Oxidized products such as aldehydes, ketones, epoxides, and acids are widely used for producing polymers, surfactants, detergents, cosmetics, etc. *(373,374)*. Gold catalysts have been widely investigated for the selective oxidation of alkanes, alkenes, and alcohols with O_2 or O_2–H_2 mixture as the oxidant.

6.2.1 O_2 activation

In the selective oxidation of alkanes, alkenes, and alcohols on gold, a key step is the activation of O_2. As shown in Figure 1.31, the dissociation of O_2 to atomic oxygen requires a huge energy of 497 kJ mol^{-1}, which is even greater than the C—H bond energy (431 kJ mol^{-1}) in the most stable hydrocarbon, methane *(374)*. It is difficult to control the reactivity of atomic oxygen. Therefore, the search for suitable catalysts to efficiently lower the activation temperature of O_2 is crucial to achieve high selectivity to partially oxidized products.

O_2 activation on gold catalysts depends on the size of the gold particles. Gold clusters smaller than 2.0 nm in diameter (such as Au_{55}) deposited on inactive metal oxides such as SiO_2 and TS-1 catalyzed epoxidation of styrene in the liquid phase and epoxidation of propylene in the gas phase with O_2 as the oxidant *(332,375,376)*. This result indicates that gold clusters themselves

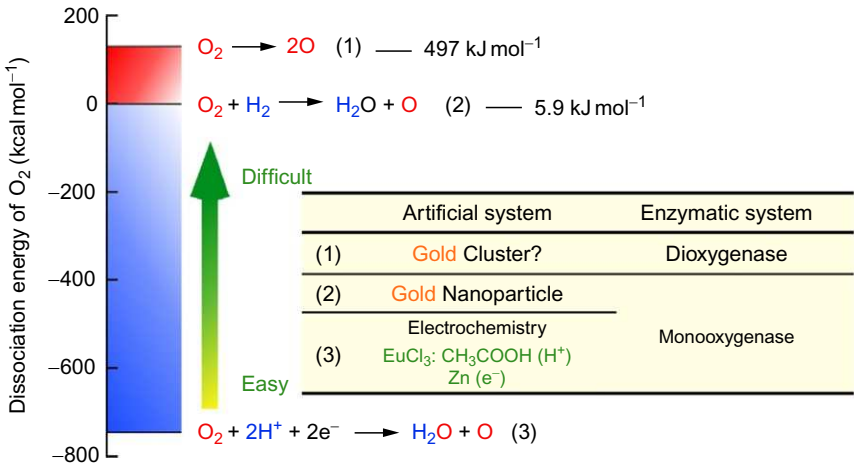

Figure 1.31 Dissociation energies of O_2 for various reactions catalyzed by artificial and enzymatic systems *(375)*.

can efficiently activate O_2. Recently, Corma *et al.* *(377,378)* used XPS, $^{16}O_2$–$^{18}O_2$ exchange reactions, and theoretical calculations to characterize their catalysts and found that gold clusters directly dissociate O_2. Moreover, the atomic oxygen that was formed catalyzed CO oxidation and styrene epoxidation. *(377)*

However, further experiments also showed that gold NPs (>2.0 nm in diameter) failed to catalyze oxidation of styrene in the liquid phase and propylene in the gas phase with O_2 as the oxidant *(332,375)*. Therefore, it is likely that gold NPs supported on inactive SiO_2 and TS-1 cannot efficiently activate O_2. So far, two routes to activation of O_2 on gold NPs have been elucidated. Route 1 involves the formation of reactive perimeter interfaces between gold NPs and suitable metal oxides, such as TiO_2, Fe_2O_3, and Co_3O_4 *(175,236)*. Oxygen can be activated at these perimeter interfaces to form negatively charged molecular oxygen. Route 2 involves the introduction of reductive reagents such as H_2 *(5)* and CO into the feed gas *(379,380)*. As shown in Figure 1.31, the addition of H_2 greatly lowers the dissociation energy of O_2 from 497 to only 5.9 kJ mol^{-1}. Indeed, in the presence of the reductant H_2 gold NPs supported on TiO_2 and on titanosilicates such as mesoporous Ti–SiO_2 and titanosilicalites efficiently catalyze the direct epoxidation of propylene with O_2 as the oxidant under relatively mild conditions *(5,381,382)*.

Tiny gold clusters have also been investigated in O_2 activation *(216,383–385)*. Yoon *et al.* *(216)* found that Au_8 clusters supported on defect-rich MgO were active for CO oxidation, whereas Au_8 clusters supported on defect-poor MgO were almost inactive. Further characterizations showed that partial electron transfer took place from defect-rich MgO to Au_8 clusters, and the negative Au_8 clusters that formed activated O_2 to give superoxo (O_2^-) species, which oxidized CO to CO_2 *(216)*. Further experiments indicated that even-numbered gold cluster anions (Au_4^- and Au_6^-) donate electrons to the $\pi^\star$ orbital of O_2 and thus activate O_2 to give superoxo species *(383)*; however, cations with even numbers of gold atoms (Au_n^+) did not activate O_2 *(384)*. Significantly, on cations with even numbers of gold atoms, the introduction of H_2 promoted O_2 activation to form hydroperoxides *(384)*.

6.2.2 Selective oxidation of alkanes

The selective oxidation of cheap and abundant light alkanes such as methane, ethane, and propane is still a challenge for both academic research and industrial application. In 1999, Kalvachev *et al.* *(386)* reported that, in the

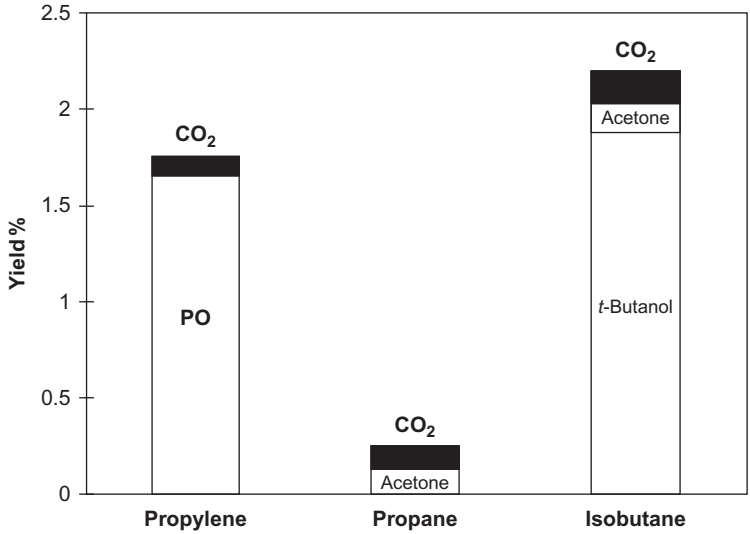

Figure 1.32 Yield of products in the oxidation of propylene at 373 K, propane at 393 K, and isobutane at 393 K on 1.20 wt% Au/Ti-MCM-41 (Ti/Si = 2.8/100) in the presence of O_2 and H_2. Reactant gases: propylene, propane, or isobutane/O_2/H_2/Ar = 1/1/1/7; space velocity, 4000 $mLg_{cat}^{-1}h^{-1}$ *(386)*.

presence of H_2, Au/Ti-MCM-41 catalyzed selective oxidation of propane and isobutane (Figure 1.32). At a temperature of 393 K, propane conversion and isobutane conversion were found to be 0.3% and 2.2%, respectively, and the selectivities to acetone and to *tert*-butyl alcohol were found to be 48% and 85%, respectively. In the reaction to form *tert*-butyl alcohol, a steady-state space time yield of $23gkg_{cat.}^{-1}h^{-1}$ was achieved. Bravo-Suárez *et al. (387,388)* reported that Au/TS-1 catalyzed selective oxidation of propane with an O_2 and H_2 mixture to give acetone and isopropanol with high selectivity (95%) at 443 K. *In situ* UV–vis spectra showed that this reaction proceeded by three steps: (1) O_2 reacted with H_2 on gold surfaces to form H_2O_2; (2) H_2O_2 was transferred from gold surfaces to neighboring isolated Ti sites to form Ti-OOH species; and (3) Ti-OOH species oxidized propane to give acetone and isopropanol.

Brávo-Suárez *et al. (389)* observed that propane epoxidation could be realized by sequential propane dehydrogenation–propylene epoxidation steps with a two-catalyst bed and O_2 and H_2 as an oxidant mixture. Propane dehydrogenation to give propylene took place on Au/TiO_2, and propylene epoxidation to give propylene oxide (PO) took place on Au/TS-1.

Lang *et al. (390,391)* inferred, on the basis of theoretical simulations and gas-phase ion-trap reaction kinetics measurements, that free (unsupported),

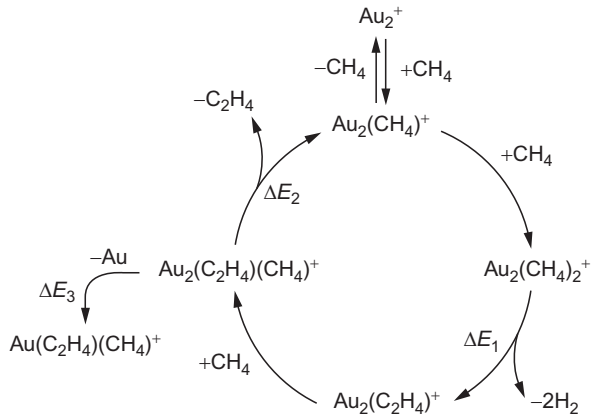

Figure 1.33 Methane activation and catalytic ethylene formation in the presence of free Au_2^+ ions. *Published with permission from Ref.* (390,391).

tiny Au_2^+ ions catalyzed the coupling of methane to ethylene (Figure 1.33). This finding suggests that gold catalysts potentially offer a capability for methane utilization—if they can be carefully optimized.

6.2.3 Epoxidation of alkenes

The epoxidation of alkenes, especially ethylene and propylene, is important in the chemical industry because epoxidized products are widely used to manufacture a variety of commodity chemicals. For example, PO is widely used for the production of propylene glycols, polyurethane, polyether polyols, and other compounds. The annual worldwide production of PO in 2007 grew at a rate more than 4.0% and amounted to about 7.5 million tons *(392)*.

Although silver catalysts have been used commercially for decades to catalyze ethylene epoxidation with O_2 alone to give ethylene oxide, these catalysts are not appropriate for propylene epoxidation with O_2 alone *(392)*. This difference in reactivity between ethylene and propylene can be explained as follows. As shown in Figure 1.34, in the propylene molecule, the allylic C—H bond is the weakest. Thus, once atomic oxygen is formed by the dissociation of O_2 on silver, it preferentially attacks the methyl groups to oxidize propylene to acrolein but not to PO. Therefore, so far, PO has been produced by an indirect route with hazardous chlorine (Cl_2) or costly hydroperoxides such as organic hydroperoxides and hydrogen peroxide (H_2O_2) as oxidants *(393–395)*. Furthermore, these processes usually require multiple reaction steps in the liquid phase. Therefore, a simple (one-step), productive (gas-phase), energy-saving (O_2 as an oxidant), and green process

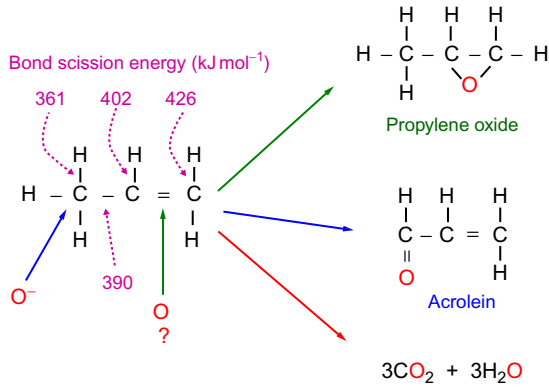

Figure 1.34 Three routes for propylene oxidation and bond scission energies in the propylene molecule *(392)*.

(not producing toxic organic wastes) is highly desired to produce PO. Gold catalysts offer good prospects, as summarized below.

6.2.3.1 Propylene epoxidation with O_2 and H_2 mixture

In 1998, Hayashi *et al. (5)* reported that in the presence of H_2 as a reductant, gold NPs supported on TiO_2 catalyze propylene epoxidation with O_2, giving a PO selectivity greater than 90%. Since then, gold catalysts have been widely investigated for the epoxidation of a variety of alkenes, including propylene, styrene, and cyclohexene *(332,375,376,379,380,396–398)*. The epoxidation of alkenes other than propylene is usually carried out with liquid-phase reactants, but only propylene epoxidation with gas-phase reactants is described here.

6.2.3.1.1 Effect of supports The reported experiments indicate that materials containing titanium should be used as supports, including TiO_2 (anatase) *(5,399–405)*, mesoporous titanosilicates (Ti–SiO_2) *(406–420)*, and microporous titanosilicalites (TS-1, TS-2, and Ti-Beta) *(381,421–431)*. The catalytic performance of gold on three representative supports, TiO_2, Ti–SiO_2, and TS-1, is shown in Table 1.3 and Figure 1.35. On 1.0 wt% Au/TiO_2, a PO selectivity of about 99% was achieved at a temperature of 323 K, although the propylene conversion was very low, only 1.1% *(5)*. Nijhuis *et al. (425)* tried to improve the catalytic performance of Au/TiO_2 by raising the temperature but failed because at a higher temperature, such as 363 K, only a poor propylene conversion of 0.3% and a poor PO selectivity of 20% were obtained. In comparison with Au/TiO_2, Au/mesoporous Ti–SiO_2 and Au/TS-1 were

Table 1.3 Effect of support and preparation method on the performances of gold catalysts in propylene epoxidation with gas-phase O_2 and H_2[a]

Support	Preparation method/gold loading (wt%)	Reaction temperature (K)	Relative $C_3H_6/O_2/H_2$/carrier gas partial pressures,[b] space velocity (mL $g_{cat.}^{-1}$ h^{-1})	C_3H_6 conversion (%)	PO selectivity (%)	PO STY ($g_{PO} kg_{cat.}^{-1} h^{-1}$)	Reference
TiO_2 (anatase)	DP/1.0	323	10/10/10/70, 4000	1.1	>99	12	*(5)*
Ti–SiO_2	DP/0.3	423	10/10/10/70, 4000	8.5	91	80	*(406)*
TS-1	DP/0.081	473	10/10/10/70, 7000	10.0	76	134	*(421)*
TiO_2 (anatase)	IMP/1.0	353	10/10/10/70, 4000	0.20	0.0	0.0	*(5)*
TS-1	Colloids/1.0	573	10/10/10/70, 7000	14.6	72	164	*(431)*
Alkali-treated TS-1	SG/0.25	473	10/10/10/70, 8000	8.8	82	137	*(422)*
Ti-MCM-48	LG/0.4	423	10/10/10/70, 4000	1.5	94	15	*(432)*

DP, deposition–precipitation; IMP, impregnation; LG, liquid grafting; SG, solid grinding.
[a]Total pressure of the reactant feed was 0.1 MPa.
[b]The carrier gas was argon, helium, or N_2.

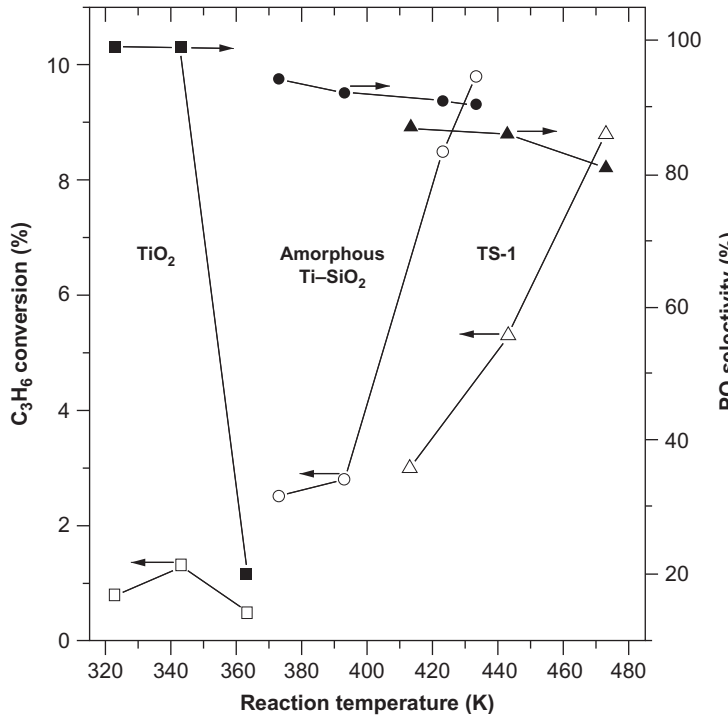

Figure 1.35 Effect of supports (TiO_2, mesoporous Ti–SiO_2, and TS-1) on the catalytic performance of gold in propylene epoxidation with O_2 and H_2 mixtures {Au/TiO_2 (□, ■), Au/mesoporous Ti–SiO_2 (○,●), and Au/TS-1 (Δ,▲)} *(392)*. Reaction conditions: feed gas, $C_3H_6/O_2/H_2/Ar$ (or He) = 1/1/1/7; space velocity, 4000 mL $g_{cat.}^{-1}h^{-1}$ (Au/TiO_2 and Au/mesoporous Ti–SiO_2) and 7000 mL $g_{cat.}^{-1}h^{-1}$ (Au/TS-1). Open symbols denote propylene conversion, and closed symbols denote PO selectivity.

characterized by greatly enhanced catalytic performance—because they could be used at much higher temperatures. For example, Chowdhury *et al. (406)* found that Au/mesoporous Ti–SiO_2 gave a propylene conversion of 8.5% and a PO selectivity of 91% at 423 K. Cumaranatunge and Delgass *(421)* observed that Au/TS-1 gave a propylene conversion of 10% with a PO selectivity of 76% at 473 K.

6.2.3.1.2 Effect of preparation methods Preparation methods are crucial to the performance of gold catalysts (Figure 1.36 and Table 1.3). As shown in Figure 1.36, when the IMP method was used, only large spherical gold particles were formed on TiO_2, resulting in propylene combustion to CO_2 and H_2O *(5)*. However, when the DP method was used, hemispherical gold NPs were formed on TiO_2, leading to high activity in PO synthesis.

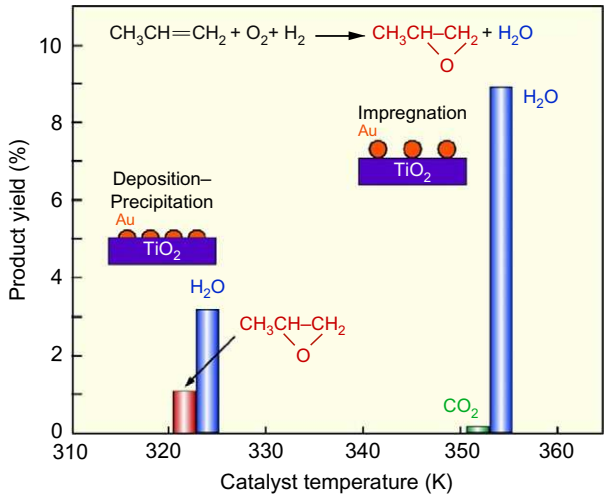

Figure 1.36 Product yields in the reaction of propylene on Au/TiO_2 catalysts prepared by various methods *(5)*. Catalyst mass, 0.5 g; feed gas composition, $C_3H_6/O_2/H_2/Ar = 10/10/10/70$; space velocity, 4000 mL $g_{cat}^{-1} h^{-1}$.

Recently, SG *(422)*, colloid immobilization *(431)*, and LG *(432)* techniques were developed to prepare active gold catalysts. By the SG method, gold clusters were deposited on alkaline-treated TS-1, and they showed high activity, with a propylene conversion of 8.8% and a PO selectivity of 82% at 473 K *(422)*. Du *et al.* *(431)* prepared highly active Au/TS-1 by colloid immobilization (the mean diameter of the gold colloids was 3.6 nm) and obtained a propylene conversion of 14.6% with a PO selectivity of 72% at 573 K.

6.2.3.1.3 Effect of gold particle size In propylene epoxidation with O_2 and H_2, the size of the gold particles markedly affects the catalytic performance. Hayashi *et al.* *(5)* found that on Au/TiO_2, gold NPs (2.0–5.0 nm in diameter) favored propylene epoxidation, whereas gold clusters (<2.0 nm in diameter) were active for propylene hydrogenation. Recently, Chen *et al.* *(433)* reported that on gold clusters supported on TiO_2, the introduction of 1.0 vol% CO to the feed gas (10% H_2, 10% O_2, and 10% propylene in helium) led to a switch from propylene hydrogenation to propylene epoxidation. Recently, Qi *et al.* *(434)* found that there was a clear gold particle size effect in the reaction of propylene with O_2 and H_2 on Au/Ti-based oxides. As shown in Figure 1.37, on gold NPs with diameters of 2.0–5.0 nm, propylene epoxidation always proceeded and PO could be produced with selectivities exceeding 90%. In contrast, on gold NPs larger than 5.0 nm in

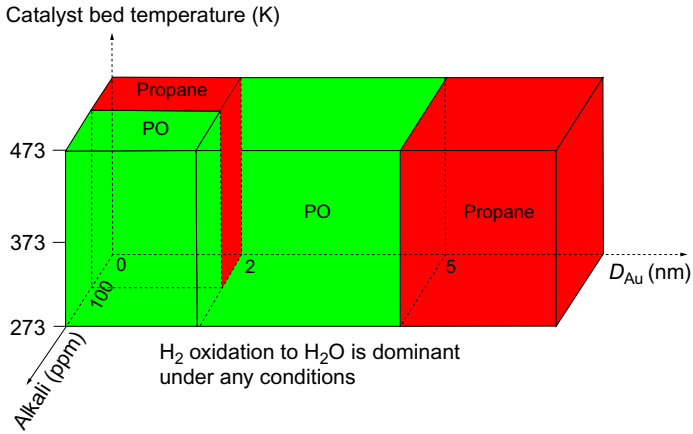

Figure 1.37 Schematic representation of the epoxidation and hydrogenation of propylene on Au/Ti-containing oxides in the presence of O_2 and H_2 *(434)*. D_{Au} is the gold particle diameter.

diameter, only propylene hydrogenation took place. On gold clusters less than 2.0 nm in diameter, both propylene epoxidation and propylene hydrogenation took place, depending on the degree of alkali contamination. A small amount of alkali in the catalyst led to a switch from propylene hydrogenation to propylene epoxidation.

For propylene epoxidation with O_2 and H_2, the most active gold particle size or size range has not yet been clarified. We observed that gold clusters that were 1.0–2.0 nm in diameter were much more active for PO synthesis than gold NPs greater than 2.0 nm in diameter *(422)*. Joshi *et al.* *(435,436)* proposed on the basis of theoretical calculations that tiny gold clusters incorporated in microporous channels of TS-1 (∼0.55 nm in diameter), such as Au_3 clusters, are highly active for PO synthesis. Recently, we used the SG method to deposit gold clusters (1.0–2.0 nm in diameter) selectively on the exterior surfaces of TS-1-Na1 and the DP method to deposit gold clusters (1.0–2.0 nm in diameter) and tiny clusters (<0.55 nm in diameter) on the exterior surfaces and into the microporous channels of TS-1-Na1, respectively *(437)*. A PO formation rate of $74 g_{PO} kg_{cat.}{}^{-1} h^{-1}$ was obtained on Au/TS-1-Na1(DP), whereas a much higher PO formation rate of $127 g_{PO} kg_{cat.}{}^{-1} h^{-1}$ was achieved on Au/TS-1-Na1(SG). Because the only difference between the two gold catalysts was the location of the gold clusters, it was clear that gold clusters 1.0–2.0 nm in diameter on the exterior surface of TS-1-Na1 are more active for PO synthesis than tiny gold clusters

(<0.55 nm in diameter) inside the microporous channels of TS-1-Na1 (Figure 1.38).

6.2.3.1.4 Reaction mechanism Recent theoretical calculations *(435,436)*, *in situ* UV–vis spectra *(407,413)*, and *in situ* XANES spectra *(407)* confirmed that Ti-OOH species were indeed the reaction intermediates in propylene epoxidation with O_2 and H_2 mixtures. Bravo-Suárez *et al.* *(407)* proposed a possible mechanism for this reaction (Figure 1.39),

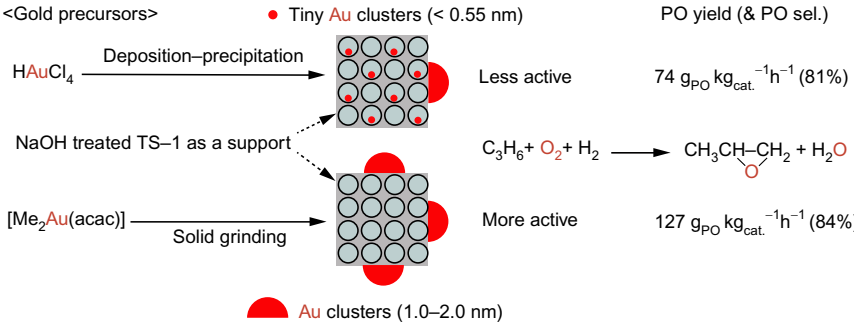

Figure 1.38 The most active gold sites in propylene epoxidation on Au/TS-1 catalysts *(437)*.

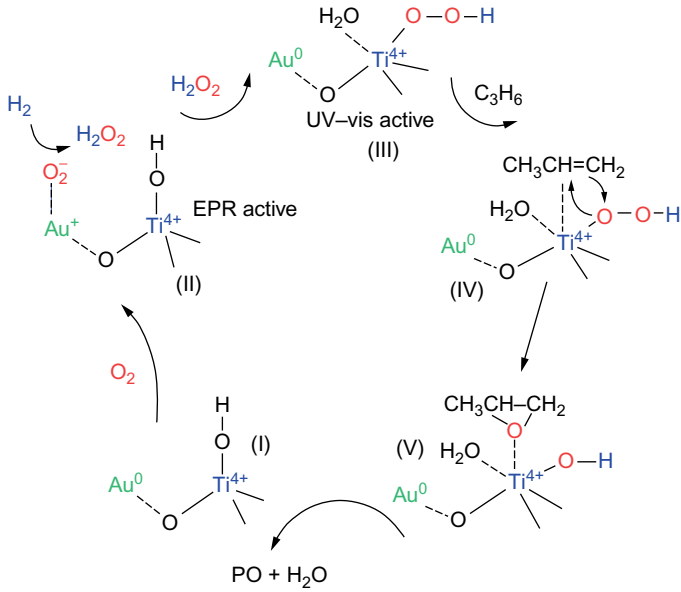

Figure 1.39 A possible sequence of steps for propylene epoxidation with O_2 and H_2 on Au/titanosilicates *(407)*.

consisting of three key steps: (1) O_2 reacted with H_2 on gold surfaces to form H_2O_2; (2) the H_2O_2 that formed was transferred from gold surfaces to neighboring isolated Ti sites to form Ti-OOH species; and (3) the Ti-OOH species epoxidized propylene to give PO.

6.2.3.2 Propylene epoxidation with O_2 alone

Although gold supported on materials containing titanium can catalyze propylene epoxidation with O_2 and H_2, its capability in epoxidizing propylene with O_2 alone has been only seldom reported. A few recent papers concerned with gold catalysts reported propylene epoxidation with O_2 alone when the gold particle size was carefully controlled *(375,376)*. Ojeda and Iglesia *(438)* reported that Au/TiO_2 catalyzed propylene epoxidation with $O_2 + H_2O$, giving a PO selectivity of 20–70%. However, the propylene conversion was lower than 0.1%. Lee *et al.* *(376)* reported that Au_{6-10} clusters deposited on amorphous Al_2O_3 catalyzed propylene conversion with O_2 alone, giving a PO selectivity of ~33.3%. Significantly, when some water was introduced into the feed gas, the PO selectivity was remarkably enhanced to values greater than 90% *(376)*.

Gold clusters (1.0–2.0 nm in diameter) were deposited by the SG method on alkali-treated TS-1 and used to catalyze propylene epoxidation with O_2 alone with a small amount of water (~2.0 vol%) introduced into the feed gas. A PO selectivity of 52% and a propylene conversion of 0.88% were achieved *(375)*. When water was absent from the feed gas, PO could not be produced at all, and CO_2 was formed as the main product (Figure 1.40).

In situ UV–vis spectroscopy was used to explore the mechanism of propylene epoxidation with $O_2 + H_2O$ *(375)*. The results showed that Ti-OOH species could be formed when $O_2 + H_2O$ passed through a bed of gold catalyst, and the intensity of a band indicating Ti-OOH species increased gradually with time on stream for about 100 min and then leveled off (Figure 1.41). After the introduction of propylene to the feed gas, the intensity of the band decreased gradually. These results indicate that the Ti-OOH species were consumed to produce PO and that the rate of consumption of the Ti-OOH species was more rapid than the rate of their formation. Once water had been removed from the feed gas, the intensity of the band characterizing the Ti-OOH species decreased quickly, a result that strongly suggests that H_2O was indispensable for the formation of the Ti-OOH species.

A plausible reaction pathway was proposed for PO formation (Figure 1.42) *(375)*. First, O_2 reacts with H_2O on the gold clusters to form

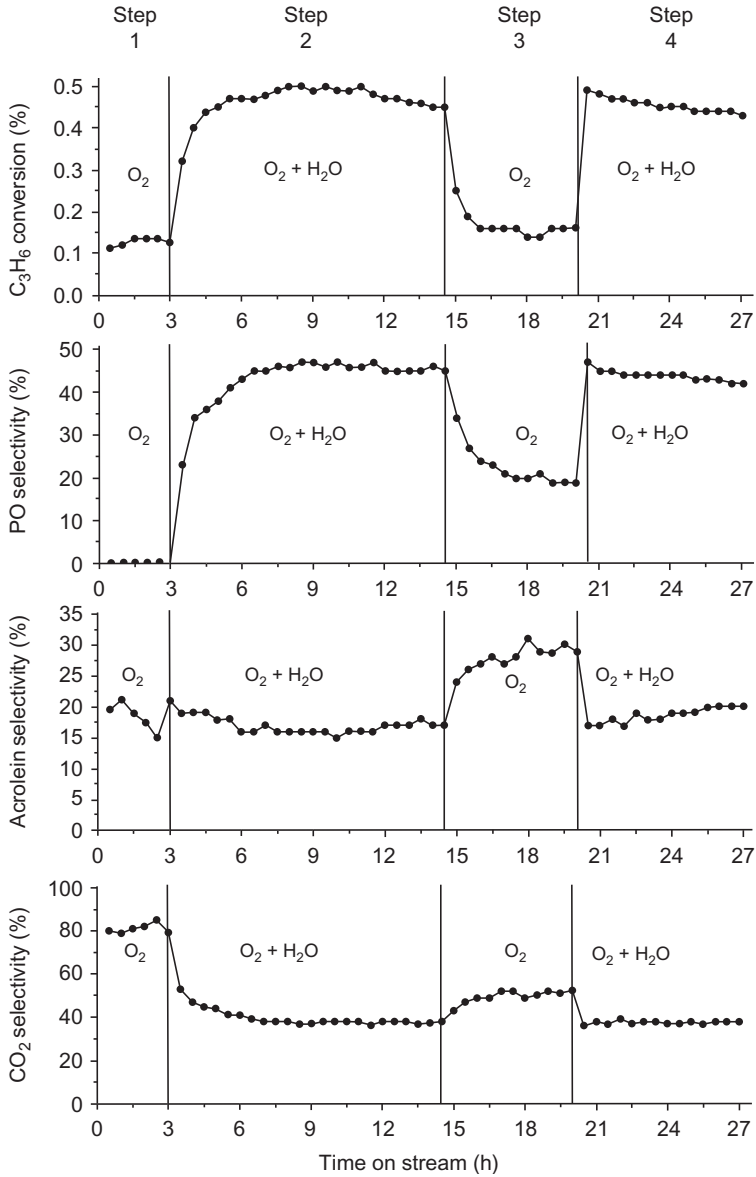

Figure 1.40 Enhancing effect of H_2O on propylene epoxidation with O_2 on 0.10 wt%Au/alkali-treated TS-1. Reaction conditions: temperature 473 K; feed gas composition $C_3H_6/O_2/Ar = 10/10/80$ or $C_3H_6/O_2/H_2O/Ar = 10/10/2/78$; space velocity 4000 mL $g_{cat.}^{-1} h^{-1}$ *(375)*.

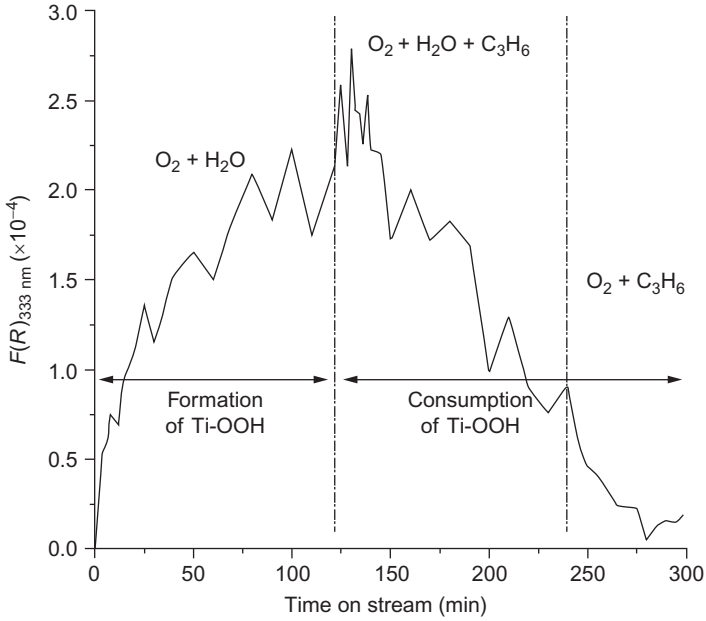

Figure 1.41 Intensity of UV–vis peak at 333 nm (assigned to Ti-OOH) measured under *in situ* conditions with various feed gas compositions characterizing reaction on 0.19 wt% Au/alkaline-treated TS-1. Reaction conditions: catalyst mass, 40 mg; temperature, 473 K; feed flow rate, 20 mL min^{-1}; space velocity, 30000 mL $g_{cat.}{}^{-1}h^{-1}$ *(375)*.

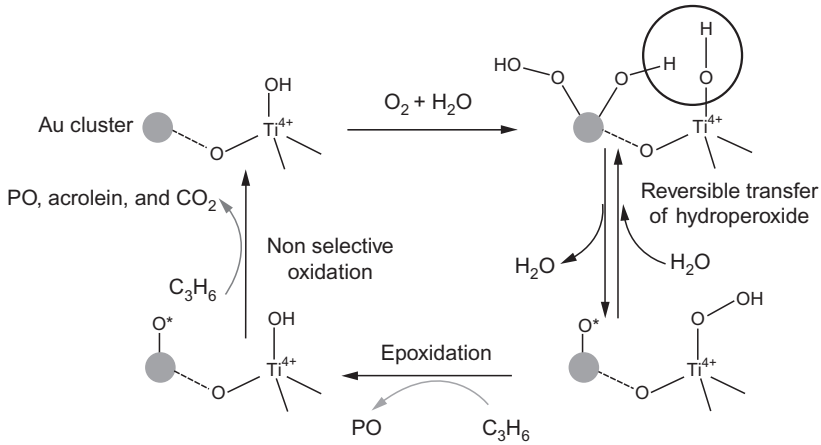

Figure 1.42 A possible pathway for propylene epoxidation with O_2 and H_2O on Au/alkaline-treated TS-1 *(375)*.

$^{\bullet}$OOH species. Then the $^{\bullet}$OOH species are reversibly transferred from the surfaces of the gold clusters to neighboring Ti sites to form Ti-OOH species, which epoxidize propylene to PO. It is possible that some $O^{\bullet}$ radicals would be co-produced, which would oxidize propylene to PO, acrolein, and CO_2. Accordingly, if we could control the reactivity of these $O^{\bullet}$ radicals, the PO selectivity could be greatly improved. Recent theoretical calculations also confirm that on gold clusters such as Au_{10} and Au_{38}, O_2 reacts with H_2O to form $^{\cdot}$OOH species, which are responsible for PO formation *(439)*.

6.2.4 Selective oxidation of alcohols

Selective oxidation of alcohols to the corresponding aldehydes, ketones, and acids is a key step numerous organic syntheses. Most of these reactions have been carried out in the liquid phase and only a few in the gas phase *(440–447)*. Rossi *et al*. *(440)* first reported that supported gold catalysts catalyze the selective oxidation of ethanol to acetaldehyde with the reactants in the gas phase. Later, Biella and Rossi *(441)* found that Au/SiO_2 catalyzes selective oxidation of some primary and secondary aliphatic alcohols with air to give the corresponding aldehydes and ketones, such as 1-propanol, 2-propanol, 1-butanol, 1-pentanol, etc.

Zheng and Stucky *(442)* investigated the effect of gold particle sizes on the selective oxidation of ethanol on Au/SiO_2. As shown in Figure 1.43, 6.3-nm-diameter gold NPs supported on SiO_2 gave the highest conversion of ethanol, 45% at 473 K, and smaller gold NPs (3.5 nm in diameter) and larger gold NPs (8.2 nm in diameter) gave lower conversions of ethanol, 24% and 22%, respectively. However, a different trend was observed for acetaldehyde selectivity: the 3.5-nm-diameter and 8.2-nm-diameter gold NPs gave slightly higher acetaldehyde selectivities of ~90% relative to the value of 75% observed with the 6.3-nm-diameter gold NPs. When the reaction temperature was lowered from 473 to 373 K, the 6.3-nm-diameter gold NPs selectivity produced ethyl acetate as the main product instead of acetaldehyde; the ethyl acetate selectivities were 86% and greater.

Takei *et al*. *(443)* extensively investigated the selective oxidation of ethanol on gold catalysts, with the reactant in the gas phase; the authors screened 23 kinds of metal oxides as supports. Mild oxidation of ethanol to acetaldehyde took place on gold NPs supported on inert metal oxides such as strongly acidic MoO_3 or weakly basic La_2O_3. Deep oxidation of ethanol to acetic acid proceeded on gold NPs deposited on n-type semiconductor metal oxides such as ZnO and V_2O_5. Complete oxidation of ethanol to CO_2 and H_2O took place on p-type semiconductor metal oxides such as

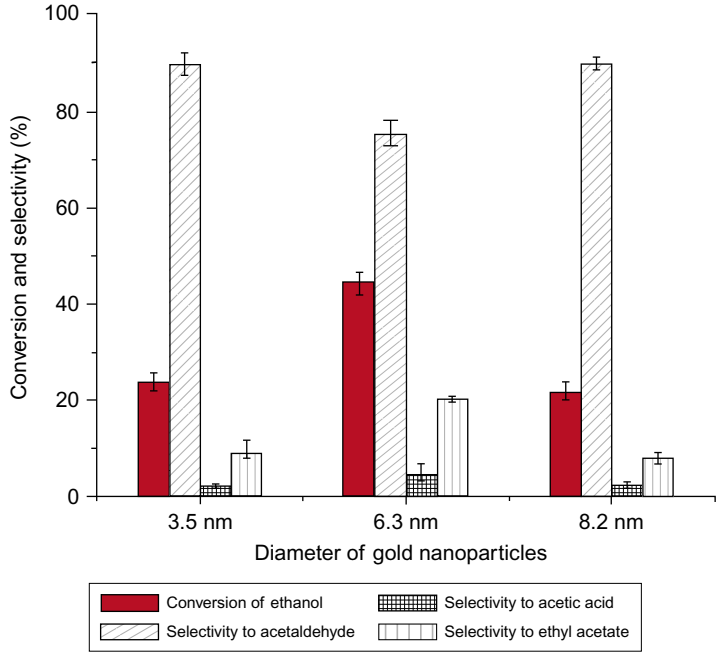

Figure 1.43 Gold particle size-dependent catalysis of ethanol oxidation by O_2 on 0.5 wt% Au/SiO_2 at 473 K. The sizes of the gold NPs were 3.5, 6.3, and 8.2 nm. Catalyst mass, 1.0 g; ethanol feed flow rate, 0.6 mL h^{-1}; O_2 feed flow rate, 10 mL min^{-1} (*no N_2 was fed*). *Published with permission from Ref.* (442).

MnO_2, Co_3O_4, and CeO_2. The tunability of product selectivity over a wide range was explained by the structures of adsorbed ethanol and by the reactivities of oxygen species present on the metal oxide supports (Figure 1.44).

Recently, Wittstock *et al.* *(444)* reported that nanoporous gold, prepared by the dealloying of Au–Ag alloys, catalyzed selective oxidative coupling of methanol to methyl formate with a selectivity of 97% at 353 K (Figure 1.45). In this reaction, the residual amount of silver in nanoporous gold was crucial to the selectivity for methyl formate formation. When the silver loading was increased from <1.0 to 2.5 atom%, the selectivity to methyl formate at 353 K decreased from 97% to 67%. When the silver loading was further increased to 10 atom%, no methyl formate was produced at all at 353 K, and the only product was CO_2.

Han *et al.* *(445)* investigated the catalytic properties of nanoporous gold for selective oxidation of benzyl alcohol, which was present in the gas phase. At a temperature of 513 K, a benzyl alcohol conversion exceeding 61% was achieved with a benzaldehyde selectivity of 95%.

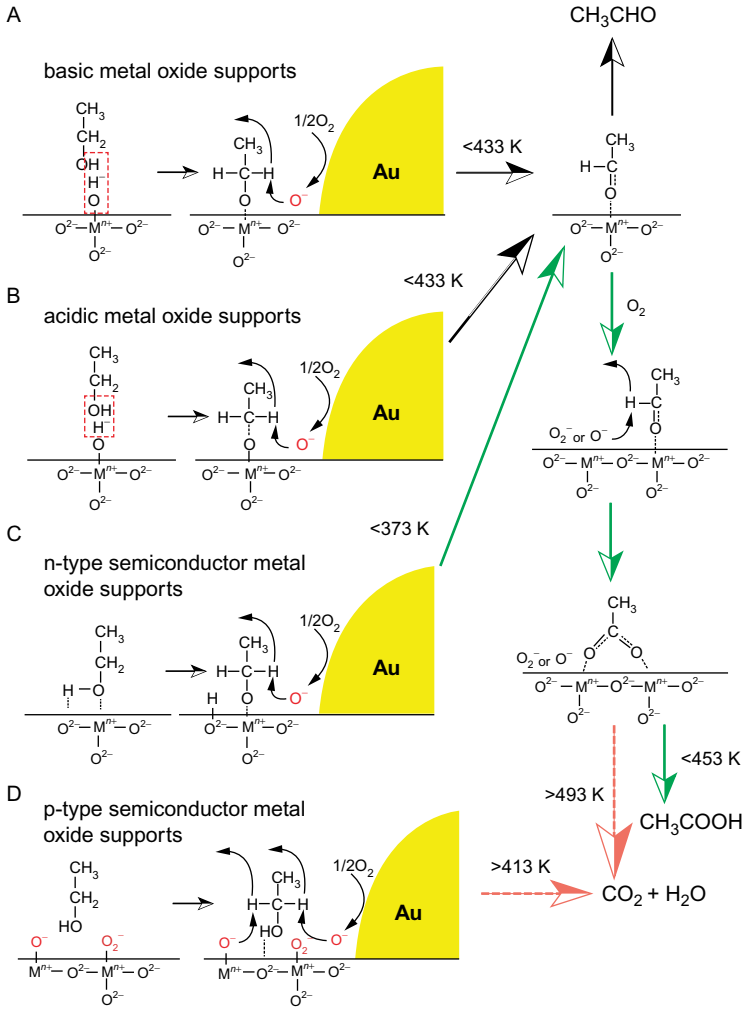

Figure 1.44 Probable routes for the formation of surface ethoxide from ethanol and its transformation to acetaldehyde, acetic acid, and CO_2 on supported gold catalysts *(443)*.

6.3. Complete oxidation

VOCs are produced mainly by industrial plants and motor vehicles; they are usually harmful to human health, and they also promote the formation of ozone and smog *(448,449)*. Therefore, processes for the efficient removal of VOCs have long been sought. Among the potential technologies for VOCs removal, catalytic combustion is preferred because it can be carried

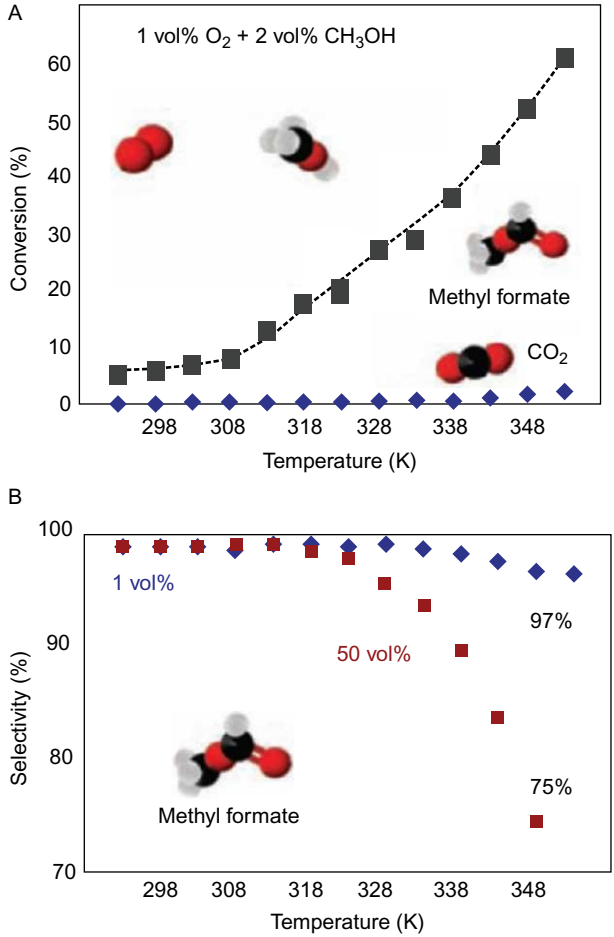

Figure 1.45 Effect of reaction temperature on methanol conversion (A) and methyl formate selectivity (B) in catalytic oxidation of methanol on nanoporous gold. *Published with permission from Ref.* (444). Reaction conditions: 0.1 mg of nanoporous gold contaminated with a small amount of Ag (<1.0 atom%); gas feed flow rate, 50 mL min^{-1}. (A) Feed gas, 1.0 vol% O_2 plus 2.0 vol% CH_3OH; CO_2, blue rhombuses; methyl formate, gray squares. (B) Feed gas, 1.0 vol% O_2 plus 2.0 vol% CH_3OH (blue rhombuses); 50 vol% O_2 plus 2.0 vol% CH_3OH (red squares).

out at relatively low temperatures and thus suppress the emission of NO_x *(450–453)*. The catalysts used for combustion of VOCs are usually supported noble metals (palladium and platinum). Because gold NPs supported on base metal oxides are highly active for low-temperature CO oxidation *(32,330)*, they have been tested for the combustion of VOCs such as formaldehyde and ethylene (Table 1.4).

Table 1.4 The combustion of formaldehyde and ethylene on gold catalysts

Catalyst	Calcination temperature (K)[a]	Gold content[b] (wt%)	Gold particle diameter (nm)	VOC/ concentration (ppm)	T_x (K)[c] or x (%) (T, K)[d]	SV[e] (mL $g_{cat.}^{-1}$ h^{-1})	Reference
Au/α-Fe_2O_3	673	1.0	3.6	HCHO, 5000	356 (T_{50})[c]	20,000	*(454)*
Au/FeO_x	473	7.1	10–15	HCHO, 4.7	353 (T_{100})[c]	54,000	*(455)*
Au/TiO_2	473	2.0	~5.0	HCHO[f]	503 (T_{100})[c]	–	*(456)*
Au/CeO_2	473	2.0	–	HCHO[f]	353 (T_{100})[c]	–	*(456)*
Au/CeO_2	473	0.56	~5.0	HCHO, 600	346 (T_{100})[c]	66,000	*(457)*
Au/CeO_2	573	3.0	2.0–4.0	HCHO, 500	323 (T_{100})[c]	120,000	*(458)*
Cu–Mn oxide (Hopcalite)	573	–	–	C_2H_4, 1800	50% (454)[d]	16,000	*(459)*
Au/Co_3O_4	673	1.0	4.0–5.0	C_2H_4, 10000	50% (~443)[d]	6000	*(460)*
Au/Fe_2O_3	673	2.0	<5.0	C_2H_4, 1050	3.4% (293)[d]	4000	*(461)*
Au/TiO_2	673	2.0	<5.0	C_2H_4, 1050	0.0% (293)[d]	4000	*(461)*
Au/Co_3O_4	673	2.0	<5.0	C_2H_4, 1050	7.4% (293)[d]	4000	*(461)*
Au/mesoporous Co_3O_4	573	2.5	<5.0	C_2H_4, 50	76% (273)[d]	14,400	*(462)*
Au/Co_3O_4 nanorods	523	2.0	3.0–3.5	C_2H_4, 50	94% (273)[d]	9000	*(463)*
Au/Co_3O_4 nanopolyhedra	523	1.9	3.0–3.5	C_2H_4, 50	86% (273)[d]	9000	*(463)*
Au/Co_3O_4 nanocubes	523	2.0	3.0–3.5	C_2H_4, 50	27% (273)[d]	9000	*(463)*

[a]Calcined in air.
[b]Gold loading.
[c]T_x means the temperature required to achieve x% conversion of HCHO.
[d]Ethylene conversion of x% obtained at the reaction temperature of T (K).
[e]SV, space velocity.
[f]Air was passed through HCHO liquid at 273 K.

6.3.1 Formaldehyde

Formaldehyde (HCHO) is a typical hazardous indoor air pollutant and is usually considered as a carcinogen. Even an indoor concentration of HCHO as low as a few parts per million is seriously harmful to human health after long exposure times *(464)*. Accordingly, the catalytic oxidation of HCHO at room temperature has been a great concern. In 1996, Haruta *et al. (454)* reported that Au/α-Fe_2O_3 exhibited catalytic activity comparable to that of Pd/γ-Al_2O_3 and Pt/γ-Al_2O_3, giving a conversion of 50% at $\sim$356 K. Later, various types of gold catalysts were used to catalyze HCHO combustion; the catalysts included Au/TiO_2 *(456)*, Au/CeO_2 *(456–458,465)*, and Au/FeO_x *(455)*. Among the catalysts investigated, Au/CeO_2 displayed the best catalytic performance. In 2005, Jia *et al. (456)* reported that at 353 K, Au/CeO_2 gave 100% conversion of HCHO. To improve the catalytic performance of Au/CeO_2, several groups continued to modify the CeO_2 supports. Zhang *et al. (457)* synthesized three-dimensionally ordered macroporous (3DOM) CeO_2 with controlled pore sizes by a colloidal crystal template method and found that Au/3DOM-CeO_2 had an improved catalytic activity, with a 100% conversion of HCHO at $\sim$348 K. Lu *et al. (458)* prepared high-surface-area CeO_2 with a surfactant template (dodecyl sodium sulfate) and found that the catalytic activity of the resultant Au/CeO_2 was greatly enhanced as a result of the increased surface area of the CeO_2. The best catalytic activity was achieved with Au/CeO_2-270, which had the highest CeO_2 surface area, 270 $m^2\ g^{-1}$; it gave a 100% conversion of HCHO at only 323 K. Zhu *et al. (466)* reported that HCHO combustion on gold catalysts proceeded at room temperature when irradiated with visible light including red light at a wavelength of 600–700 nm and blue light at a wavelength of 400–500 nm (Figure 1.46). This discovery may be of substantial benefit for alleviation of indoor HCHO.

6.3.2 Ethylene

Ethylene is one of the harmful VOCs because it enhances photochemical pollution and because it accelerates the spoilage of fruits and vegetables. Fruits and vegetables release ethylene during storage, and this ethylene in turn accelerates the maturing and then the spoilage of fruits and vegetables. A key to maintaining the freshness of fruits and vegetables is to efficiently remove the released ethylene. Although ethylene combustion is favored thermodynamically, it has been difficult to carry out this reaction at or below room temperature because ethylene has a strong C=C double bond.

Li *et al. (459)* reported that mesoporous Cu–Mn hopcalite catalyzed ethylene combustion but at relatively high temperatures (>473 K). Because

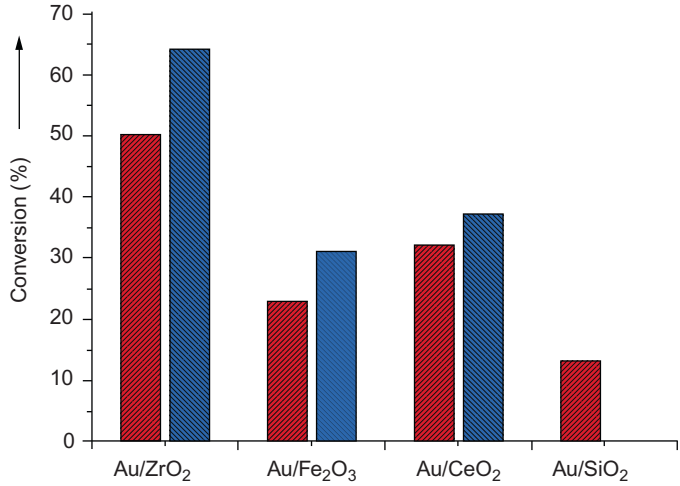

Figure 1.46 Formaldehyde combustion on gold catalysts by virtue of irradiation with blue light (blue or light grey bars) and red light (red or dark grey bars) (the blue or light grey bar for Au/SiO_2 was not shown in the original paper). *Published with permission from Ref.* (466).

fruits and vegetables are usually stored in refrigerated warehouses at temperatures of 273–293 K, novel catalysts have long been desired to work in this temperature range.

In 2006, Jin *et al.* *(460)* reported that gold catalyzed ethylene combustion to CO_2 and H_2O at 463 K. Later, Hao *et al.* *(461)* investigated the effect of supports (Fe_2O_3, Co_3O_4, TiO_2, and ZnO) on ethylene combustion catalyzed by gold and found that Au/Co_3O_4 was the most active, giving an ethylene conversion of 7.4% at 293 K and 100% at 433 K. In an investigation of the effect of the morphology of Co_3O_4 on the catalytic activity of Au/Co_3O_4 *(462,463)*, Au/mesoporous Co_3O_4 was found to be significantly more active than Au/Co_3O_4 nanosheets at 273 K, giving ethylene conversions of 76% and 7.4%, respectively *(462)*. HRTEM indicated that the exposed reactive {110} facets in mesoporous Co_3O_4 were responsible for the excellent performance of Au/mesoporous Co_3O_4. Further research results showed that Au/Co_3O_4 nanorods were more active than Au/Co_3O_4 nanopolyhedra and Au/Co_3O_4 nanocubes at 273 K, giving ethylene conversions of 94%, 86%, and 27%, respectively *(463)*. HRTEM images showed that Co_3O_4 nanorods selectively exposed {110} planes, whereas Co_3O_4 nanopolyhedra and Co_3O_4 nanocubes exposed predominantly {011} and {001} planes, respectively.

6.3.3 Other VOCs

Gold catalysts have also been used to catalyze the combustion of other VOCs, such as propylene, propane, methane, toluene, and 2-propanol (Table 1.5) *(467–477)*. Among them, propylene is often chosen as a model VOC molecule. Delannoy *et al. (468)* investigated the effect of supports (Al_2O_3, TiO_2, and CeO_2) and found that CeO_2 was the best. At ~448 K, 4.0 wt% Au/CeO_2 completely oxidized propylene at a concentration of 1200 ppm to give CO_2 and H_2O. Furthermore, the authors found that on Au/CeO_2 metallic gold was much more active than cationic gold species. Lakshmanan *et al. (469)* observed that the doping of Al_2O_3 with CeO_2 before gold deposition greatly enhanced the catalytic performance of Au/Al_2O_3 in propylene combustion. Gluhoi *et al. (470)* also found that the doping of Al_2O_3 with MO_x (M = Ce, Mn, Co, Fe) greatly enhanced the catalytic performance of Au/Al_2O_3. The promotion effect of these MO_x species on Au/Al_2O_3 follows this order: $CeO_x > FeO_x > MnO_x > CoO_x$, giving temperatures for 95% conversion of 497, 546, 567, and 592 K, respectively. TEM characterizations showed that the presence of CeO_x stabilized gold particles against sintering. Moreover, Gluhoi *et al. (473)* observed that the addition of alkali (or alkaline earth) metal oxides (MO_x, with M = Li, Rb, Mg, or Ba) was beneficial to the performance of Au/Al_2O_3 in the complete oxidation of propylene. The researchers suggested that the introduction of MO_x stabilized small gold particles against sintering.

Gluhoi *et al. (471)* also investigated the combustion of propylene and propane on Au/Al_2O_3, $Au/CuO–Al_2O_3$, $Au/Co_3O_4–Al_2O_3$, and Pt/Al_2O_3. In propylene combustion, $Au/CuO–Al_2O_3$ was almost as active as Pt/Al_2O_3, whereas $Au/Co_3O_4–Al_2O_3$ was much less active than $Au/CuO–Al_2O_3$. Furthermore, the light-off temperature in propane oxidation was much higher than that of propylene oxidation. The authors also investigated the combustion of methane and propane on Au/Al_2O_3 and $Au/MO_x–Al_2O_3$ (M: alkali or alkaline earth, transition metal, and cerium) *(467)*. Higher temperatures were required to oxidize methane (temperatures above 673 K) than to oxidize propane (temperatures above 523 K). The addition of MO_x to Au/Al_2O_3 enhanced the catalytic activity for both methane oxidation and propane oxidation. In methane oxidation, FeO_x and MnO_x were the most efficient promoters of Au/Al_2O_3. Gold catalysts have also been used to completely oxidize other VOCs such as toluene *(472)*, benzene *(475,476)*, and 2-propanol *(475,477)*.

Table 1.5 The combustion of volatile organic compounds (VOCs) on gold catalysts

Catalyst	Calcination temperature (K/gas)	Gold content (wt%)	Gold particle diameter (nm)	VOC concentration or molar ratio	T_x [a] (K)	SV[b] ($ml\,g_{cat}^{-1}h^{-1}$)	Reference
Au/Al_2O_3	573/H_2	4.1	5.2	CH_4:O_2 = 1:4	865 (T_{50})	9000	*(467)*
Au/FeO_x–Al_2O_3	573/H_2	4.2	–	CH_4:O_2 = 1:4	816 (T_{50})	9000	*(467)*
Au/MnO_x–Al_2O_3	573/H_2	4.3	4.9	CH_4:O_2 = 1:4	838 (T_{50})	9000	*(467)*
Au/TiO_2	773/O_2	1.1	3.9	C_3H_6, 1200 ppm[c]	593 (T_{50})	180,000	*(468)*
Au/Al_2O_3	773/O_2	0.96	3.3	C_3H_6, 1200 ppm[c]	683 (T_{50})	180,000	*(468)*
Au/CeO_2	773/O_2	1.0	–	C_3H_6, 1200 ppm[c]	488 (T_{50})	180,000	*(463)*
$Au/1.5CeO_2$–Al_2O_3[d]	573/H_2	0.93	2.3	C_3H_6, 1200 ppm[c]	505 (T_{50})	60,000	*(469)*
$Au/5CeO_2$–Al_2O_3[d]	573/H_2	0.89	2.2	C_3H_6, 1200 ppm[c]	498 (T_{50})	60,000	*(469)*
$Au/10CeO_2$–Al_2O_3[d]	573/H_2	0.89	2.0	C_3H_6, 1200 ppm[c]	488 (T_{50})	60,000	*(469)*
Au/MnO_x–Al_2O_3	573/H_2	4.3	4.9	C_3H_6:O_2 = 1:9	567 (T_{95})	9000	*(470)*
Au/CeO_x–Al_2O_3	573/H_2	4.5	1.7	C_3H_6:O_2 = 1:9	497 (T_{95})	9000	*(470)*
Au/Al_2O_3	573/H_2	4.1	4.3	C_3H_8:O_2 = 1:16	723 (T_{50})	9000	*(471)*
Au/Co_3O_4–Al_2O_3	573/H_2	4.3	5.0	C_3H_8:O_2 = 1:16	605 (T_{50})	9000	*(471)*
Au/CuO–Al_2O_3	573/H_2	4.0	3.0	C_3H_8:O_2 = 1:16	639 (T_{50})	9000	*(471)*
Au/CuO–Al_2O_3	573/H_2	7.4	6.8	C_3H_8:O_2 = 1:16	611 (T_{50})	9000	*(471)*
Au/CeO_2	773/O_2	0.06	–	2-Propanol:O_2 = 1.2:21	470 (T_{50})	175 h^{-1}	*(477)*
Au/CeO_2	573/air	1.5	4.5	Benzene: 0.5%	480 (T_{50})	60,000	*(476)*
Co-UVM-7[e]	773/air			C_7:O_2 = 0.1:20[f]	663 (T_{50})	40,000	*(472)*
Au/Co-UVM-7[e]	773/air	1.2	3.9	C_7:O_2 = 0.1:20 [f]	528 (T_{50})	40,000	*(472)*

[a] T_x is the temperature required to achieve x% conversion of the VOC.
[b] SV, space velocity.
[c] Feed gas: 1200 ppm C_3H_6, 9.0 vol% O_2, and helium.
[d] Weight ratio of CeO_2 to Al_2O_3.
[e] UVM, a type of mesoporous silica.
[f] C7, toluene.

7. CATALYSIS BY GOLD WITH REACTANTS IN THE LIQUID PHASE

7.1. Introduction

Selective oxidations and hydrogenations with liquid-phase reactants are of great importance in the chemical industry. These reactions have been achieved by using stoichiometric reagents and homogeneous metal complex catalysts. The motivation for green chemistry has challenged researchers to replace these reactions with reactions catalyzed by solids, which offer the advantages of being easily separated from products and recycled. Selective oxidation of reactants containing oxidizable functional groups is needed. In particular, biomass-derived compounds often have more than one hydroxyl group so that the selective oxidation of the hydroxyl group at the desired position should be achieved. Solid palladium and platinum catalysts have been used widely for hydrogenations. However, poisoning of the catalysts with toxic metals is sometimes required to improve the product selectivity. Moreover, control the chemical selectivity is a still challenging research target.

Catalysis by gold in the presence of liquid-phase reactants had not been investigated as intensively as that in the presence of gas-phase reactants. However, in the preceding decade, it has been reported that gold exhibits unique and excellent product selectivities different from those of palladium and platinum.

7.2. Oxidation

7.2.1 Alcohols

Selective oxidations of alcohols, amines, alkenes, and alkanes are of industrial importance, especially for fine chemicals synthesis. Stoichiometric oxidizing agents have been used predominantly, and the generation of unwanted by-products often exceeds that of desired products. Oxidations catalyzed by solids have been strongly desired with molecular O_2 or air as the sole oxidant.

Gold-catalyzed oxidation reactions in the presence of liquid-phase reactants have recently been investigated intensively *(478–481)*. Gold catalysts generally have advantages over palladium and platinum catalysts in terms of higher selectivity when more than one oxidizable group is present in reactant alcohols, and the gold catalysts also offer better resistance to water and oxygen. Gold preferentially oxidizes hydroxyl groups whereas palladium oxidizes both these and other functional groups or isomerization of carbon–carbon double

bonds. Various types of metal oxides *(331,482–490)*, carbons, *(6,491,492)*, and organic polymers *(82,493–497)* have been exploited as supports for gold clusters and NPs. Some kinds of organic polymers *(493,494)* and MOFs *(82,496,497)* stabilize gold as clusters smaller than 2 nm in diameter, and these exhibit catalytic activity for aerobic oxidations of alcohols. In principle, metal oxide-supported gold catalysts appear to be advantageous for base-free oxidation of alcohols to produce aldehydes, whereas carbon- and polymer-supported gold catalysts except for Au/MOFs need the addition of base to promote the reaction. Oxidation reactions are carried out in the presence of various solvents such as toluene, methanol, and water. Metal oxide-supported gold catalysts gave metal time yields (MTYs) for the oxidation of benzyl alcohol in the range of 50–500 h^{-1} *(486,489)*. Gold NPs supported on basic hydrotalcite ($Mg_6Al_2(OH)_{16}CO_3{\cdot}nH_2O$, HT) also exhibited excellent catalytic performance for the oxidation of benzyl alcohol to produce benzaldehyde in the absence of base *(498,499)*. In particular, gold NPs supported on MgCr–HT in which all Al^{3+} in the HT precursor was replaced by Cr^{3+} achieved remarkably high MTY, 1880 h^{-1} *(499)*. Gold on MgCr–HT also showed high MTY (81,000 h^{-1}) for the aerobic oxidation of 1-phenyl ethanol to acetophenone under solvent-free conditions at 423–433 K in the initial 30 min.

Even gold NPs supported on metal oxides efficiently catalyze aerobic oxidation of alcohols, and base is needed for the direct production of carboxylates and esters from alcohols. To obtain carboxylic acids from carboxylates, the neutralization of carboxylates is needed, and a large amount of inorganic salts was produced as a waste. Thus, aerobic oxidation of alcohols under base-free conditions to directly produce carboxylic acids is strongly desired but is still limited to a few cases. The base-free direct alcohol oxidation was carried out with Au/TiO_2 with an excess of hydrogen peroxide as an oxidant *(500)*. Christensen *et al.* reported the oxidation of ethanol with O_2 in the presence of aqueous solution to directly produce acetic acid on $Au/MgAl_2O_4$ *(501)* and Au/TiO_2 *(502)* without base. On gold catalysts, a selectivity greater than 80% to acetic acid was obtained at a high conversion, whereas palladium and platinum NPs supported on $MgAl_2O_4$ showed higher selectivities to acetaldehyde.

Aliphatic carboxylic acids are among the important fine chemicals for applications to surfactants but are less reactive than benzylic and lower alcohols. When highly active gold catalysts were used, MTY values characterizing the 1-octanol oxidation in the absence of base were as much as 38 h^{-1}, and the major product was octanal *(499)*. Gold NPs supported on nanometer-sized

NiO catalyzed the base-free oxidation of 1-octanol to octanal together with ocatnoic acid, but the selectivity to octanoic acid was only 31% *(503)*. Co-precipitated Au/NiO was also active and selective under the optimized reaction conditions, achieving a high selectivity to octanoic acid (e.g., 97%) at a full conversion *(504)*.

Gold catalysts also show superior product selectivities in the oxidation of diols to form mono-acids (hydroxy acids), whereas the complete oxidation takes place on palladium catalysts *(6,491)*. In the oxidation of 1,4-butanediol, the cyclization takes place to form γ-butyrolactone *(505)*. Oxidation of 1,2-propanediol to lactic acid (LA) has been focused on in view of green chemistry because 1,2-propanediol (propylene glycol) can be produced from a bio-renewable feedstock, glycerol *(6,506,507)*. Hutchings *et al.* *(507)* reported that Au/TiO_2 and $Au–Pd/TiO_2$ provide high selectivity to LA.

The reaction network characterizing gold-catalyzed alcohol oxidation is widely accepted to involve a sequence of three reactions (Scheme 1.1) *(508–513)*. The first is the deprotonation of alcohol to form alkoxide catalyzed by basic hydroxyl groups on metal oxide surfaces or by alkali added in the case of carbon- and polymer-supported gold NPs. Basic properties of metal oxide surfaces play a key role in the first reaction so that basic metal oxides such as hydrotalcite and MgO have been used as supports for gold NPs and gave good catalytic activity *(490,498)*. The β-H is eliminated in a reaction

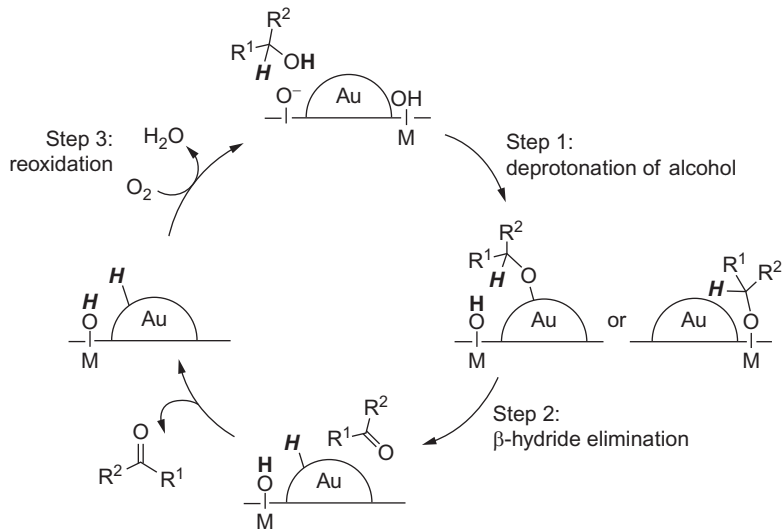

Scheme 1.1 A possible reaction pathway for the gold-catalyzed aerobic oxidation of alcohols.

catalyzed by gold to form carbonyl compounds, and the hydride is shifted to the gold surface. This transformation is considered to be the rate-determining step. The third reaction is the oxidation of Au–H groups by O_2 to produce H_2O, possibly via H_2O_2 formation *(513)*. The proton released from the hydroxyl group of the alcohol is consumed in the formation of H_2O.

It had been considered that molecular oxygen was indispensable for removing hydride from the gold surface to restore the catalytic activity. Recently, however, gold-catalyzed dehydrogenation of alcohol to give carbonyl compounds without the use of O_2 has been reported *(514–516)*. A proton can be supplied by hydroxyl groups on metal oxides, and hydrides on gold surfaces could be removed as H_2.

7.2.2 Amines

Aerobic oxidation of amines catalyzed by gold NPs to give valuable nitrogen-containing compounds has been the focus of recent research. Zhu *et al. (517,518)* first reported the aerobic oxidation of amines to imines by using bulk gold powder and Au/Al_2O_3. Several types of imine formation were demonstrated: secondary amines to the corresponding imines (Scheme 1.2A) *(517–523)*, homo-condensation of primary amines (Scheme 1.2B) *(518, 519,524)*, and cross-condensation of two kinds of primary amines (Scheme 1.2C) *(519)*. In the aerobic oxidation of amines to imines, gold NPs on inert supports were found to exhibit higher catalytic activity than those on metal oxides (or similar activities), and gold NPs with diameters greater than 10 nm or bulk gold were also found to be catalytically active.

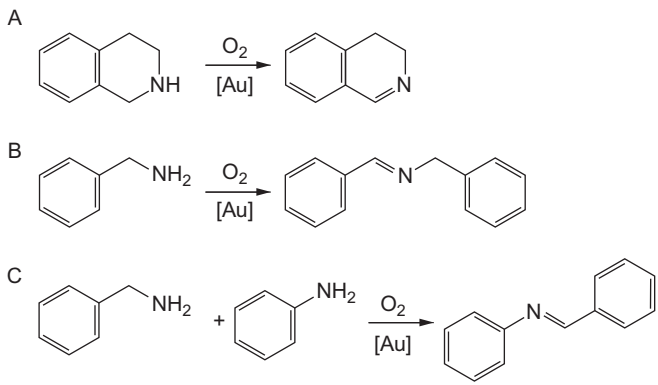

Scheme 1.2 Representatives of gold catalyzed aerobic oxidation of secondary amine to imine (A), homo-condensation of primary amine (B), and cross-condensation of primary amines (C).

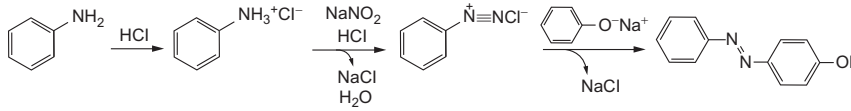

Scheme 1.3 Conventional synthetic protocol for azobenzene dye.

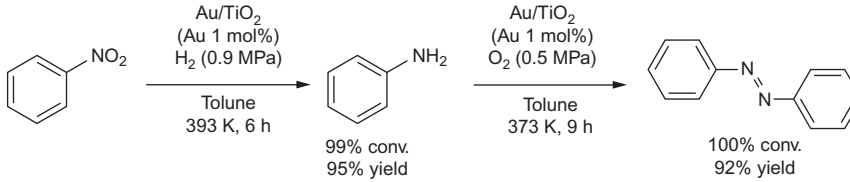

Scheme 1.4 One-pot two-step synthesis of azobenzene from nitrobenzene catalyzed by Au/TiO_2.

Another important transformation of amines is the aerobic oxidation of anilines to azobenezenes, which are widely used as dyes and optoelectronic materials. A conventional synthetic route to azobenzene includes the formation of a diazonium salt by use of stoichiometric reagents, producing high yields of wastes (Scheme 1.3). Grirrane *et al.* *(525)* reported that gold efficiently catalyzed the aerobic oxidation of aniline to produce azobenzene with excellent selectivity (98%) (the last reaction in Scheme 1.4). The type of support strongly affects the catalytic activity. Gold on TiO_2 and on CeO_2 was found to be active and selective, whereas Au/C and Au/Fe_2O_3 were not. Although TiO_2 and CeO_2 have catalytic activity themselves for aniline oxidation, gold NPs enhanced the rate of reaction. In contrast, palladium and platinum NPs on TiO_2 did not catalyze aniline oxidation. The authors *(525)* also demonstrated a one-pot two-step azobenzene synthesis from nitrobenzene catalyzed by Au/TiO_2 (Scheme 1.4).

7.2.3 Alkenes

Direct epoxidation of alkene with molecular oxygen is strongly desired by industry. However, it is one of the difficult reactions to achieve. Hughes *et al.* *(396)* first reported that supported gold NPs enabled the aerobic oxidation of cycloalkenes to give epoxides in the presence of radical initiators such as *tert*-butyl hydroperoxide (TBHP), but with epoxide yields as low as 15%. Gold-catalyzed oxidation of alkenes with peroxide as an initiator has been investigated with Au/TiO_2 *(526,527)*, Au/C *(396)*, and Au/SiO_2 *(528,529)* catalysts. Mendez *et al.* *(527)* proposed that gold NPs catalyzed

the homolytic decomposition of TBHP to begin the process (Scheme 1.5). The generated *tert*-butoxy and hydroxyl radicals were inferred to react with solvent molecules such as methylcyclohexane to form alkyl radicals, which further reacted with O_2 to form alkyl peroxy radicals. The peroxy radicals were considered to be the true oxidant.

Turner *et al.* *(332)* demonstrated that 55 Au-atom clusters deposited on inert BN and on SiO_2 enabled the epoxidation of styrene to produce styrene epoxide in the presence of molecular O_2 alone (Scheme 1.6). These gold clusters activated and dissociated O_2 into oxygen atoms which led to the epoxidation, whereas larger (e.g., 3 nm-diameter) gold NPs did not. However, the selectivity to styrene epoxide was as low as 14%. Thiolate-protected 25-atom gold clusters supported on SiO_2 also catalyzed the epoxidation of styrene, giving styrene epoxide with a selectivity of 26% *(530)*.

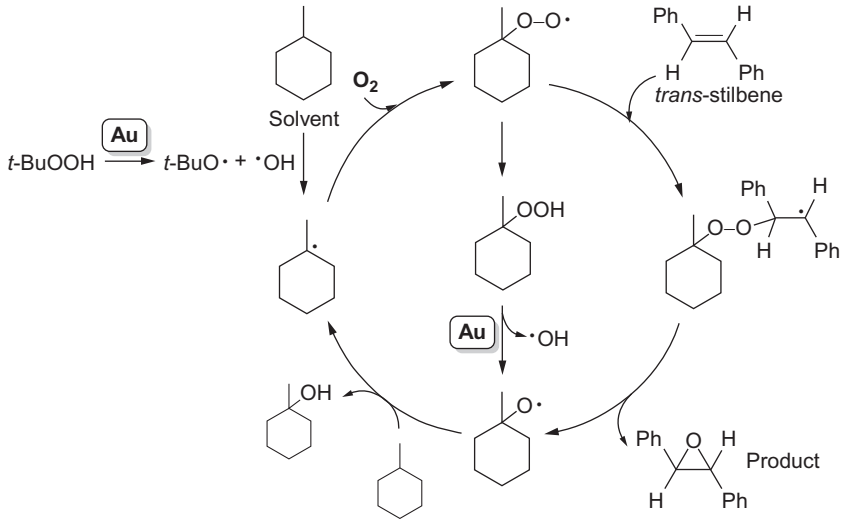

Scheme 1.5 Proposed reaction mechanism for the aerobic epoxidation of stilbene in the presence of *t*-butyl hydroperoxide in methylcyclohexane solvent *(527)*.

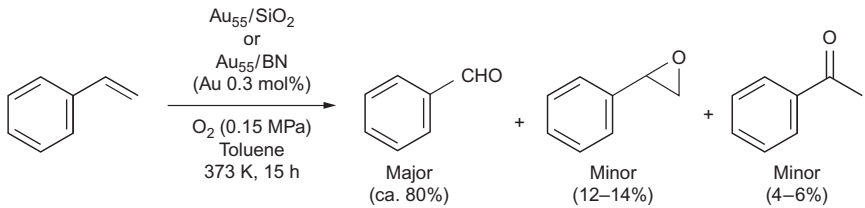

Scheme 1.6 Epoxidation of styrene with O_2 catalyzed by supported 55-atom gold clusters.

7.2.4 Alkanes

Aerobic oxidation of hydrocarbons is crucial in industrial petrochemical processes. In most cases, reducing agents and/or radical initiators have been used under severe conditions. Some catalysts have been used for cycloalkane oxidation, especially for cyclohexane to K/A oil (a mixture of cyclohexanone and cyclohexanol). The present commercial process for cyclohexane oxidation is carried out at approximately 423 K and 1–2 MPa O_2 partial pressure, affording ~4% conversion and 70–85% selectivity to K/A oil by homogeneous catalysis with, for example, cobalt salts.

Gold catalysts have been reported to be active for the aerobic oxidation of cyclohexane without radical initiators (Scheme 1.7) *(531–537)*. As in the epoxidation of alkene, SiO_2 and organically functionalized mesoporous SiO_2 have been used to support gold NPs. In most cases, conversions up to 20% were applied to maintain high selectivity to K/A oil in the range of 75–94%. Gold supported on functionalized SBA-15 exhibited an excellent selectivity to K/A oil (as much as 94%) at a conversion of 22% under 1 MPa of O_2 at 423 K *(536)*. With gold catalysts, the product ratio of cyclohexanone to cyclohexanol was about 2:1 to 4:1, which was opposite to the industrial case (about 1:2). The high ketone selectivity was ascribed to the high catalytic activity of gold NPs for the cyclohexanol oxidation. Aerobic oxidation of *n*-alkanes to alcohols or ketones without radical initiators has also been catalyzed by gold clusters encapsulated in the walls of mesoporous SiO_2 for the oxidation of *n*-hexadecane *(537)*.

7.3. Hydrogenation

7.3.1 α,β-Unsaturated carbonyl compounds

Selective hydrogenation of α,β-unsaturated aldehydes into unsaturated alcohols is an important reaction in industry for the manufacture of fragrances and pharmaceuticals. The hydrogenation of the C═C bond is thermodynamically more favorable than that of the C═O bond. For example, the equilibrium constant for the hydrogenation of crotonaldehyde to form butanal is greater than that for the production of crotyl alcohol, as shown by Gibbs free energy values (Scheme 1.8) *(538)*. Conventional palladium and platinum

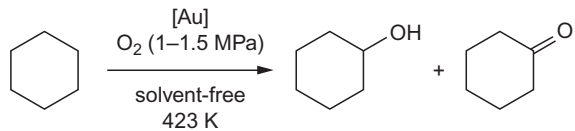

Scheme 1.7 Aerobic oxidation of cyclohexane to cyclohexanol and cyclohexanone.

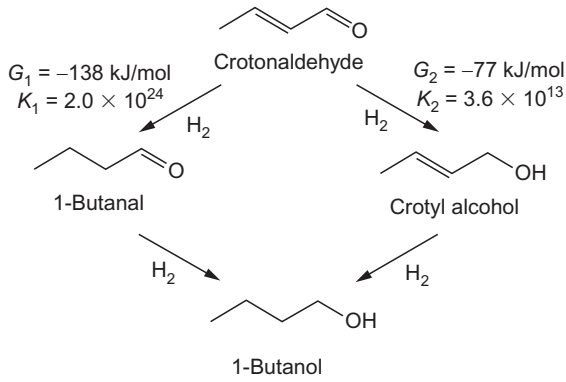

Scheme 1.8 Reaction pathway for the hydrogenation of crotonaldehyde.

catalysts accelerate C═C hydrogenation to give an undesired product, saturated aldehyde, as a major product. In contrast, gold catalysts tend to exhibit C═O selectivity. Product selectivity depends on the substituents at the C═C bond, reaction conditions, the size of the gold NPs, and the nature of the supports for the gold NPs (Table 1.6) *(363,539–547)*.

Sterically hindered α,β-unsaturated aldehydes such as cinnamaldehyde and citral afforded the desired unsaturated alcohols with excellent selectivities exceeding 90% *(539,545)*. However, the hydrogenations of small substrates, acrolein and crotonaldehyde, unsaturated alcohols are produced with lower selectivities *(539,540,542)*. H_2O appears to be an efficient solvent for the selective hydrogenation of C═O groups. The selectivity to crotyl alcohol in the crotonaldehyde hydrogenation catalyzed by Au/CeO_2 was improved to 86% in the presence of water at full conversion, whereas the selectivity was only 29% in the presence of ethanol *(541)*.

The catalytic activity of unsupported gold NPs was found to be enhanced by the addition of Lewis acids *(539)*. Thiolate-protected 25-atom gold clusters catalyzed the hydrogenation even at 273 K *(544)*. Deposition of 25-atom gold clusters onto metal oxides such as TiO_2 and Fe_2O_3 enhanced the catalytic activity of the clusters, with the product selectivity maintained *(544)*. Moreover, these 25-atom cluster catalysts afforded excellent selectivity to allyl alcohol (92%) in the hydrogenation of acrolein.

In these selective hydrogenations, the nature of the support greatly influences the selectivity to unsaturated alcohols. Reducible metal oxides such as Fe_2O_3 are better than inert supports such as Al_2O_3 *(539–541,543,545,546)*. It has been speculated that an electron transfer from metal oxides to gold NPs would enhance the catalytic activity of gold. One of the other support effects

Table 1.6 Hydrogenation of α,β-unsaturated aldehydes and ketones on gold catalysts

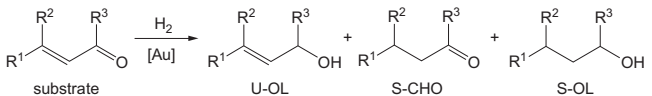

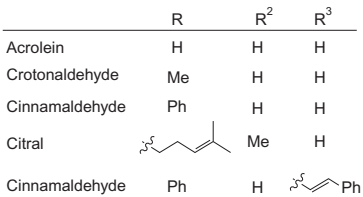

Reactant	Catalyst	Temperature (K)	H_2 partial pressure (MPa)	Conversion (%)	Selectivity (%)			MTY (h^{-1})	Reference
					S-CHO	U-OL	S-OL		
Acrolein	Au_{25}/Fe_2O_3	273	0.1	47	0	92	8	4	*(544)*
Crotonaldehyde	Au/Fe_2O_3	333	4.0	91	n.d.	76	n.d.	4	*(539)*
	Au/ZnO	333	4.0	90	n.d.	78	n.d.	5	*(539)*
	Au/Fe_3O_4	393	2.0	>99	3	78	19	4	*(540)*
	Au/CeO_2	373	1.0	>99	n.d.	87	n.d.	29	*(541)*
Cinnamaldehyde	$Au/Fe(OH)_x$	373	4.0	86	11	82	6	22	*(542)*
	Au/Fe_2O_3	373	4.0	81	72	13	5	5	*(542)*
	Au/ZnO	333	4.0	91	n.d.	95	n.d.	2	*(539)*
Benzalacetone	Au/Fe_2O_3	333	0.1	99	11	68	21	0.2	*(543)*
	Au_{25}/Fe_2O_3	273	0.1	43	0	100	0	4	*(544)*
Citral	Au/Fe_2O_3	333	0.1	90	trace	97	3	3	*(545)*

S-CHO, saturated aldehyde; U-OL, unsaturated alcohol; S-OL, saturated alcohol; n.d., no data.

proposed is that metal oxides affect the morphology of the gold NPs *(363,546)*. When the catalytic activity of gold NPs with similar diameters is compared, the metal oxide supports that stabilize gold NPs with facets lead to higher selectivities than the supports that stabilize spherical gold NPs with weak metal–support interactions. Claus *et al. (363,547)* investigated the morphological effects on the selective hydrogenation of acrolein catalyzed by Au/ZnO, whereby the terraces of the gold NPs were covered by indium, leaving the edges and the corners free from indium. The indium-modified Au/ZnO catalysts showed higher selectivities to desired allyl alcohol than the unmodified catalyst, indicating that Au atoms at edges and corners preferably catalyze the hydrogenation of C═O groups to give the desired allyl alcohol, whereas on gold terraces hydrogenation of the C═C bonds gave propanal. Dissociation of molecular H_2 at Au atoms on edges and corners has also been proposed on the basis of DFT calculations *(341)* and experimental results *(339)*. With a decrease in the size of the gold NPs, the catalytic activity and selectivity increased as a consequence of an increase in the number of edges and corners having more highly unsaturated coordination sites. We also note that recent surface science work by Fujitani *et al. (97)* demonstrated that hydrogen dissociation can take place at the perimeter interfaces between gold NPs and the support.

7.3.2 Nitroaromatics

Solid palladium catalysts have been used for the hydrogenation of nitroarenes to produce functionalized anilines. However, selective hydrogenation of the nitro group is usually difficult when other reducible functional groups are present in the same molecule *(549)*. In earlier stages of research, the selective hydrogenation of halogenated nitrobenzene without dehalogenation was addressed with supported gold catalysts *(550,551)*. Chen *et al. (550)* first reported the hydrogenation of nitro compounds on Au/SiO_2 in ethanol, achieving high selectivity to chlorinated nitroaromatics.

On the other hand, the selective hydrogenation of nitro compounds incorporating reducible functional groups such as C═C and C═O to give the corresponding amino compounds is more challenging because palladium and platinum catalysts are selective for the hydrogenation of C═C and C═O bonds rather than the nitro group. Corma and Serna *(335)* demonstrated the excellent potential of gold catalysts for the selective hydrogenation of the nitro groups in the presence of alkenyl, formyl, cyano, and carbamoyl groups, without poisoning of the catalysts (Table 1.7). Scheme 1.9 shows a possible reaction pathway. Nitrobenzene was reduced to phenylhydroxylamine via

Table 1.7 Selective hydrogenation of nitrobenzene derivatives

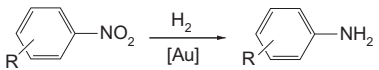

R	Catalyst	Metal (mol%)[a]	Temperature (K)	H_2 partial pressure (MPa)	Time (h)	Conversion (%)	Selectivity (%)	MTY (h^{-1})	Reference
3-Vinyl	Au/TiO_2	0.23	393	0.9	6	99	96	72	*(335)*
	Pd/C	0.11	393	9	0.03	99	0	—	*(335)*
	Pt/C	0.12	393	0.9	0.03	97	3	—	*(335)*
4-Formyl	Au/TiO_2	1.14	373	1	1.25	99	97	70	*(335)*
	Pd/C	0.35	373	1	0.03	92	30	—	*(335)*
	Pt/C	0.38	373	1	0.03	97	67	—	*(335)*
4-Acetyl	Au/SiO_2	0.17	413	4	3	100	95	196	*(550)*
	$Au/Fe(OH)_x$	0.42	388	1	0.75	>99	99	318	*(542)*
4-Cyano	Au/TiO_2	0.6	413	2.5	1.25	99	97	133	*(335)*
	Pd/C	0.6	413	2.5	0.42	>99	80	—	*(335)*

[a]Metal mol%: molar ratio in percentage of catalytic metal with respect to reactant. Catalytic metals are indicated in the "Catalyst" column (Au, Pd, or Pt).

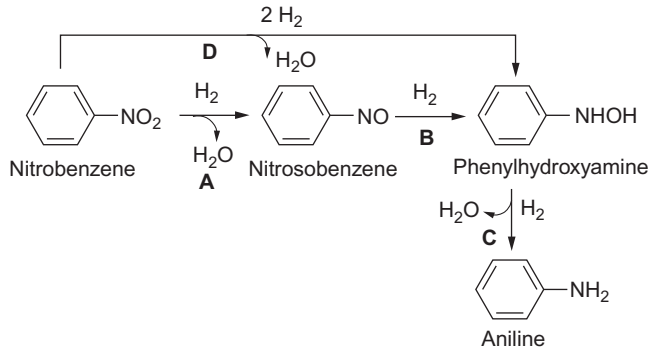

Scheme 1.9 A possible reaction pathway for the hydrogenation of nitrobenzene catalyzed by supported gold NPs.

nitrosobenzene as an intermediate (routes **A** and **B**) and by a direct route (**D**) (Scheme 1.9) *(552)*. Hydrogenation of phenylhydroxylamine to give aniline (route **C**) was considered to be rate limiting.

In the selective hydrogenation, the choice of proper supports is crucial. Accordingly, Au/TiO_2 preferentially hydrogenates nitrobenzene to aniline in the presence of styrene, whereas Au/SiO_2 tends to do the opposite. Theoretical investigations combined with *in situ* IR measurements showed that the nitro group was strongly bonded to TiO_2 (or on Au/TiO_2 at the interface) but weakly adsorbed on Au/SiO_2 *(553)*. On the other hand, no large difference between Au/TiO_2 and Au/SiO_2 was observed for the bonding of the C═C bond. Thus, preferential bonding of nitro groups over the C═C bond on the support or gold–support interface is inferred to be responsible for the chemical selectivity. Shimizu *et al. (554)* mentioned that the metal oxide, Al_2O_3, worked not only for the preferential adsorption through nitro groups but also for the assistance by this support in the formation of the H^+/H^- pair generated by H_2 dissociation at the Au/Al_2O_3 interface.

When nitroalkenes were used as reactants, gold catalysts gave oxime as a major product (Scheme 1.10A and B) *(335,555)*. The hydrogenation of 1-nitro-1-cyclohexene catalyzed by Au/TiO_2 selectively produces cyclohexanone oxime, which is an important chemical for the production of nylon-6. Cyclohexanone oxime can also be obtained by the hydrogenation of nitrocyclohexane (Scheme 1.10C) *(556,557)*.

7.4. Deoxygenation

Gold NPs supported on HT can catalyze deoxygenation of epoxides to give alkenes with high selectivities in the presence of reducing agents (Scheme 1.11) *(558–560)*. Alcohols (such as 2-propanol), CO/H_2O, and

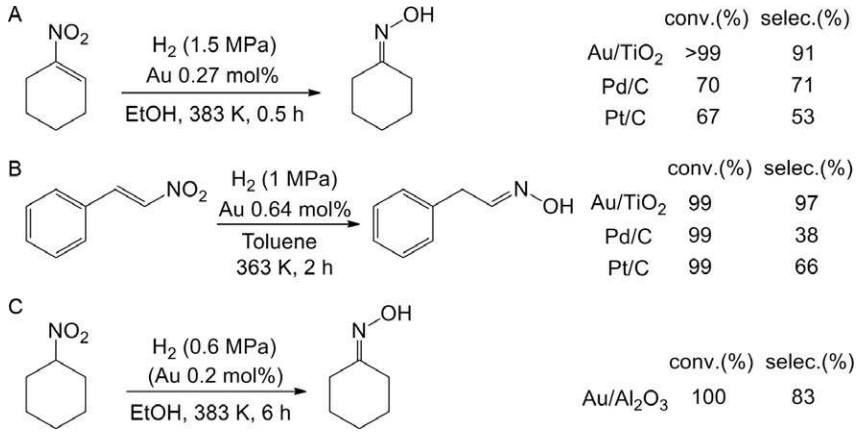

Scheme 1.10 Selective hydrogenation of 1-nitro-1-cyclehexene (A) *(335)*, *trans*-β-nitrostyrene (B) *(555)*, and nitrocyclohexane (C) *(554)* to the corresponding oximes.

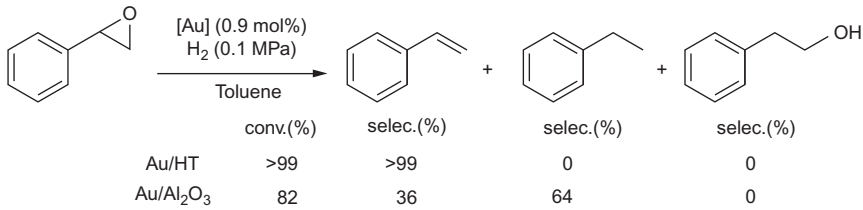

Scheme 1.11 Deoxygenation of epoxide.

H_2 can also be used as reducing agents. In the proposed mechanism, $[Au–H]^-$ species, which form by the dehydrogenation of alcohols, water, or heterolytic dissociation of H_2, were considered to be responsible for the selective deoxygenation of epoxide. Basic HT worked to preserve H^+, which opened the epoxide ring.

7.5. Coupling

7.5.1 Suzuki–Miyaura coupling

Metal-catalyzed C—C bond-forming reactions have been among the most important research topics in the field of fine chemical and pharmaceutical synthesis *(561)*. The Suzuki–Miyaura cross-coupling is the most frequently used reaction to produce biaryl compounds in industry, and palladium catalysts have been the most intensively investigated *(562)*. Unsupported gold clusters *(563–565)* as well as supported gold catalysts *(566,567)* are active for the homo-coupling of boronic acid to give symmetrical biaryl compounds (Scheme 1.12A), but they do not catalyze the formation of the cross-coupling

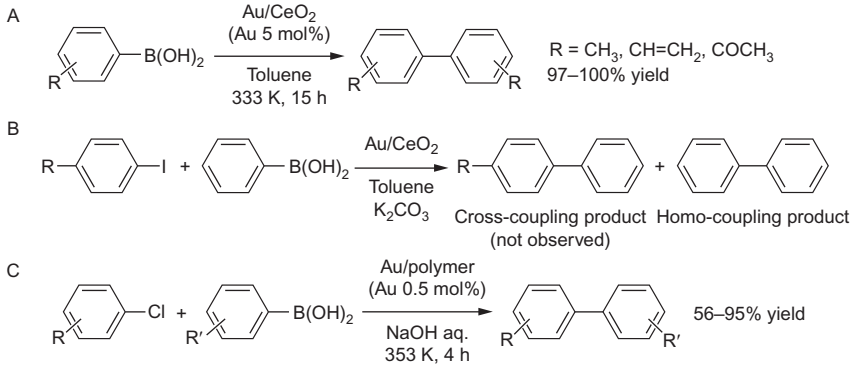

Scheme 1.12 Biphenyl synthesis catalyzed by gold.

products (Scheme 1.12B). These observations suggested that the oxidative addition of gold to aryl halides could not take place. Later, Han *et al. (568)* demonstrated Suzuki–Miyaura cross-coupling catalyzed by polymer-supported gold NPs by using less reactive aryl chlorides as cross-coupling partners (Scheme 1.12C). The product derived from the homo-coupling of phenyl boronic acid was not observed. Although the reaction mechanism is not clear, this result indicated that Au(0) NPs have a potential to activate aryl halides.

7.5.2 Sonogashira coupling

Gold-catalyzed Sonogashira coupling of iodobenzene (IB) with phenylacetylene has been reported to produce diphenylacetylene (DPA) (Scheme 1.13) *(337,569–574)*. The order of catalytic activities was found to be the following: Au(I) complex > supported Au(0) NPs > Au(III) complex *(337)*. Thus, the catalytically active gold species was thought to be Au(I) but not the Au(0) that was present in the Au/CeO_2 catalysts. On the other hand, Lambert *et al. (571)* demonstrated by TPR measurements that the Sonogashira coupling reaction occurs on the smooth Au(111) surface, and the cross-coupling product was detected together with the two homo-coupling products (diphenyldiacetylene (DPDA) and biphenyl (BP)). These authors further examined the catalytic performance of Au(I), Au(III), and

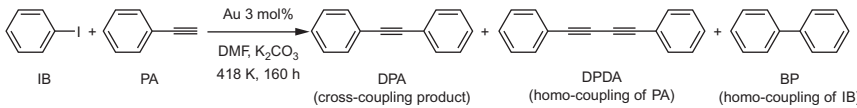

Scheme 1.13 Sonogashira coupling of iodobenzene (IB) and phenylacetylene (PA) to give diphenylacetylene (DPA) together with homo-coupling products, diphenyldiacetylene (DPDA) and biphenyl (BP).

Au(0) NPs supported on La_2O_3 *(573)*. Metallic gold on La_2O_3 was catalytically active even when the diameter of the gold NPs was as great as 20 nm, whereas Au(I) and Au(III) on La_2O_3 did not catalyze the reaction. Corma *et al. (575)* also reported that the cleavage of the C—I bond in IB took place on the surfaces of zerovalent gold NPs but that the oxidative addition of IB to Au(I) to form Au(III) hardly occurred. These results suggest that the catalytically active species was Au(0). It is likely that the catalytic activity obtained with the Au(I) complex was a consequence of the reduction of Au(I) to Au(0) and aggregation to form gold NPs in the reaction medium.

The nature of the support affects the product selectivity in this coupling reaction. The data lead to the following comparison of selectivities *(573)*: CeO_2 (92%) > La_2O_3 (82%) > Al_2O_3 (65%) and BaO (62%) > SiO_2 (38%) > TiO_2 (22%). The selectivity pattern was not correlated with acidity/basicity, redox properties, or oxygen-vacancy sites on the metal oxides.

7.5.3 Mannich reaction

The A^3 (alkyne, aldehyde, amine) coupling, Mannich reaction to obtain propargylamines on Au/CeO_2 and Au/ZrO_2, was reported by Zhang and Corma (Scheme 1.14) *(576)*. Au(III) supported on metal hydroxide ($Mg_{1-x}Al_x(OH)_2(Cl)_x \cdot zH_2O$) also catalyzed the reaction, whereas the reduced Au(0) catalysts showed no catalytic activity *(577)*. The catalytically active species was thought to be Au(III) in Au/CeO_2 and Au/ZrO_2. Gold (III) would activate alkyne to form gold acetylide which reacted with imine intermediate to give the final product *(576)*. In contrast, Zhu *et al. (578)* demonstrated that the Mannich reaction took place on Au(0) NPs supported on mesoporous organosilica in excellent yields (81–99%).

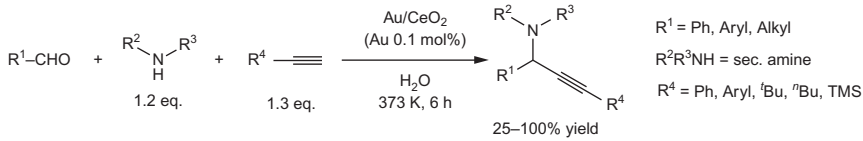

Scheme 1.14 Mannich reaction.

7.6. Addition reaction

7.6.1 Hydrosilylation

Hydrosilylation of aldehyde and imine to convert alcohol and secondary amine by a homogeneous Au(I) complex was first reported by Ito *et al. (579)*. Later, Caporusso *et al. (580,581)* demonstrated the hydrosilylation of 1-hexyne with silanes into (*E*)-alkenylsilane in the presence of Au(0) NPs

on various supports such as C, Al_2O_3, and Fe_2O_3 (Scheme 1.15A). Corma *et al.* *(582)* demonstrated the hydrosilylation of alkenes, aldehydes, and alkynes catalyzed by Au/CeO_2 (Scheme 1.15B and C). They proposed that Au(III) in Au/CeO_2 was the catalytically active species for the hydrosilylation because colloidal Au(0) NPs showed much lower catalytic activity. These results indicate that the interaction of gold NPs with the support may be important to generate catalytic activity, although it is still unclear which species, Au(I), Au (III), or Au(0), are catalytically active in this reaction.

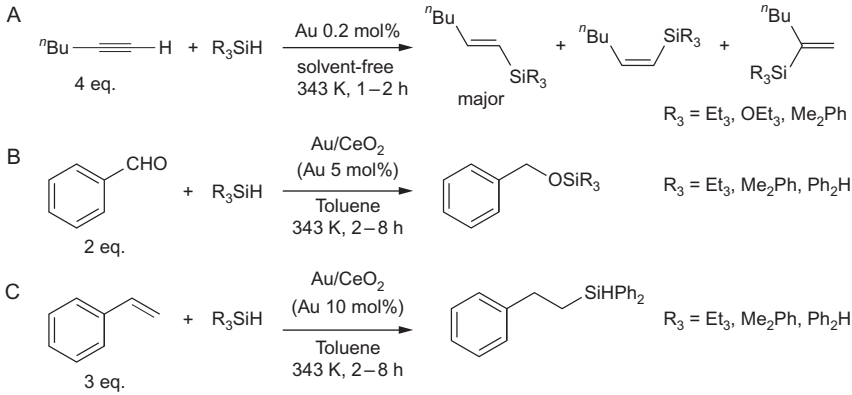

Scheme 1.15 Hydrosilylation of alkyne (A), aldehyde (B), and alkene (C) *(580-582)*.

7.6.2 Hydroamination

Hydroamination of alkynes or alkenes to produce aminoalkenes or aminoalkanes has been reported to be catalyzed by homogeneous Au(I) and Au(III) catalysts and by supported Au(III) catalysts *(583,584)*. Unsupported Au(0) clusters (Au:PVP) catalyzed the intramolecular hydroamination in the presence of O_2 and base *(548,585)*. Molecular oxygen was required to make gold surfaces partially cationic under basic conditions to activate C═C bonds of anionic alkene. Intramolecular hydroaminations were achieved in the presence of various supported Au(0) catalysts such as Au/Fe_2O_3 *(586)* and Au/mesoporous organosilica *(578)*. Intermolecular reaction was promoted by a Au/chitosan–SiO_2 hybrid (Scheme 1.16) *(587)*.

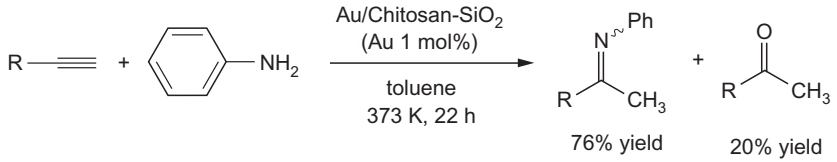

Scheme 1.16 Hydroamination of alkyne *(587)*.

Intramolecular hydroalkoxylation was also catalyzed by Au:PVP in a manner similar to that of hydroamination *(588)*.

7.7. Transformations of biomass-derived compounds

The transformation of biomass-derived feedstocks such as glucose, glycerol, and bioethanol into valuable chemicals has been attracting growing attention owing to a significant contribution to the goal of global environmental maintenance. Because these raw materials are usually obtained as aqueous solutions, catalysts for their conversions should be highly stable in water as well as active and selective. Although palladium and platinum catalysts have been investigated most often for biomass transformations, they sometimes cause over-oxidation of reactants and are deactivated by surface oxidation in water. Because catalysis by gold NPs is usually enhanced by water, it offers the prospect of being useful for biomass transformations.

7.7.1 Glucose

Aerobic oxidation of glucose to gluconic acid in aqueous solution is one of the simplest reactions in the presence of liquid-phase reactants and has been used as a test reaction for gold catalysts (Scheme 1.17) *(65,83,589–596)*. The catalytic performance of gold depends on the type of support and the size of the gold NPs. Carbons, Al_2O_3, ZrO_2, and TiO_2 have been used frequently as supports of the catalysts for glucose oxidation. The size dependency investigated by using unsupported gold NPs showed that the catalytic activity of gold was inversely proportional to the mean diameter of the gold NPs in the range of 3–6 nm and was almost zero when the NP diameters became larger than 10 nm *(590)*. Gold NPs supported on metal oxides were more active than Au/C, and their performance was characterized by lower activation energies and a weaker dependence on the glucose concentration *(83,592)*. Gold present as small NPs and clusters less than 3 nm in diameter on well-chosen supports such as Al_2O_3 and ZrO_2 exhibited remarkably high values of TOF, such as 56 s^{-1} *(83)*.

The reaction is influenced by the pH of the reaction solution and favored by basic conditions (pH > 9). However, more strongly basic conditions

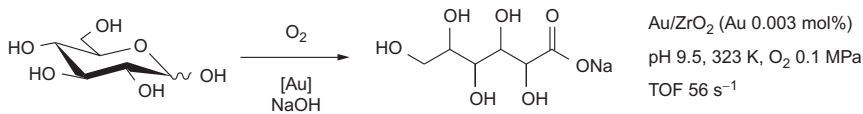

Scheme 1.17 Glucose oxidation to gluconic acid *(83)*.

(pH > 10) lead to the isomerization of glucose to fructose, and so the pH is kept in the range of 9–10 during the reaction. The oxidation of glucose to give free gluconic acid is a more desirable process because neutralization with inorganic acid is not necessary after the reaction. However, lower pH slows down the reaction. Comotti *et al.* *(593)* reported that Au–Pt/C is characterized by catalytic activity under conditions of base-free glucose oxidation. However, the TOF value ($0.3\ h^{-1}$) was much lower than that observed under basic conditions.

A direct transformation of cellulose into gluconic acid could have a significant practical impact because cellulose is the most abundant and non-edible natural biomass resource. From this point of view, the conversion of cellobiose into gluconic acid has recently been investigated *(597–599)*. Cellobiose is a disaccharide consisting of a linear chain of glucose connected by a β-1,4-glycosidic linkage; thus, cellobiose can be regarded as a model of cellulose. The transformation involves two steps: (1) hydrolysis of cellobiose into two glucose molecules and (2) the oxidation of glucose to gluconic acid. Acidic supports, nitric acid-treated carbon nanotubes and polyoxometalate, were used for the hydrolysis of cellobiose. The base-free oxidation of glucose was catalyzed by gold NPs. Whereas Au/SiO_2 catalyzed deep oxidation to give formic acid and glycolic acid (GLYCA), $Au/Cs_2HPW_{12}O_{40}$ exhibited excellent selectivity to gluconic acid (99%) at a conversion of 98%. Direct conversion of cellulose to gluconic acid was also reported to occur in the presence of a combination of $Au/Cs_3PW_{12}O_{40}$ with the more acidic $H_3PW_{12}O_{40}$ as a hydrolysis catalyst *(599)*. Gluconic acid was obtained in 85% yield at 97% conversion of cellulose.

One of the other disaccharides, lactose, is also a candidate reactant in biomass-derived chemistry because a large amount of lactose is produced as a by-product of cheese manufacturing. Valuable lactobionic acid can be obtained by the oxidation of lactose at the 1-OH position (Scheme 1.18). Whereas palladium catalysts are active for the oxidation of lactose at the 2-OH position, resulting in 2-keto-lactobionic acid, gold catalysts give lactobionic acid selectively *(600,601)*.

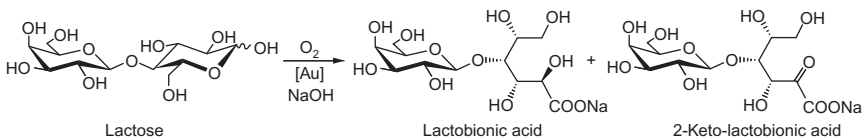

Scheme 1.18 Lactose oxidation.

7.7.2 Glycerol

Glycerol is a raw material obtained as a by-product in the production of biodiesel fuels from vegetable oils. Transformation of cheap glycerol to high-value chemicals has been an important research and development target as the production of biodiesel fuels has been increasing in recent years. Selective oxidation of glycerol with gold catalysts has been investigated intensively because gold is more resistant to oxygen poisoning than palladium and platinum *(602–611)*. As shown in Scheme 1.19, there are several reaction pathways for glycerol oxidation. Glycerol oxidation on gold catalysts

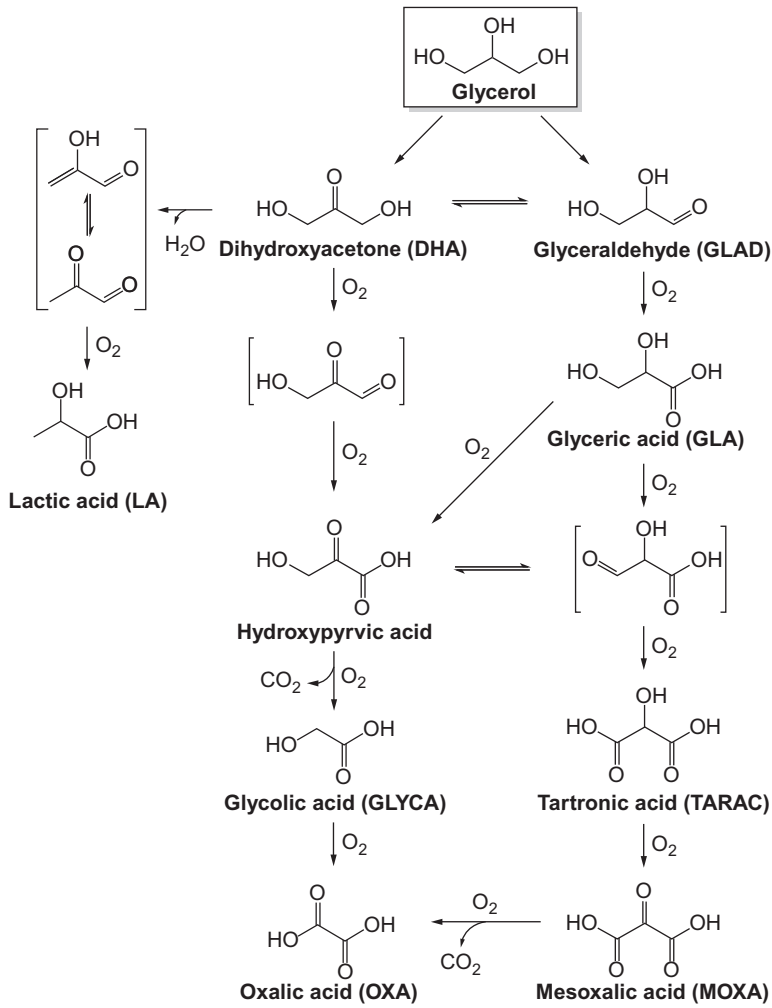

Scheme 1.19 Reaction pathways for glycerol oxidation.

frequently requires strongly basic conditions. Base promotes the deprotonation of hydroxyl groups in the first oxidation step to form glyceraldehyde (GLAD) or dihydroxyacetone (DHA). Under basic conditions, DHA is easily converted to GLAD. Because aldehyde is much more reactive than the hydroxyl group, glyceric acid (GLA) is obtained as a major product by rapid oxidation of GLAD. Hutchings *et al.* *(602–605)* first reported that GLA was produced with 100% selectivity with 50% in the conversion catalyzed by Au/C but that the selectivity gradually decreased to 86% at 72% conversion, caused by the subsequent oxidation of GLA to tartronic acid (TARAC) and mesoxalic acid (MOXA) and by C—C bond cleavage to form GLYCA and oxalic acid (OXA).

The oxidation of glycerol is influenced by the type of support, the size of the gold particles, and the reaction conditions, such as the temperature, partial pressure of O_2, and the pH of the reactant solution. Metal oxide supports were found to be inferior to carbons in terms of GLA selectivity because of the further oxidation and C—C bond cleavage encountered with the latter *(606)*. When various kinds of carbon supports were used, the catalytic activity of gold was altered by the nature of the carbon materials. Damirel *et al.* *(612)* demonstrated that the catalytic activity of gold was independent on the specific surface area but dependent on the microporosity of the carbon supports. On the other hand, Rodrigues *et al.* *(613)* in an investigation of the effects of AC surfaces on the catalytic activity of gold found that the number of oxygenated groups on the carbon affects the catalytic activity of gold, because groups such as carboxylic acid groups give acidic surfaces, causing the deactivation of the gold. Large gold NPs (ca. 20 nm in diameter) were characterized by lower catalytic activities but higher GLA selectivities than smaller ones (ca. 5 nm in diameter) as a consequence of limiting over-oxidation and C—C bond cleavage in GLA *(608,609)*. The effect of reaction temperature *(610)* and oxygen partial pressure *(602)* was also investigated. An increase in the temperature and oxygen partial pressure enhanced the reaction but caused over-oxidation and C—C bond cleavage. Optimized reaction conditions were 0.3 MPa of O_2 and a temperature of approximately 313 K for the selective production of GLA. The pH of the reaction solution also significantly affected the reaction rate and the product selectivity. An increase in the molar ratio of NaOH to glycerol up to the molar ratio of 2 led to an acceleration of the reaction *(614)*, but when this ratio increased to 4, GLA was further oxidized to form TARAC *(610,614)*.

Strong basic reaction conditions limit the industrial applications of gold catalysts because the neutralization of carboxylic acids is required after the

reaction. Accordingly, base-free oxidation of glycerol on gold-containing catalysts has recently become a hot research topic *(615–618)*. Ebitani *et al. (615,616)* used gold NPs supported on basic HT under base-free conditions, but the major product was a C_2 compound, GLYCA. Villa *et al. (617)* reported that an acidic support, H-mordenite, was suitable for base-free oxidation to produce GLA as a consequence of the suppression of C—C bond cleavage. The introduction of platinum into the gold particles significantly improved the catalytic activity and GLA selectivity *(617,618)*.

The formation of DHA, TARAC, MOXA, and LA has also been reported to be catalyzed by gold. DHA is one of the most interesting compounds derived from glycerol because it is used for cosmetics such as tanning agents. Introduction of platinum into carbon-supported gold catalysts improved both the activity and DHA selectivity *(612)*. Although the DHA selectivity was only 20% in the reaction catalyzed by Au/AC *(606,612–614,619)*, the selectivity was improved to 60% at 93% conversion when carbon nanotubes were used as a support *(75)*.

MOXA is a fully oxidized C_3 product and can be used as a monomer to produce poly(ketomalonate) *(620)*. Taarning *et al. (621)* reported that dimethyl mesoxalate was obtained in the reactions catalyzed by Au/TiO_2 and Au/Fe_2O_3, with a selectivity of 89% at full conversion. Shen *et al. (622)* reported that LA could be obtained with a selectivity of 74% at a slightly higher temperature (363 K) and lower O_2 partial pressure than those for the GLA production.

7.7.3 5-Hydroxymethylfurfural

Hexose monosaccharides such as glucose and fructose are dehydrated to give 5-hydroxymethylfurfural (HMF) in the presence of acid catalysts. This compound can be further converted into high-value chemicals such as 2,5-furandicarboxylic acid (FDA), levulinic acid (LVA), and γ-valerolactone (GVL) (Scheme 1.20). FDA and its esters are regarded as potential replacements of terephthalic acid, which is used as a monomer for the manufacture of polyethylene terephthalate (PET). Supported gold catalysts have been found to be active in the aerobic oxidation of HMF to FDA and its methyl ester *(623–628)*. Because this conversion involves two oxidation reactions (oxidation of formyl and hydroxyl groups), harsh reaction conditions are required to carry out the second oxidation—for example, high temperatures with base. Recently, the use of basic HT as a support for gold NPs led to the oxidation of HMF to FDA with a high selectivity, >99%, at complete conversion without additional base *(629)*.

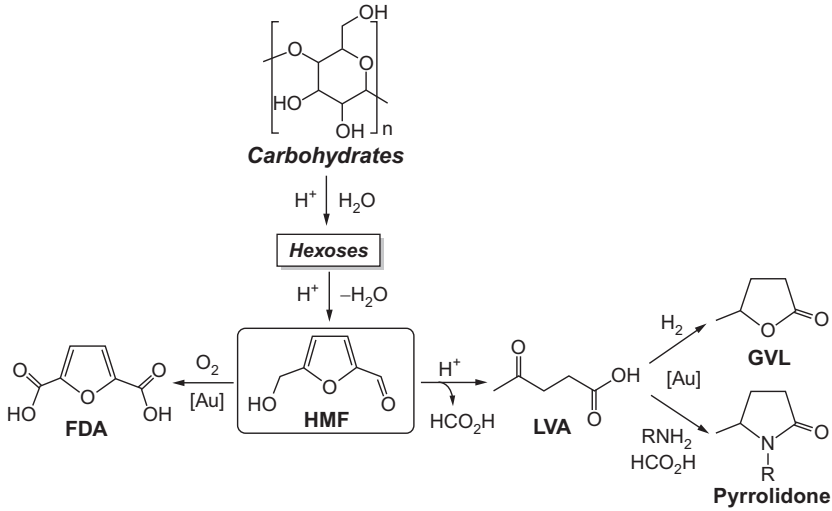

Scheme 1.20 Transformations of carbohydrates into valuable chemicals via HMF.

LVA and GVL are derived from HMF, by acid-catalyzed hydrolysis and that hydrolysis followed by reduction in H_2, respectively (Scheme 1.20). The hydrolysis of HMF produces LVA together with an equimolar amount of formic acid. Du *et al.* *(630)* demonstrated the reduction of LVA by using formic acid as a hydrogen source in the conversion catalyzed by Au/ZrO_2. GVL was obtained from LVA in a 99% yield in the conversion catalyzed by Au/ZrO_2 at 423 K for 6 h. Combining the acid-catalyzed hydrolysis of carbohydrates and the subsequent gold-catalyzed reduction gave GVL with yields of 33–60%. Gold NPs assisted the decomposition of formic acid into H_2 and CO_2.

Succinic acid, which is also an alternative feedstock derived from glucose, was transformed into γ-butyrolactone with H_2 and into pyrrolidone in the reaction with amine on Au/TiO_2 *(631)*. However, these transformations require high temperatures (>423 K).

7.8. One-pot reactions

Performing multiple reactions in a single reactor with solid catalysts offers great potential to reduce wastes, simplify purification processes, and save energy. Gold catalysts exhibit excellent selectivity in reactions such as alcohol oxidation and alcohol hydrogenations, even when other reactive functional groups coexist in the same molecules—thus facilitating efficient one-pot reactions.

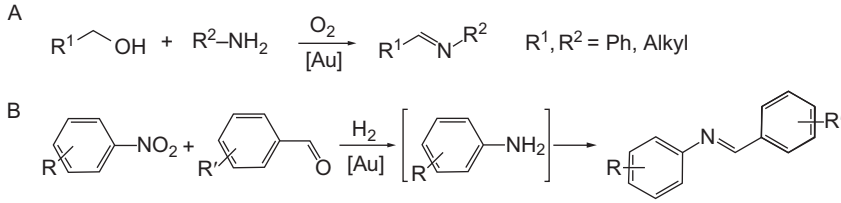

Scheme 1.21 One-pot imine synthesis by the selective oxidation of alcohols (A) *(524,632)* and by the selective hydrogenation of nitrobenzene (B) *(633)*.

7.8.1 Synthesis of imines

Supported gold catalysts have been found to be efficient for oxidation of alcohols even in the presence of amines. Once aldehyde is formed, it reacts with amine to form hemiaminal followed by dehydration to yield imine (Scheme 1.21A) *(524,632)*. In this reaction, the oxidative coupling of two amine molecules should be avoided when there are α-H groups in the primary amine. Supported gold catalysts gave high selectivities to the corresponding imine. Oxime can be obtained by using hydroxylamine instead of a primary amine *(634)*. Another one-pot synthetic route for imine has been proposed by the use of nitroarenes with aldehydes as substrates—by selective hydrogenation (Scheme 1.21B) *(633)*. In the first reaction, Au/TiO_2 selectively hydrogenates the NO_2 groups, leaving C—O groups intact. Aniline derivatives react with aldehydes to produce imine. In this catalytic system, imine is not hydrogenated until the nitro groups are completely reduced, resulting in high selectivities to imine.

7.8.2 N-Alkylation for secondary amine synthesis

N-Alkylation of primary amines with alcohols to produce secondary amines proceeds by three reactions in one pot: (1) the dehydrogenation of alcohol to aldehyde, (2) the condensation of aldehyde with primary amine to form imine via a hemiaminal intermediate, and (3) hydrogen transfer to produce secondary amine (Scheme 1.22). The hydrogen generated by reaction (1) is stored as gold hydride and can be used for reaction (3) so that neither O_2 nor H_2 is necessary and water is the only by-product. Supported gold catalyzes N-alkylation in the presence of N_2 *(516,524,635–637)*. However, excess primary amine, Lewis acid, or base was required in some cases *(524,635)*. Minimizing the size of the gold particles *(637)* and the selection of proper supports enabled N-alkylation under mild conditions without additives. Gold NPs supported on ZrO_2 were found to give a

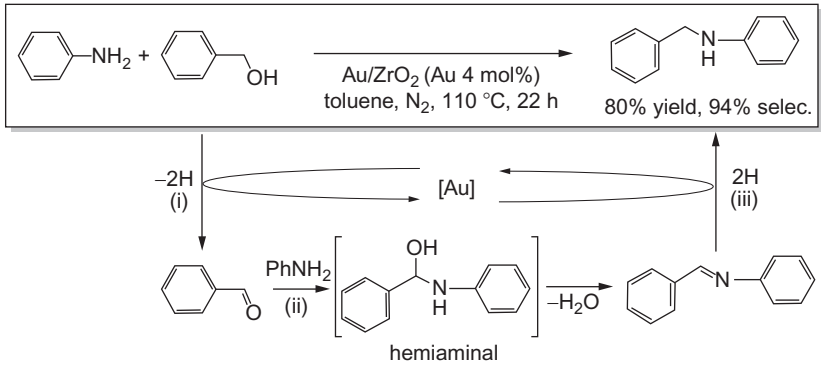

Scheme 1.22 N-Alkylation of primary amine with alcohol to produce secondary amine *(516)*.

secondary amine selectivity of 94% when equimolar amounts of primary amine and alcohol were used under ambient pressure of N_2 *(516)*.

7.8.3 Amide synthesis

In the selective oxidation of alcohol in the presence of amine, if catalysts can drive the oxidation of OH in hemiaminal rather than the dehydration to give imine, then amide can be obtained in a one-pot reaction (Scheme 1.23) *(638–643)*. When methanol was used as the reactant alcohol, formamides were obtained via the formation of methyl formate as an intermediate when the solvent was methanol *(641)* or formamide when the solvent was aqueous methanol *(642,643)*. The one-pot synthesis of amide by the oxidation of amine to imine followed by the hydration of imine was also proposed to occur in the presence of gold powder and silica gel *(644)*; gold worked as an oxidation catalyst and silica gel accelerated the hydration. This procedure enables the facile synthesis of five-, six-, and seven-membered cyclic amides, which are useful intermediates for nylon production from cyclic amines (Scheme 1.24).

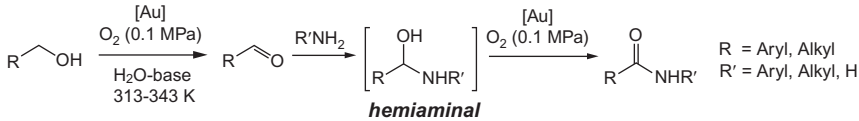

Scheme 1.23 One-pot synthesis of amide from alcohols and amines.

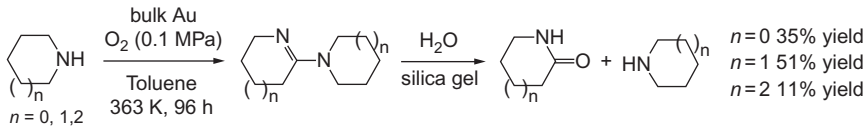

Scheme 1.24 One-pot amide synthesis by the oxidation of amines to imines followed by the hydration of imine in the presence of gold catalyst and silica gel *(644)*.

7.8.4 Other reactions

One-pot sequential synthesis of indoles has been performed by the hydrogenation of nitroarenes and the subsequent intramolecular hydroamination (Scheme 1.25) *(586)*. H_2 at a partial pressure of 1 atm. and an increase in the temperature were necessary for the second cyclization reaction. Aromatic dicarbamate, which can be used as a monomer for the synthesis of polyurethane, was obtained by the one-pot hydrogenation of dinitroarenes and carbamoylation with dimethyl carbonate (Scheme 1.26) *(645)*. Cerium oxide (CeO_2) catalyzes the carbamoylation, but the deposition of gold NPs improved the dicarbamate yield.

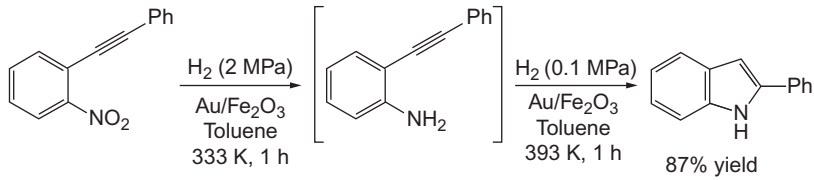

Scheme 1.25 One-pot sequential indole synthesis *(586)*.

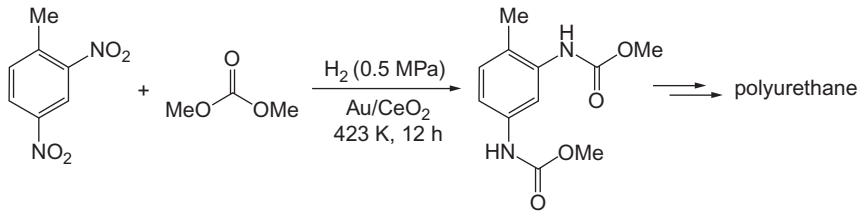

Scheme 1.26 One-pot synthesis of dicarbamate *(645)*.

8. CONCLUSIONS AND PROSPECTS

Highly dispersed gold exhibits an enormous variety of catalytic properties for reactions including oxidation, hydrogenation, coupling, and numerous others. When one takes into account the capability of gold catalysts in room-temperature oxidation, the unique selectivity, and the subtle roles of water in the catalysis, one imagines that gold catalysts may become major players in green and sustainable chemistry. In addition to gold NPs with diameters of 2–5 nm, tiny clusters having specific numbers of gold atoms may be expected to show unique catalytic properties for targeted reactions that are considered to hardly take place in the presence

of conventional catalysts. Selection of the support materials is also crucial because it defines the bonding strength with gold clusters and affects their three-dimensional structures much more than those of gold NPs. As has been shown by the example of direct propylene epoxidation with molecular oxygen alone, gold clusters can provide new catalytic routes to stoichiometrically simple chemical conversions *(375,376)*.

8.1. Size and structure specificity

An emerging approach is to discover magic numbers and structures of gold to provide novel catalytic activities and selectivities. Tsukuda *et al.* *(646)* prepared gold clusters stabilized by polymers—with one-atom resolution—and measured the catalytic activity for the aerobic oxidation of alcohols as a function of the number of gold atoms. They also deposited gold clusters on hydroxyapatite and found that 39-atom clusters exhibited the highest catalytic activity in the aerobic oxidation of cyclohexane *(647)*. For predicting magic numbers of Au atoms for a specific reaction, the interplay between experiment and theory is expected to be especially fruitful.

The next challenge to be faced might be the creation of gold catalysts with specific selectivities tailored to individual reactants, functional groups, or/and products. Many gold cluster compounds with defined numbers of atoms have already been synthesized by using phosphine as a ligand, for example, $Au_{11}(PPh_3)_8Cl_3$ *(648)*, $Au_{55}(PPh_3)_{12}Cl_{l6}$ *(649)*, and $Au_{101}(PPh_3)_{21}Cl_5$ *(650)*. For monodisperse gold NPs, a thiol ligand, $SCH_2(CH_2)_{10}CH_3$ *(651)* is used to stabilize the clusters. It is critical to remove these organic ligands while preventing the initially present gold cluster frames from aggregating. Fortunately, it was found that oxygen plasma at room temperature combined with calcination in air at 573 K could be applied without serious coagulation *(652,653)*.

Another topic of great interest is single gold atoms *(654)* or clusters *(655)* incorporated in the small cages of zeolites. Until now, atomic species of gold were reported to be less active than metallic NPs, but it was a story restricted to CO oxidation. If catalytic tests are extended to address selectivity aspects, atomic gold may be expected to exhibit unique selectivity in oxidation and hydrogenation.

8.2. Creative design of supports

Another approach involves the creative designing of supports by means of morphology control; incorporation of functional groups; control of acid–base properties, electrical conductivity, oxygen absorption–discharge properties; and so on. The surface atomic configuration of a support depends

markedly on the crystal structure and exposed crystal planes and therefore affects the contact strength of supported gold clusters, resulting in various cluster shapes. For example, the (110) plane of Co_3O_4 exposes catalytically active Co^{3+} ions, whereas the (111) and (100) planes expose only Co^{2+} ions *(656,657)*. Another example is polymer-incarcerated gold clusters which exhibit excellent catalytic performance depending on the size of gold clusters and cooperative functional groups in the polymer *(523)*.

8.3. Stability of clusters

A serious constraint to metal cluster catalysts is the chemical and thermal stability during catalytic reactions. Concerning chemical stability, Gibbs free energies for the formation of metal oxides from palladium, platinum, silver, and gold are −130, −168, −22.4, and +53.3 kJ mol^{-1} of O_2, respectively. Only gold among these metals does not spontaneously form oxides. Consequently, gold clusters present advantages over the clusters of other noble metals.

As for thermal stability, gold is inferior to the other noble metals because its melting point is 1336 K, lower than that of palladium and platinum by 492 and 710 K, respectively. The melting point of gold clusters is markedly lowered as the clusters become smaller: 649 K at a diameter of 3.2 nm; 495 K at a diameter of 2.3 nm; and 592 K at diameters of 2.0, 1.5, and 1.2 nm *(658)*. It appears that the melting point does not decrease monotonically as the clusters become smaller, but instead levels off at approximately 592 K. Indeed, even after propylene epoxidation at 473 K for 17 h, gold clusters smaller than 2 nm in diameter were largely retained *(375)*. If the bonding strength of gold clusters with the support is not weak (the selection of the support is important), the gold clusters can be stable enough during catalysis provided that the reaction temperature is below 473 K. It is fortunate that most reactions on supported gold catalysts take place in the presence of gas and liquid phases at temperatures below about 473 K.

8.4. Promoting action of water

It is beneficial that water is indispensable enhancing the catalytic activity of supported gold NPs for room-temperature oxidation of CO *(97,246)*. It is also surprising that PO can be produced on Au/TS-1 catalysts only when water is added to the propylene and oxygen mixtures *(375)*. DFT calculations led to a scheme showing that water and oxygen molecules adsorb on a gold cluster and then react with each other to form hydroperoxide and OH

(329). The hydroperoxo species are assumed to react with CO to form CO_2 and with propylene to produce PO *(375)*:

$$H_2O + O_2 \rightarrow OOH^* + OH^* \quad [1.3]$$

$$CO + OOH^* \rightarrow CO_2 + OH^* \quad [1.4]$$

where * represents a site on the gold surface.

In the aerobic oxidation of glucose in the presence of aqueous alkali solutions, the rate is extremely high—the rate per exposed surface Au atom is approximately $50\ s^{-1}$ *(83)*, which is one to two orders of magnitude greater than that for CO oxidation with gas-phase reactants. Such a high rate can be understood if molecular oxygen regenerates hydroxide ions and does not dissociate into atomic oxygen *(659)*. Because the promoting effect of water appears to be closely related to the basic conditions, detailed work is needed to elucidate the effects of acidity and basicity.

ACKNOWLEDGMENT

We are indebted to Mayumi Morikawa, who worked hard to make the references in this chapter complete.

REFERENCES

1. Holmyard, E.J. *Alchemy*. Penguin Books: London, 1957.
2. Haruta, M.; Yamada, N.; Kobayashi, T.; Iijima, S. *J. Catal.* **1989**, *115*, 301–309.
3. Hutchings, G.J. *J. Catal.* **1985**, *96*, 292–295.
4. Nkosi, B.; Coville, J.; Hutchings, G.J. *Appl. Catal.* **1988**, *43*, 33–39.
5. Hayashi, T.; Tanaka, K.; Haruta, M. *J. Catal.* **1998**, *178*, 566–575.
6. Prati, L.; Rossi, M. *J. Catal.* **1998**, *176*, 552–560.
7. Bond, G.C.; Louis, C.; Thompson, D. *Catalysis by Gold*. Imperial College Press: London, 2006.
8. Corti, C.; Holliday, R. *Gold Science and Applications*. CRC Press: Boca Raton, 2010.
9. *Faraday Discussions Volume 152 Gold*. Royal Society of Chemistry: Cambridge, 2011.
10. Louis, C.; Pluchery, O. *Gold Nanoparticles for Physics, Chemistry and Biology*. World Scientific: Singapore, 2012.
11. Hashmi, A.S.K.; Toste, F.D. *Modern Gold Catalyzed Synthesis*. Wiley-VCH: Weinheim, 2012.
12. Toste, F.D.; Michelet, V. *Gold Catalysis: An Homogeneous Approach*. World Scientific: Singapore, 2012; scheduled for publication in 2013.
13. Bond, G.C.; Thompson, D. *Catal. Rev. Sci. Eng.* **1999**, *41*, 319–388.
14. Haruta, M.; Date, M. *Appl. Chem. A Gen.* **2001**, *222*, 427–437.
15. Hutchings, G.J. *Catal. Today* **2005**, *100*, 55–61.
16. Hashmi, A.S.K.; Hutchings, G.J. *Angew. Chem. Int. Ed. Engl.* **2006**, *45*, 7896–7936.
17. Min, B.K.; Friend, C.M. *Chem. Rev.* **2007**, *107*, 2709–2724.
18. Ma, Z.; Dai, S. *Nano Res.* **2011**, *4*, 3–32.
19. Haruta, M. *Catal. Today* **1997**, *36*, 153–166.
20. Delannoy, L.; El Hassen, N. El; Musi, A.; To, N.N.L.; Krafft, J.-M.; Louis, C. *J. Phys. Chem. B* **2006**, *110*, 22471–22478.

21. Li, W.-C.; Comotti, M.; Schüth, F. *J. Catal.* **2006**, *237*, 190–196.
22. Bowker, M.; Nuhu, A.; Soares, J. *Catal. Today* **2007**, *122*, 245–247.
23. Baatz, C.; Decker, N.; Prüβe, U. *J. Catal.* **2008**, *258*, 165–169.
24. Yuan, Y.; Asakura, K.; Wan, H.; Tsai, K.; Iwasawa, Y. *Chem. Lett.* **1996**, 755–756.
25. Yuan, Y.; Kozlova, A.P.; Asakura, K.; Wan, H.; Tsai, K.; Iwasawa, Y. *J. Catal.* **1997**, *170*, 191–199.
26. Choudhary, T.V.; Sivadinarayana, C.; Chusuei, C.C.; Datye, A.K.; Fackler, J.P., Jr.; Goodman, D.W. *J. Catal.* **2002**, 247–255.
27. Okumura, M.; Haruta, M. *Chem. Lett.* **2000**, 396–397.
28. Guzman, J.; Gates, B.C. *Angew. Chem. Int. Ed. Engl.* **2003**, *42*, 690–693.
29. Tian, B.; Zhang, J.; Tong, T.; Chen, F. *Appl. Catal. B* **2008**, *79*, 394–401.
30. Bonelli, R.; Lucarelli, C.; Pasini, T.; Liotta, L.F.; Zacchini, S.; Albonetti, S. *Appl. Catal. A Gen.* **2011**, *400*, 54–60.
31. Sakurai, H.; Takeuchi, T.; Koga, K.; Kiuchi, M. International Patent Application No. PCT/JP2012/060494, National Institute of Advanced Industrial Science and Technology (AIST).
32. Haruta, M.; Kobayashi, T.; Sano, H.; Yamada, N. *Chem. Lett.* **1987**, *16*, 405–408.
33. Haruta, M.; Kageyama, H.; Kamijo, N.; Kobayashi, T.; Delannay, F. *Stud. Surf. Sci. Catal.* **1988**, *44*, 33–42.
34. Herzing, A.A.; Kiely, C.J.; Carley, A.F.; Landon, P.; Hutchings, G.J. *Science* **2008**, *321*, 1331–1335.
35. Takei, T.; Okuda, I.; Bando, K.K.; Akita, T.; Haruta, M. *Chem. Phys. Lett.* **2010**, *493*, 207–211.
36. Tsubota, S.; Cunningham, D.A.H.; Bando, Y.; Haruta, M. *Stud. Surf. Sci. Catal.* **1995**, *91*, 227–235.
37. Wolf, A.; Schüth, F. *Appl. Catal. A Gen.* **2002**, *226*, 1–13.
38. Moreau, F.; Bond, G.C.; Taylor, A.O. *J. Catal.* **2005**, *231*, 105–114.
39. Moreau, F.; Bond, G.C. *Catal. Today* **2007**, *122*, 260–265.
40. Qian, K.; Fang, J.; Huang, W.; He, B.; Jiang, Z.; Ma, Y.; Wei, S. *J. Mol. Catal. A Chem.* **2010**, *320*, 97–105.
41. Zanella, R.; Sandoval, A.; Santiago, P.; Basiuk, V.A.; Saniger, J.M. *J. Phys. Chem. B* **2006**, *110*, 8559–8565.
42. Zhu, H.; Ma, Z.; Clark, J.C.; Pan, Z.; Overbury, S.H.; Dai, S. *Appl. Catal. A Gen.* **2007**, *326*, 89–99.
43. Zhu, H.; Liang, C.; Yan, W.; Overbury, S.H.; Dai, S. *J. Phys. Chem. B* **2006**, *110*, 10842–10848.
44. Gutierrez, L.-F.; Hamoudi, S.; Belkacemi, K. *Appl. Catal. A Gen.* **2012**, *425–426*, 213–223.
45. Somodi, F.; Borbath, I.; Hegedus, M.; Tompos, A.; Sajo, I.E.; Szegedi, A.; Rojas, S.; Fierro, J.L.G.; Margitfalvi, J.L. *Appl. Catal. A Gen.* **2008**, *347*, 216–222.
46. Kirichenko, O.A.; Kapustin, G.I.; Nissenbaum, V.D.; Tkachenko, O.P.; Poluboyarov, V.A.; Tarasov, A.L.; Kucherov, A.V.; Kustov, L.M. *Stud. Surf. Sci. Catal.* **2010**, *175*, 537–540.
47. Zanella, R.; Giorgio, S.; Henry, C.R.; Louis, C. *J. Phys. Chem. B* **2002**, *106*, 7634–7642.
48. Zanella, R.; Delannoy, L.; Louis, C. *Appl. Catal. A Gen.* **2005**, *291*, 62–72.
49. Milone, C.; Trapani, M.; Zanella, R.; Piperopolulos, E.; Galvagno, S. *Mater. Res. Bull.* **2010**, *45*, 1925–1933.
50. Miquel, P.; Granger, P.; Jaglap, N.; Umbarkar, S.; Dongare, M.; Dujardin, C. *J. Mol. Catal. A Chem.* **2010**, *322*, 90–97.
51. Wang, L.-C.; Huang, X.-S.; Liu, Q.; Liu, Y.-M.; Cao, Y.; He, H.-Y.; Fan, K.-N.; Zhuang, J.-H. *J. Catal.* **2008**, *259*, 66–74.

52. Wang, L.-C.; Liu, Y.-M.; Chen, M.; Cao, Y.; He, H.-Y.; Fan, K.-N. *J. Phys. Chem. C* **2008**, *112*, 6981–6987.
53. Longo, A.; Liotta, L.F.; Carilo, F.; Venezia, A.M.; Martorana, A. *Chem. Mater.* **2010**, *22*, 3952–3960.
54. Khoudiakov, M.; Gupta, M.C.; Deevi, S. *Appl. Catal. A Gen.* **2005**, *291*, 151–161.
55. Delannoy, L.; Fajerwerg, K.; Lakshmanan, P.; Potivin, C.; Methivier, C.; Louis, C. *Appl. Catal. B* **2010**, *94*, 117–124.
56. Rio, E.; Blanco, G.; Collins, S.; Haro, M.L.; Chen, X.; Delgado, J.J.; Calvino, J.J.; Bernal, S. *Top. Catal.* **2011**, *54*, 931–940.
57. Huang, J.; Wang, L.-C.; Liu, Y.-M.; Cao, Y.; He, H.-Y.; Fan, K.-N. *Appl. Catal. B* **2011**, *101*, 560–569.
58. Ishida, T.; Kuroda, K.; Kinoshita, N.; Minagawa, W.; Haruta, M. *J. Colloid Interface Sci.* **2008**, *323*, 105–111.
59. Kuroda, K.; Ishida, T.; Haruta, T. *J. Mol. Catal. A Chem.* **2009**, *298*, 7–11.
60. Ishida, T.; Okamoto, S.; Makiyama, R.; Haruta, M. *Appl. Catal. A Gen.* **2009**, *353*, 243–248.
61. Villa, A.; Chan-Thaw, C.E.; Prati, L. *Appl. Catal. B* **2010**, *96*, 541–547.
62. Sunagawa, Y.; Yamamoto, K.; Takahashi, H.; Muramatsu, A. *Catal. Today* **2008**, *132*, 81–87.
63. Prati, L.; Martra, G. *Gold Bull.* **1999**, *32*, 96–101.
64. Porta, F.; Prati, L.; Rossi, M.; Coluccia, S.; Martra, G. *Catal. Today* **2000**, *61*, 165–172.
65. Önal, Y.; Schimpf, S.; Claus, P. *J. Catal.* **2004**, *223*, 122–133.
66. Dimitratos, N.; Villa, A.; Bianchi, C.L.; Prati, L.; Makkee, M. *Appl. Catal. A Gen.* **2006**, *311*, 185–192.
67. Hammer, N.; Kvande, I.; Xu, X.; Gunnarsson, V.; Tøtdal, B.; Chen, D.; Rønning, M. *Catal. Today* **2007**, *123*, 245–256.
68. Zhong, Z.; Lin, J.; Teh, S.-P.; Teo, J.; Dautzenberg, F.M. *Adv. Funct. Mater.* **2007**, *17*, 1402–1408.
69. Zhan, G.; Du, M.; Huang, J.; Li, Q. *Catal. Commun.* **2011**, *12*, 830–833.
70. Alhumaimess, M.; Lin, Z.; Weng, W.; Dimitratos, N.; Dummer, N.F.; Taylor, S.H.; Bartley, J.K.; Kiely, C.J.; Hutchings, G.J. *ChemSusChem* **2012**, *5*, 125–131.
71. Biella, S.; Porta, F.; Prati, L.; Rossi, M. *Catal. Lett.* **2003**, *90*, 23–29.
72. Dimitratos, N.; Porta, F.; Prati, L. *Appl. Catal. A Gen.* **2005**, *291*, 210–214.
73. Bawaked, S.; Dummer, N.F.; Dimitratos, N.; Bethell, D.; He, Q.; Kiely, C.J.; Hutchings, G.J. *Green Chem.* **2009**, *11*, 1037–1044.
74. Li, B.; He, P.; Yi, G.; Lin, H.; Yuan, Y. *Catal. Lett.* **2009**, *133*, 33–40.
75. Rodrigues, E.G.; Carabineiro, S.A.C.; Delgado, J.J.; Chen, X.; Pereira, M.F.R.; Orfuäo, J.J.M. *J. Catal.* **2012**, *285*, 83–91.
76. Okumura, M.; Nakamura, S.; Tsubota, S.; Nakamura, T.; Azuma, M.; Haruta, M. *Catal. Lett.* **1998**, *51*, 53–58.
77. Chen, Y.-J.; Yeh, C.-T. *J. Catal.* **2001**, *200*, 59–68.
78. Okumura, M.; Tsubota, M.; Haruta, M. *J. Mol. Catal. A Chem.* **2003**, *199*, 73–84.
79. Guzman, J.; Gates, B.C. *Langmuir* **2003**, *19*, 3897–3903.
80. Moroz, B.L.; Pyrjaev, P.A.; Zaikovskii, V.I.; Bukhtiyarov, V.I. *Catal. Today* **2009**, *144*, 292–305.
81. Hermes, S.; Schröter, M.-K.; Schmid, R.; Khodeir, L.; Muhler, M.; Tissler, A.; Fischer, R.W.; Fischer, R.A. *Angew. Chem. Int. Ed. Engl.* **2005**, *44*, 6237–6241.
82. Ishida, T.; Nagaoka, M.; Akita, T.; Haruta, M. *Chem. Eur. J.* **2008**, *14*, 8456–8460.
83. Ishida, T.; Kinoshita, N.; Okatsu, H.; Akita, T.; Haruta, M. *Angew. Chem. Int. Ed. Engl.* **2008**, *47*, 9265–9268.
84. Ishida, T.; Watanabe, H.; Bebeko, T.; Akita, T.; Haruta, M. *Appl. Catal. A Gen.* **2010**, *377*, 42–46.

85. Jiang, H.-L.; Lin, Q.-P.; Akita, T.; Liu, B.; Ohashi, H.; Oji, H.; Honma, T.; Takei, T.; Haruta, M.; Xu, Q. *Chem. Eur. J.* **2011**, *17*, 78–81.
86. Brey, L. A.; Wood, T. E.; Buccellato, G. M.; Jones, M.E.; Chamberlain, C. S.; Siedle, A. R. WO Patent 2005/030382, 3M Innovative Properties Co., 2005.
87. Brady, J. T.; Brey, L. A.; Buccellato, G. M.; Chamberlain, C. S.; Huberty, J. S.; Siedle, A. R.; Wood, T. E. WO Patent 2006/074126 A2, 3M Innovative Properties Co., 2006.
88. Corti, C.W.; Holliday, R.J.; Thompson, D.T. *Top. Catal.* **2007**, *44*, 331–343.
89. Veith, G.M.; Lupini, A.R.; Dudney, N.J. *J. Phys. Chem. C* **2009**, *113*, 269–280.
90. Cojocaru, B.; Neatu, S.; Sacaliuc-Parvulescu, E.; Levy, F.; Parvulescu, V.I.; Garcia, H. *Appl. Catal. B* **2011**, *107*, 140–149.
91. Veith, G.M.; Lupini, A.R.; Rashkeev, S.; Pennycook, S.J.; Mullins, D.R.; Schwartz, V.; Bridges, C.A.; Dudney, N.J. *J. Catal.* **2009**, *262*, 92–101.
92. Zheng, X.; Veith, G.M.; Redekop, E.; Lo, C.S.; Yablonsky, G.S.; Gleaves, J.T. *Ind. Eng. Chem. Res.* **2010**, *49*, 10428–10437.
93. Veith, G.M.; Lupini, A.R.; Pennycook, S.J.; Ownby, G.W.; Dudney, N.J. *J. Catal.* **2005**, *231*, 151–158.
94. Veith, G.M.; Lupini, A.R.; Pennycook, S.J.; Villa, A.; Prati, L.; Dudney, N.J. *Catal. Today* **2007**, *122*, 248–253.
95. Singh, J.A.; Overbury, S.H.; Dudney, N.J.; Li, M.; Veith, G.M. *ACS Catal.* **2012**, *2*, 1138–1146.
96. Guo, H.; Kemell, M.; Al-Hunaiti, A.; Rautiainen, S.; Leskelä, M.; Repo, T. *Catal. Commun.* **2011**, *12*, 1260–1264.
97. Fujitani, T.; Nakamura, I.; Akita, T.; Okumura, M.; Haruta, M. *Angew. Chem. Int. Ed. Engl.* **2009**, *48*, 9515–9518.
98. Fujitani, T.; Nakamura, I. *Angew. Chem. Int. Ed. Engl.* **2011**, *50*, 10144–10147.
99. Iijima, S. *Optik* **1977**, *48*, 193–214.
100. Akita, T.; Tanaka, K.; Tsubota, S.; Haruta, M. *J. Electron Microsc.* **2000**, *49*, 657–662.
101. Akita, T.; Okumura, M.; Tanaka, K.; Kohyama, M.; Tsubota, S.; Haruta, M. *J. Electron Microsc.* **2005**, *54*(Suppl. 1), i81–i85.
102. Uzun, A.; Ortalan, V.; Hao, Y.; Browning, N.D.; Gates, B.C. *J. Phys. Chem. C* **2009**, *113*, 16847–16849.
103. Batson, P.E. *Microsc. Microanal.* **2008**, *14*, 89–97.
104. Treacy, M.M.J.; Rice, S.B. *J. Microsc.* **1989**, *156*, 211–234.
105. Wang, Z.W.; Toikkanen, O.; Yin, F.; Li, Z.Y.; Quinn, B.M.; Palmer, R.E. *J. Am. Chem. Soc.* **2010**, *132*, 2854–2855.
106. Akita, T.; Lu, P.; Ichikawa, S.; Tanaka, K.; Haruta, M. *Surf. Interface Anal.* **2001**, *31*, 73–78.
107. Akita, T.; Tanaka, T.; Kohyama, M.; Haruta, M. *Mater. Res. Soc. Symp. Proc.* **2008**, *1026*, C17–C.
108. Zanella, R.; Louis, C. *Catal. Today* **2005**, *107–108*, 768–777.
109. Okazaki, K.; Morikawa, Y.; Tanaka, S.; Tanaka, K.; Kohyama, M. *Phys. Rev. B* **2004**, *69*, 235404–235408.
110. Akita, T.; Tanaka, K.; Kohyama, M. *J. Mater. Sci.* **2008**, *43*, 3917–3922.
111. Akita, T.; Tanaka, T.; Kohyama, M.; Haruta, M. *Catal. Today* **2007**, *122*, 233–238.
112. Allard, L.F.; Borisevich, A.; Deng, W.; Si, R.; Flytzani-Stephanopoulos, M.; Overbury, S.H. *J. Electron Microsc.* **2009**, *58*, 199–212.
113. Allard, L.F.; Flytzani-Stephanopoulos, M.; Overbury, S.H. *Microsc. Microanal.* **2010**, *16*, 375–385.
114. Iijima, S.; Ichihashi, T. *Jpn. J. Appl. Phys.* **1985**, *24*, L125–L128.
115. Iijima, S.; Ichihashi, T. *Phys. Rev. Lett.* **1986**, *56*, 616–619.
116. Smith, D.J.; Petford-Long, A.K.; Wallenberg, L.R.; Bovin, J.O. *Science* **1986**, *233*, 872–875.

117. Ajayan, P.M.; Marks, L.D. *Nature* **1989**, *338*, 139–141.
118. Ajayan, P.M.; Marks, L.D. *Phys. Rev. Lett.* **1989**, *63*, 279–282.
119. Marks, L.D. *Rep. Prog. Phys.* **1994**, *57*, 603–649.
120. Ascencio, J.A.; Gutierrez-Wing, C.; Espinosa, M.E.; Marin, M.; Tehuacanero, S.; Zorrilla, C.; José-Yacamán, M. *Surf. Sci.* **1998**, *396*, 349–368.
121. Koga, K.; Sugawara, K. *Surf. Sci.* **2003**, *529*, 23–35.
122. Haruta, M. *Faraday Discuss.* **2011**, *152*, 11–32.
123. Giorgio, S.; Chapton, C.; Henry, C.R.; Nihoul, G.; Penisson, J.M. *Philos. Mag. A* **1991**, *64*, 87–96.
124. Giorgio, S.; Henry, C.R.; Pauwels, B.; Van Tendeloo, G. *Mater. Sci. Eng. A* **2001**, *297*, 197–202.
125. Cosandey, F.; Madey, T.E. *Surf. Rev. Lett.* **2001**, *8*, 73–93.
126. Akita, T.; Tanaka, K.; Kohyama, M.; Haruta, M. *Surf. Interface Anal.* **2008**, *40*, 1760–1763.
127. Sivaramakrishnan, S.; Wen, J.; Scarpelli, M.E.; Pierce, B.J.; Zuo, J.M. *Phys. Rev. B* **2010**, *82*, 195421.
128. Akita, T.; Okumura, M.; Tanaka, K.; Kohyama, M.; Haruta, M. *J. Mater. Sci.* **2005**, *40*, 3101–3106.
129. Akita, T.; Tanaka, S.; Tanaka, K.; Haruta, M.; Kohyama, M. *J. Mater. Sci.* **2011**, *46*, 4384–4391.
130. Cochrane, H.D.; Hutchison, J.L.; White, D.; Parkinson, G.M.; Dupas, C.; Scott, A.J. *Ultramicroscopy* **1990**, *34*, 10–16.
131. Majimel, J.; Lamirand-Majimel, M.; Moog, I.; Feral-Martin, C.; Tréguer-Delapierre, M. *J. Phys. Chem. C* **2009**, *113*, 9275–9283.
132. Akita, T.; Okumura, M.; Tanaka, K.; Kohyama, M.; Haruta, M. *Catal. Today* **2006**, *117*, 62–68.
133. Hasegawa, T.; Kobayashi, K.; Ikarashi, N.; Takayanagi, K.; Yagi, K. *Jpn. J. Appl. Phys.* **1986**, *25*, L366–L368.
134. Kawasaki, T.; Takai, T.; Shimizu, R. *Appl. Phys. Lett.* **2001**, *79*, 3509–3511.
135. Shibata, N.; Goto, A.; Matsunaga, K.; Mizoguchi, T.; Findlay, S.D.; Yamamoto, T.; Ikuhara, Y. *Phys. Rev. Lett.* **2009**, *102*, 136105.
136. Gai, P.L.; Boyes, E.D. *Microsc. Res. Tech.* **2009**, *72*, 153–164.
137. Hansen, P.L.; Wagner, J.B.; Helveg, S.; Rostrup-Nielsen, J.R.; Clausen, B.S.; Topsøe, H. *Science* **2002**, *295*, 2053–2055.
138. Yoshida, H.; Matsuura, K.; Kuwauchi, Y.; Kohno, H.; Shimada, S.; Haruta, M.; Takeda, S. *Appl. Phys. Expr.* **2011**, *4*, 065001.
139. Giorgio, S.; Sao Joao, S.; Nitsche, S.; Chaudanson, D.; Sitja, G.; Henry, C.R. *Ultramicroscopy* **2006**, *106*, 503–507.
140. Giorgio, S.; Cabié, M.; Henry, C.R. *Gold Bull.* **2008**, *41*, 167–173.
141. Ueda, K.; Kawasaki, T.; Hasegawa, H.; Tanji, T.; Ichihashi, M. *Surf. Interface Anal.* **2008**, *40*, 1725–1727.
142. Tanaka, T.; Sano, K.; Ando, M.; Sumiya, A.; Sawada, H.; Hosokawa, F.; Okunishi, E.; Kondo, Y.; Takayanagi, K. *Surf. Sci.* **2010**, *604*, L75–L78.
143. Uchiyama, T.; Yoshida, H.; Kuwauchi, Y.; Ichikawa, S.; Shimada, S.; Haruta, M.; Takeda, S. *Angew. Chem. Int. Ed. Engl.* **2011**, *50*, 10157–10160.
144. Yoshida, H.; Kuwauchi, K.; Jinschek, J.R.; Sun, K.; Tanaka, S.; Kohyama, M.; Shimada, S.; Haruta, M.; Takeda, S. *Science* **2012**, *335*, 317–319.
145. Okunishi, E.; Ishikawa, I.; Sawada, H.; Hosokawa, F.; Hori, H.; Kondo, Y. *Microsc. Microanal.* **2009**, *15*(Suppl. 2), 164–165.
146. Findlay, S.D.; Saito, T.; Shibata, N.; Sato, Y.; Matsuda, J.; Asano, K.; Akiba, E.; Hirayama, T.; Ikuhara, Y. *Appl. Phys. Expr.* **2010**, *3*, 116603.
147. Ishikawa, R.; Okunishi, E.; Sawada, H.; Kondo, Y.; Hosokawa, F.; Abe, E. *Nat. Mater.* **2011**, *10*, 278–281.

148. González, J.C.; Hernández, J.C.; López-Haro, M.L.; del Río, E.; Delgado, J.J.; Hungría, A.B.; Trasobares, S.; Bernal, S.; Midgley, P.A.; Calvino, J.J. *Angew. Chem. Int. Ed. Engl.* **2009**, *48*, 5313–5315.
149. Hernandez-Garrido, J.C.; Yoshida, K.; Gai, P.L.; Boyes, E.D.; Christensen, C.H.; Midgley, P.A. *Catal. Today* **2011**, *160*, 165–169.
150. Scott, M.C.; Chen, C.C.; Mecklenburg, M.; Zhu, C.; Xu, R.; Ercius, P.; Dahmen, U.; Regan, B.C.; Miao, J. *Nature* **2012**, *483*, 444.
151. Ichikawa, S.; Akita, T.; Okumura, M.; Haruta, M.; Tanaka, K.; Kohyama, M. *J. Electron Microsc.* **2003**, *52*, 21–26.
152. Okazaki, K.; Ichikawa, S.; Maeda, Y.; Haruta, M.; Kohyama, M. *Appl. Catal. A Gen.* **2005**, *291*, 45–54.
153. Akita, T.; Hiroki, T.; Tanaka, S.; Kojima, T.; Kohyama, M.; Iwase, A.; Hori, F. *Catal. Today* **2008**, *131*, 90–97.
154. Ferrer, D.; Blom, D.A.; Allard, L.F.; Mejı´a, S.; Pérez-Tijerina, E.; José-Yacamán, M. *J. Mater. Chem.* **2008**, *18*, 2442–2446.
155. Min, B.K.; Alemozafar, A.R.; Pinnaduwage, D.; Deng, X.; Friend, C.M. *J. Phys. Chem. B* **2006**, *110*, 19833–19838.
156. Gong, J.L.; Ojifinni, R.A.; Kim, T.S.; Stiehl, J.D.; McClure, S.M.; White, J.M.; Mullins, C.B. *Top. Catal.* **2007**, *44*, 57–63.
157. Lazaga, M.A.; Wickham, D.T.; Parker, D.H.; Kastanas, G.N.; Koel, B.E. *ACS Symp. Ser.* **1993**, *523*, 90–109.
158. Outka, D.A.; Madix, R.J. *Surf. Sci.* **1987**, *179*, 351–360.
159. Gottfried, J.M.; Christmann, K. *Surf. Sci.* **2004**, *566–568*, 1112–1117.
160. Kim, J.; Samano, E.; Koel, B.E. *J. Phys. Chem. B* **2006**, *110*, 17512–17517.
161. Samano, E.; Kim, J.; Koel, B.E. *Catal. Lett.* **2009**, *128*, 263–267.
162. Diebold, U. *Surf. Sci. Rep.* **2003**, *48*, 53–229.
163. Chen, M.S.; Goodman, D.W. *Acc. Chem. Res.* **2006**, *39*, 739–746.
164. Meyer, R.; Lemire, C.; Shaikhutdinov, Sh.K.; Freund, H.-J. *Gold Bull.* **2004**, *37*, 72–124.
165. Zhang, L.; Persaud, R.; Madey, T.E. *Phys. Rev. B* **1997**, *56*, 10549–10557.
166. Lai, X.; Clair, T.P.St.; Valden, M.; Goodman, D.W. *Prog. Surf. Sci.* **1998**, *59*, 25–52.
167. Parker, S.C.; Grant, A.W.; Bondzie, V.A.; Campbell, C.T. *Surf. Sci.* **1999**, *441*, 10–20.
168. Guo, Q.L.; Luo, K.; Davis, K.A.; Goodman, D.W. *Surf. Interface Anal.* **2001**, *32*, 161–165.
169. Santra, A.K.; Kolmakov, A.; Yang, F.; Goodman, D.W. *Jpn. J. Appl. Phys.* **2003**, *42*, 4795–4798.
170. Valden, M.; Lai, X.; Goodman, D.W. *Science* **1998**, *281*, 1647–1650.
171. Zhang, L.; Cosandey, F.; Persaud, R.; Madey, T.E. *Surf. Sci.* **1999**, *439*, 73–85.
172. Cosandey, F.; Zhang, L.; Madey, T.E. *Surf. Sci.* **2001**, *474*, 1–13.
173. Lazzari, R.; Renaud, G.; Jupille, J.; Leroy, F. *Phys. Rev. B* **2007**, *76 125412-1–125412-18.*
174. Matthey, D.; Wang, J.G.; Wendt, S.; Matthiesen, J.; Schaub, R.; Lægsgaard, E.; Hammer, B.; Besenbacher, F. *Science* **2007**, *315*, 1692–1696.
175. Haruta, M. *CATTECH* **2002**, *6*, 102–115.
176. Green, I.X.; Tang, W.; Neurock, M.; Yates, J.T., Jr. *Science* **2011**, *333*, 736–739.
177. Widmann, D.; Behm, R.J. *Angew. Chem. Int. Ed. Engl.* **2011**, *50*, 10241–10245.
178. Pyykkö, P. *Chem. Soc. Rev.* **2008**, *37*, 1967–1997.
179. Molina, L.M.; Rasmussen, M.D.; Hammer, B. *J. Chem. Phys.* **2004**, *120*, 7673–7680.
180. Arenz, M.; Landman, U.; Heiz, U. *Chem. Phys. Chem.* **2006**, 7, 1871–1879.
181. Chen, M.S.; Goodman, D.W. *Science* **2004**, *306*, 252–255.
182. Choudhary, T.V.; Goodman, D.W. *Appl. Catal. A* **2005**, *291*, 32–36.
183. Chen, M.S.; Goodman, D.W. *Chem. Soc. Rev.* **2008**, *37*, 1860–1870.

184. Kung, M.C.; Davis, R.J.; Kung, H.H. *J. Phys. Chem. C* **2007**, *111*, 11767–11775.
185. Lopez, N.; Janssens, T.V.W.; Clausen, B.S.; Xu, Y.; Mavrikakis, M.; Bligaard, T.; Nørskov, J.K. *J. Catal.* **2004**, *223*, 232–235.
186. Valden, M.; Pak, S.; Lai, X.; Goodman, D.W. *Catal. Lett.* **1998**, *56*, 7–10.
187. Kung, H.H.; Kung, M.C.; Costello, C.K. *J. Catal.* **2003**, *216*, 425–432.
188. Campbell, C.T.; Grant, A.W.; Starr, D.E.; Parker, S.C.; Bondzie, V.A. *Top. Catal.* **2001**, *14*, 3–51.
189. Lee, S.S.; Fan, C.Y.; Wu, T.P.; Anderson, S.L. *J. Am. Chem. Soc.* **2004**, *126*, 5682–5683.
190. Meier, D.C.; Goodman, D.W. *J. Am. Chem. Soc.* **2004**, *126*, 1892–1899.
191. Tong, X.; Benz, L.; Kemper, P.; Metiu, H.; Bowers, M.T.; Buratto, S.K. *J. Am. Chem. Soc.* **2005**, *127*, 13516–13518.
192. Miller, J.T.; Kropf, A.J.; Zha, Y.; Regalbuto, J.R.; Delannoy, L.; Louis, C.; Bus, E.; van Bokhoven, J.A. *J. Catal.* **2006**, *240*, 222–234.
193. Shaikhutdinov, Sh.K.; Meyer, R.; Naschitzki, M.; Bäumer, M.; Freund, H.-J. *Catal. Lett.* **2003**, *86*, 211–219.
194. Bondzie, V.A.; Parker, S.C.; Campbell, C.T. *Catal. Lett.* **1999**, *63*, 143–151.
195. Kim, T.S.; Stiehl, J.D.; Reeves, C.T.; Meyer, R.J.; Mullins, C.B. *J. Am. Chem. Soc.* **2003**, *125*, 2018–2019.
196. Bondzie, V.A.; Parker, S.C.; Campbell, C.T. *J. Vac. Sci. Technol. A* **1999**, *17*, 1717–1720.
197. Stiehl, J.D.; Kim, T.S.; Reeves, C.T.; Meyer, R.J.; Mullins, C.B. *J. Phys. Chem. B* **2004**, *108*, 7917–7926.
198. Boyen, H.-G.; Kästle, G.; Weigl, F.; Koslowski, B.; Dietrich, C.; Ziemann, P.; Spatz, J.P.; Riethmüller, S.; Hartmann, C.; Möller, M.; Schmid, G.; Garnier, M.G.; Oelhafen, P. *Science* **2002**, *297*, 1533–1536.
199. Lopez, N.; Nørskov, J.K. *J. Am. Chem. Soc.* **2002**, *124*, 11262–11263.
200. Mavrikakis, M.; Stoltze, P.; Nørskov, J.K. *Catal. Lett.* **2000**, *64*, 101–106.
201. Lemire, C.; Meyer, R.; Shaikhutdinov, Sh.K.; Freund, H.-J. *Surf. Sci.* **2004**, *552*, 27–34.
202. Janssens, T.V.W.; Carlsson, A.; Puig-Molina, A.; Clausen, B.S. *J. Catal.* **2006**, *240*, 108–113.
203. Chrétien, S.; Buratto, S.K.; Metiu, H. *Curr. Opin. Solid State Mater. Sci.* **2007**, *11*, 62–75.
204. Janssens, T.V.W.; Clausen, B.S.; Hvolbæk, B.; Falsig, H.; Christensen, C.H.; Bligaard, T.; Nørskov, J.K. *Top. Catal.* **2007**, *44*, 15–26.
205. Hvolbæk, B.; Janssens, T.V.W.; Clausen, B.S.; Falsig, H.; Christensen, C.H.; Nørskov, J.K. *Nano Today* **2007**, *2*, 14–18.
206. Zielasek, V.; Jürgens, B.; Schulz, C.; Biener, J.; Biener, M.M.; Hamza, A.V.; Bäumer, M. *Angew. Chem. Int. Ed. Engl.* **2006**, *45*, 8241–8244.
207. Xu, C.X.; Su, J.X.; Xu, X.H.; Liu, P.P.; Zhao, H.J.; Tian, F.; Ding, Y. *J. Am. Chem. Soc.* **2007**, *129*, 42–43.
208. Fierro-Gonzalez, J.C.; Gates, B.C. *Chem. Soc. Rev.* **2008**, *37*, 2127–2134.
209. Bond, G.C.; Thompson, D.T. *Gold Bull.* **2000**, *33*, 41–51.
210. Centeno, M.A.; Hadjiivanov, K.; Venkov, Tz; Klimev, Hr; Odriozola, J.A. *J. Mol. Catal. A* **2006**, *252*, 142–149.
211. Naya, K.; Ishikawa, R.; Fukui, K. *J. Phys. Chem. C* **2009**, *113*, 10726–10730.
212. Weststrate, C.J.; Resta, A.; Westerström, R.; Lundgren, E.; Mikkelsen, A.; Andersen, J.N. *J. Phys. Chem. C* **2008**, *112*, 6900–6906.
213. Škoda, M.; Cabala, M.; Matolínová, I.; Prince, K.C.; Skála, T.; Šutara, F.; Veltruská, K.; Matolín, V. *J. Chem. Phys.* **2009**, *130*, 034703–1–7.
214. Manzoli, M.; Boccuzzi, F.; Chiorino, A.; Vindigni, F.; Deng, W.; Flytzani-Stephanopoulos, M. *J. Catal.* **2007**, *245*, 308–315.

215. Carrettin, S.; Concepción, P.; Corma, A.; López Nieto, J.M.; Puntes, V.F. *Angew. Chem. Int. Ed. Engl.* **2004**, *43*, 2538–2540.
216. Yoon, B.; Häkkinen, H.; Landman, U.; Wörz, A.S.; Antonietti, J.-M.; Abbet, S.; Judai, K.; Heiz, U. *Science* **2005**, *307*, 403–407.
217. Risse, T.; Shaikhutdinov, S.; Nilius, N.; Sterrer, M.; Freund, H.-J. *Acc. Chem. Res.* **2008**, *41*, 949–956.
218. Campbell, C.T. *Science* **2004**, *306*, 234–235.
219. Carrettin, S.; Hao, Y.; Aguilar-Guerrero, V.; Gates, B.C.; Trasobares, S.; Calvino, J.J.; Corma, A. *Chem. Eur. J.* **2007**, *13*, 7771–7779.
220. Schwartz, V.; Mullins, D.R.; Yan, W.; Chen, B.; Dai, S.; Overbury, S.H. *J. Phys. Chem. B* **2004**, *108*, 15782–15790.
221. Yang, J.H.; Henao, J.D.; Raphulu, M.C.; Wang, Y.; Caputo, T.; Groszek, A.J.; Kung, M.C.; Scurrell, M.S.; Miller, J.T.; Kung, H.H. *J. Phys. Chem. B* **2005**, *109*, 10319–10326.
222. Calla, J.T.; Bore, M.T.; Datye, A.K.; Davis, R.J. *J. Catal.* **2006**, *238*, 458–467.
223. Sterrer, M.; Yulikov, M.; Fischbach, E.; Heyde, M.; Rust, H.-P.; Pacchioni, G.; Risse, T.; Freund, H.-J. *Angew. Chem. Int. Ed. Engl.* **2006**, *45*, 2630–2632.
224. Yan, Z.; Chinta, S.; Mohamed, A.A.; Fackler, J.P.; Goodman, D.W. *J. Am. Chem. Soc.* **2005**, *127*, 1604–1605.
225. Chen, M.; Cai, Y.; Yan, Z.; Goodman, D.W. *J. Am. Chem. Soc.* **2006**, *128*, 6341–6346.
226. Minato, T.; Susaki, T.; Shiraki, S.; Kato, H.S.; Kawai, M.; Aika, K. *Surf. Sci.* **2004**, *566*, 1012–1017.
227. Stiehl, J.D.; Kim, T.S.; McClure, S.M.; Mullins, C.B. *J. Am. Chem. Soc.* **2004**, *126*, 1606–1607.
228. Stiehl, J.D.; Gong, J.L.; Ojifinni, R.A.; Kim, T.S.; McClure, S.M.; Mullins, C.B. *J. Phys. Chem. B* **2006**, *110*, 20337–20343.
229. Chen, M.S.; Goodman, D.W. *Catal. Today* **2006**, *111*, 22–33.
230. Kobayashi, Y.; Nasu, S.; Tsubota, S.; Haruta, M. *Hyperfine Interact.* **2000**, *126*, 95–99.
231. Guzman, J.; Gates, B.C. *J. Am. Chem. Soc.* **2004**, *126*, 2672–2673.
232. Daniells, S.T.; Overweg, A.R.; Makkee, M.; Moulijn, J.A. *J. Catal.* **2005**, *230*, 52–65.
233. Boyd, D.; Golunski, S.; Hearne, G.R.; Magadzu, T.; Mallick, K.; Raphulu, M.C.; Venugopal, A.; Scurrell, M.S. *Appl. Catal. A* **2005**, *292*, 76–81.
234. Hutchings, G.J.; Hall, M.S.; Carley, A.F.; Landon, P.; Solsona, B.E.; Kiely, C.J.; Herzing, A.; Makkee, M.; Moulijn, J.A.; Overweg, A.; Fierro-Gonzalez, J.C.; Guzman, J.; Gates, B.C. *J. Catal.* **2006**, *242*, 71–81.
235. Guzman, J.; Carrettin, S.; Corma, A. *J. Am. Chem. Soc.* **2005**, *127*, 3286–3287.
236. Haruta, M. *Chem. Rec.* **2003**, *3*, 75–87.
237. Schubert, M.M.; Hackenberg, S.; van Veen, A.C.; Muhler, M.; Plzak, V.; Behm, R.J. *J. Catal.* **2001**, *197*, 113–122.
238. Schubert, M.M.; Kahlich, M.J.; Gasteiger, H.A.; Behm, R.J. *J. Power Sour.* **1999**, *84*, 175–182.
239. Grunwaldt, J.-D.; Baiker, A. *J. Phys. Chem. B* **1999**, *103*, 1002–1012.
240. Remediakis, I.N.; Lopez, N.; Nørskov, J.K. *Appl. Catal. A* **2005**, *291*, 13–20.
241. Molina, L.M.; Hammer, B. *Appl. Catal. A* **2005**, *291*, 21–31.
242. Molina, L.M.; Hammer, B. *Phys. Rev. Lett.* **2003**, *90 206102-1–206102-4.*
243. Remediakis, I.N.; Lopez, N.; Nørskov, J.K. *Angew. Chem. Int. Ed. Engl.* **2005**, *44*, 1824–1826.
244. Liu, Z.-P.; Gong, X.-Q.; Kohanoff, J.; Sanchez, C.; Hu, P. *Phys. Rev. Lett.* **2003**, *91 266102-1–266102-4.*
245. Daté, M.; Haruta, M. *J. Catal.* **2001**, *201*, 221–224.

246. Daté, M.; Okumura, M.; Tsubota, S.; Haruta, M. *Angew. Chem. Int. Ed. Engl.* **2004**, *43*, 2129–2132.
247. Kim, T.S.; Gong, J.; Ojifinni, R.A.; White, J.M.; Mullins, C.B. *J. Am. Chem. Soc.* **2006**, *128*, 6282–6283.
248. Costello, C.K.; Yang, J.H.; Law, H.Y.; Wang, Y.; Lin, J.-N.; Marks, L.D.; Kung, M.C.; Kung, H.H. *Appl. Catal. A* **2003**, *243*, 15–24.
249. Tanaka, K. *Catal. Today* **2010**, *154*, 105–112.
250. Tanaka, K. *Catal. Today* **2011**, *175*, 467–470.
251. Gao, F.; Wood, T.E.; Goodman, D.W. *Catal. Lett.* **2010**, *134*, 9–12.
252. Yan, T.; Gong, J.L.; Flaherty, D.W.; Mullins, C.B. *J. Phys. Chem. C* **2011**, *115*, 2057–2065.
253. Pyykkö, P. *Angew. Chem. Int. Ed. Engl.* **2004**, *43*, 4412–4456.
254. Pyykkö, P. *Inorg. Chim. Acta* **2005**, *358*, 4113–4130.
255. Coquet, R.; Howard, K.L.; Willock, D.J. *Chem. Soc. Rev.* **2008**, *37*, 2046–2076.
256. Assadollahzadeh, B.; Schwerdtfeger, P. *J. Chem. Phys.* **2009**, *131*, 064306–064311.
257. Mantina, M.; Valero, R.; Truhlar, G. *J. Chem. Phys.* **2009**, *131*, 064706(1)–064706(5).
258. Gruene, P.; Rayner, D.M.; Redlich, B.; van der Meer, A.F.G.; Lyon, J.T.; Meijer, G.A.; Fielicke, A. *Science* **2008**, *321*, 674–676.
259. De, H.S.; Krishnamurty, S.; Pal, S. *J. Phys. Chem. C* **2009**, *113*, 7101–7106.
260. Vargas, A.; Santarossa, G.; Iannuzzi, M.; Baiker, A. *Phys. Rev. B* **2009**, *80*, 195421 (1)–195421(13).
261. Landon, P.; Collier, J.; Papworth, A.J.; Kiely, C.J.; Hutchings, G.J. *Chem. Commun.* **2005**, 2351–2353.
262. Edwards, J.K.; Solsona, B.; Landon, P.; Carley, A.F.; Herzing, A.; Kiely, C.J.; Hutchings, G.J. *J. Catal.* **2005**, *236*, 69–79.
263. Okumura, M.; Kitagawa, Y.; Yamaguchi, K.; Akita, T.; Tsubota, S.; Haruta, M. *Chem. Lett.* **2003**, *32*, 822–823.
264. Ishihara, T.; Ohura, Y.; Yoshida, S.; Hata, Y.; Nishiguchi, H.; Takita, Y. *Appl. Catal.* **2005**, *291*, 215–221.
265. Tsiplakides, D.; Balomenou, S. *Catal. Today* **2008**, *146*, 312–318.
266. Zhang, H.; Watanabe, T.; Okumura, M.; Haruta, M.; Toshima, N. *Nat. Mater.* **2012**, *11*, 49–52.
267. Shan, B.; Wang, L.; Yang, S.; Hyun, J.; Kapur, N.; Zhao, Y.; Nicholas, J.B.; Cho, K. *Phys. Rev. B* **2009**, *80*, 035404–035408.
268. Kim, Y.D. *Int. J. Mass Spectrom.* **2004**, *238*, 17–31.
269. Schwerdtfeger, P.; Lein, M.; Krawczyk, R.P.; Jacob, C.R. *J. Chem. Phys.* **2008**, *128*, 124302–124310.
270. Kang, G.-J.; Chen, Z.-X.; Li, Z. *J. Chem. Phys.* **2009**, *131*, 034710–034718.
271. Shafai, G.S.; Shetty, S.; Krishnamurty, S.; Shah, V.; Kanhere, D.G. *J. Chem. Phys.* **2007**, *126*, 014704–014708.
272. Lyalin, A.; Taketsugu, T. *J. Phys. Chem. C* **2009**, *113*, 12930–12934.
273. Campo, B.; Volpe, M.; Ivanova, S.; Tonrade, R. *J. Catal.* **2006**, *242*, 162–171.
274. You, K.-J.; Chang, C.-T.; Liaw, B.-J.; Huang, C.-T.; Chen, Y.-Z. *Appl. Catal. A Gen.* **2009**, *361*, 65–71.
275. Okumura, M.; Kitagawa, Y.; Kawakami, T.; Haruta, M. *Chem. Phys. Lett.* **2008**, *459*, 133–136.
276. Häkkinen, H.; Landman, U. *J. Am. Chem. Soc.* **2001**, *123*, 9704–9705.
277. Okumura, M.; Kitagawa, Y.; Haruta, M.; Yamaguchi, K. *Chem. Phys. Lett.* **2001**, *364*, 163–170.
278. Deka, A.; Deka, R.C.; Choudhury, A. *Chem. Phys. Lett.* **2010**, *490*, 184–188.
279. Josh, A.M.; Delgass, W.N.; Thomson, K.T. *Top. Catal.* **2007**, *44*, 27–39.

280. Varganov, S.A.; Olson, R.M.; Gordon, M.S.; Mills, G.; Metiu, H. *J. Chem. Phys.* **2004**, *120*, 5169–5175.
281. Wang, F.; Zhang, D.; Sun, H.; Ding, Y. *J. Phys. Chem. C* **2007**, *111*, 11590–11597.
282. Joshi, A.M.; Delgass, W.N.; Thomson, K.T. *J. Phys. Chem. B* **2005**, *109*, 22392–22406.
283. Sivadinarayana, C.; Choudhary, T.V.; Daemen, L.L.; Eckert, J.; Goodman, D.W. *J. Am. Chem. Soc.* **2004**, *126*, 38–39.
284. Landon, P.; Collier, P.J.; Carley, A.F.; Chadwick, D.; Papworth, A.J.; Burrows, A.; Kiely, C.J.; Hutchings, G.J. *Phys. Chem. Chem. Phys.* **2003**, *5*, 1917–1923.
285. Xu, Y.; Mavrikakis, M. *J. Phys. Chem. B* **2003**, *107*, 9298–9307.
286. Hammer, B.; Hansen, L.B.; Nørskov, J.K. *Phys. Rev. B* **1999**, *59*, 7413–7421.
287. Greeley, J.; Nørskov, J.K.; Mavrikakis, M. *Annu. Rev. Phys. Chem.* **2002**, *53*, 319–348.
288. Landmann, M.; Rauls, E.; Schmidt, W.G. *Phys. Rev. B* **2009**, *79*, 045412–045419.
289. Mehmood, F.; Kara, A.; Rahman, T.S.; Henry, C.R. *Phys. Rev. B* **2009**, *79*, 075422–075426.
290. Shi, H.; Stampfl, C. *Phys. Rev. B* **2007**, *76*, 075327(1)–075327(14).
291. Kersse, G.; Furthmuller, J. *Phys. Rev. B* **1994**, *47*, 558–561 **1994,** *49*, 14251-14269.
292. Okazaki-Maeda, K.; Kohyama, M. *Chem. Phys. Lett.* **2010**, *492*, 266–271.
293. Hayashi, T.; Morikawa, Y.; Liew, C.C.; Nozoe, H. *J. Chem. Phys.* **2001**, *114*, 7615–7621.
294. Morikawa, Y.; Hayashi, T.; Liew, C.C.; Nozoe, H. *Surf. Sci.* **2002**, *46*, 507–510.
295. Wang, G.-C.; Jiao, J.; Bu, X.-H. *J. Phys. Chem. C* **2007**, *111*, 12335–12339.
296. Yuan, D.; Gong, X.; Wu, R. *Phys. Rev. B* **2007**, *75*, 085428.
297. Ham, H.C.; Hwang, G.S.; Han, J.; Nam, S.W.; Lim, T.H. *J. Phys. Chem. C* **2010**, *114*, 14922–149228.
298. Senanayake, S.D.; Stacchiola, D.; Liu, P.; Mullins, C.B.; Hrbek, J.; Rodriguez, J.A. *J. Phys. Chem. C* **2009**, *113*, 19536–19544.
299. Su, H.-Y.; Yang, M.-M.; Bao, X.-H.; Li, W.-X. *J. Phys. Chem. C* **2008**, *112*, 17303–17310.
300. Qian, K.; Zhang, W.; Sun, H.; Fang, J.; He, B.; Ma, Y.; Jiang, Z.; Wei, S.; Yang, J.; Huang, W. *J. Catal.* **2011**, *277*, 95–103.
301. Wang, G.-C.; Jiang, L.; Pang, X.-Y.; Nakamura, J. *J. Phys. Chem. B* **2005**, *109*, 17943–17950.
302. Zhang, W.; Li, Z.; Luo, Y.; Yang, J. *J. Chem. Phys.* **2008**, *129*, 134708(1)–134708(5).
303. Hussain, A.; Ferre, D.C.; Gracia, J.; Nieuwenhuys, B.E.; Niemantsverdriet, J.W. *Surf. Sci.* **2009**, *603*, 2734–2741.
304. Baker, T.A.; Friend, C.M.; Kaxiras, E. *J. Chem. Phys.* **2008**, *129*, 104702–104705.
305. Baker, T.A.; Friend, C.M.; Kaxiras, E. *J. Chem. Phys.* **2009**, *130*, 084701–084708.
306. Chang, C.M.; Cheng, C.; Wei, C.M. *J. Chem. Phys.* **2008**, *128*, 124710–124714.
307. Xie, Y.-P.; Gong, X.-G. *J. Chem. Phys.* **2010**, *132*, 244302–244306.
308. Boronat, M.; Corma, A.; Illas, F.; Radilla, J.; Rodenas, T.; Sabater, M.J. *J. Catal.* **2011**, *278*, 50–58.
309. Ortmann, F.; Schmidt, W.G.; Bechstedt, F. *Phys. Rev. Lett.* **2005**, *95*, 186101–186104.
310. Ortmann, F.; Bechstedt, F.; Schmidt, W.G. *Phys. Rev. B* **2006**, *73*, 205101–205110.
311. Rauls, E.; Blankenburg, S.; Schmidt, W.G. *Phys. Rev. B* **2010**, *81*, 125401–125405.
312. Camellone, M.F.; Kowalski, P.M.; Marx, D. *Phys. Rev. B* **2011**, *84*, 035413–035418.
313. Chretien, S.; Metiu, H. *J. Chem. Phys.* **2007**, *127*, 084704–084709.
314. Chretien, S.; Metiu, H. *J. Chem. Phys.* **2007**, *127*, 244708–244713.
315. Pabisiak, T.; Kiejna, A. *Phys. Rev. B* **2009**, *79*, 085411(1)–85411(10).
316. Shi, H.; Kohyama, M.; Tanaka, S.; Takeda, S. *Phys. Rev. B* **2009**, *80,*155413(1)–155413(10).
317. Chen, D.; Ma, X.L.; Wang, Y.M. *Phys. Rev. B* **2007**, *75,* 125409(1)–125409(7).

318. Branda, M.M.; Castellani, N.J.; Grau-Crespo, R.; de Leeuw, N.H.; Hernandez, N.C.; Sanz, J.F.; Neyman, K.M.; Illas, F. *J. Chem. Phys.* **2009**, *131*, 094702–094711.
319. Frondelius, P.; Hellman, A.; Honkala, K.; Hakkinen, H.; Gronbeck, H. *Phys. Rev. B* **2008**, *78*, 085426–085427.
320. Ammal, S.C.; Heyden, A. *J. Chem. Phys.* **2010**, *133*, 164703–164715.
321. Quek, S.Y.; Friend, C.M.; Kaxiras, E. *Surf. Sci.* **2006**, *600*, 3388–3393.
322. Rashkeev, S.N.; Lupini, A.; Overbury, S.H. *Phys. Rev. B* **2007**, *76 035438 (8 pages).*
323. Chretien, S.; Metiu, H. *J. Chem. Phys.* **2008**, *128*, 044714(1)–044714(13).
324. Moronat, M.; Concepcion, P.; Corma, A. *J. Phys. Chem. C* **2009**, *113*, 16772–16784.
325. Laursen, S.; Linic, S. *Phys. Chem. Chem. Phys.* **2009**, *11*, 11006–11012.
326. Zhou, M.; Zhang, A.; Dai, Z.; Feng, Y.P.; Zhang, C. *J. Phys. Chem. C* **2010**, *114*, 16541–16546.
327. Zhou, M.; Zhang, A.; Dai, Z.; Zhang, C.; Feng, Y.P. *J. Chem. Phys.* **2010**, *132*, 194704(1)–194704(3).
328. Zhu, W.-J.; Zhang, J.; Gong, X.-Q.; Lu, G. *Catal. Today* **2011**, *165*, 19–24.
329. Bongiorno, A.; Landman, U. *Phys. Rev. Lett.* **2005**, *95*, 106102–106104.
330. Haruta, M.; Tsubota, S.; Kobayashi, T.; Kageyama, H.; Genet, M.J.; Delmon, B. *J. Catal.* **1993**, *144*, 175–192.
331. Abad, A.; Concepcion, P.; Corma, A.; Garcia, H. *Angew. Chem. Int. Ed. Engl.* **2005**, *44*, 4066–4069.
332. Turner, M.; Golovko, V.B.; Vaughan, O.P.H.; Abdulkin, P.; Berenguer-Murcia, A.; Tikhov, M.S.; Johnson, B.F.G.; Lambert, R.M. *Nature* **2008**, *454*, 981–984.
333. Kesavan, L.; Tiruvalam, R.; Rahim, M.H.A.; Saiman, M.I.B.; Enache, D.I.; Jenkins, R.L.; Dimitratos, N.; Lopez-Sanchez, J.A.; Taylor, S.H.; Knight, D.W.; Kiely, C.J.; Hutchings, G.J. *Science* **2011**, *331*, 195–199.
334. Landon, P.; Collier, P.J.; Padpworth, A.J.; Kiely, C.J.; Hutchings, G.J. *Chem. Commun.* **2002**, 2058–2059.
335. Corma, A.; Serna, P. *Science* **2006**, *313*, 332–334.
336. Fu, Q.; Saltsburg, H.; Flytzani-Stephanopoulos, M. *Science* **2003**, *301*, 935–938.
337. González-Arellano, C.; Abad, A.; Corma, A.; García, H.; Iglesias, M.; Sánchez, F. *Angew. Chem. Int. Ed. Engl.* **2007**, *46*, 1536–1538.
338. Bond, G.C.; Sermon, P.A.; Webb, G.; Buchanan, D.A.; Wells, P.B. *J. Chem. Soc. Chem. Commun.* **1973**, 444–445.
339. Bus, E.; Miller, J.T.; van Bokhoven, J.A. *J. Phys. Chem. B* **2005**, *109*, 14581–14587.
340. Corma, A.; Boronat, M.; González, S.; Illas, F. *Chem. Commun.* **2007**, 3371–3373.
341. Boronat, M.; Illas, F.; Corma, A. *J. Phys. Chem. A* **2009**, *113*, 3750–3757.
342. Barrio, L.; Liu, P.; Rodríguez, J.A.; Campos-Martín, J.M.; Fierro, J.L.G. *J. Chem. Phys.* **2006**, *125*, 164715.
343. Nakamura, I.; Mantoku, H.; Furukawa, T.; Fujitani, T. *J. Phys. Chem. C* **2011**, *115*, 16074–16080.
344. Zhang, X.; Shi, H.; Xu, B. *Angew. Chem. Int. Ed. Engl.* **2005**, *44*, 7132–7135.
345. Zhang, X.; LlabrésiXamena, F.X.; Corma, A. *J. Catal.* **2009**, *265*, 155–160.
346. Jia, J.; Haraki, K.; Kondo, J.N.; Domen, K.; Tamaru, K. *J. Phys. Chem. B* **2000**, *104*, 11153–11156.
347. Choudhary, T.V.; Sivadinarayana, C.; Dantye, A.; Kumar, D.; Goodman, D.W. *Catal. Lett.* **2003**, *86*, 1–8.
348. Lopez-Sanchez, J.A.; Lennon, D. *Appl. Catal. A* **2005**, *291*, 230–237.
349. Segura, Y.; Lopez, N.; Perez-Ramirez, J. *J. Catal.* **2007**, *247*, 383–386.
350. Okumura, M.; Akita, T.; Haruta, M. *Catal. Today* **2002**, *74*, 265–269.
351. Hugon, A.; Delannoy, L.; Louis, C. *Gold Bull.* **2008**, *41*, 127–138.
352. Hugon, A.; Delannoy, L.; Krafft, J.M.; Louis, C. *J. Phys. Chem. C* **2010**, *114*, 10823–10835.

353. Zhang, X.; Shi, H.; Xu, B. *Catal. Today* **2007**, *122*, 330–337.
354. Zhang, X.; Shi, H.; Xu, B. *J. Catal.* **2011**, *279*, 75–87.
355. Liu, Z.; Wang, C.; Fan, K. *Angew. Chem. Int. Ed. Engl.* **2006**, *45*, 6865–6868.
356. Bailie, J.E.; Hutchings, G.J. *Chem. Commun.* **1999**, 2151–2152.
357. Bailie, J.E.; Abdullah, H.A.; Anderson, J.A.; Rochester, C.H.; Richardson, N.V.; Hodge, N.; Zhang, J.; Burrows, A.; Kiely, C.J.; Hutchings, G.J. *Phys. Chem. Chem. Phys.* **2001**, *3*, 4113–4121.
358. Zanella, R.; Louis, C.; Giorgio, S.; Touroude, R. *J. Catal.* **2004**, *223*, 328–339.
359. Campo, B.; Volpe, M.; Ivanova, S.; Touroude, R. *J. Catal.* **2006**, *242*, 162–171.
360. Campo, B.; Petit, C.; Volpe, M.A. *J. Catal.* **2008**, *254*, 71–78.
361. Campo, B.; Ivanova, S.; Gigola, C.; Petit, C.; Volpe, M.A. *Catal. Today* **2008**, *133–135*, 661–666.
362. Mohr, C.; Hofmeister, H.; Claus, P. *J. Catal.* **2003**, *213*, 86–94.
363. Mohr, C.; Hofmeister, H.; Radnik, J.; Claus, P. *J. Am. Chem. Soc.* **2003**, *125*, 1905–1911.
364. Sakuri, H.; Tsubota, S.; Haruta, M. *Appl. Catal. A* **1993**, *102*, 125–136.
365. Sakurai, H.; Haruta, M. *Appl. Catal. A* **1995**, *127*, 93–105.
366. Sakurai, H.; Haruta, M. *Catal. Today* **1996**, *29*, 361–365.
367. Słoczyński, J.; Grabowski, R.; Kozłowska, A.; Olszewski, P.; Stoch, J.; Skrzypek, J.; Lachowska, M. *Appl. Catal. A* **2004**, *278*, 11–23.
368. Mpela, A.; Hildebrandt, D.; Glasser, D.; Scurrell, M.S.; Hutchings, G.J. *Gold Bull.* **2007**, *40*, 219–224.
369. Strunk, J.; Kähler, K.; Xia, X.; Comotti, M.; Schüth, F.; Reinecke, T.; Muhler, M. *Appl. Catal. A* **2009**, *359*, 121–128.
370. Vilchis-Nestor, A.R.; Avalos-Borja, M.; Gómez, S.A.; Hernández, J.A.; Olivas, A.; Zepeda, T.A. *Appl. Catal. B* **2009**, *90*, 64–73.
371. Trimm, D.L.; Önsan, Z.I. *Catal. Rev.* **2001**, *43*, 31–84.
372. Ghenciu, A.F. *Curr. Opin. Solid State Mater. Sci.* **2002**, *6*, 389–399.
373. Thayer, A.M. *Chem. Eng. News* **1992**, *70*(10), 27–49.
374. Haruta, M. *Nature* **2005**, *437*, 1098–1099.
375. Huang, J.; Akita, T.; Faye, J.; Fujitani, T.; Takei, T.; Haruta, M. *Angew. Chem. Int. Ed. Engl.* **2009**, *48*, 7862–7866.
376. Lee, S.; Molina, L.M.; López, M.J.; Alonso, J.A.; Hammer, B.; Lee, B.; Seifert, S.; Winans, R.E.; Elam, J.W.; Pellin, M.J.; Vajda, S. *Angew. Chem. Int. Ed. Engl.* **2009**, *48*, 1467–1671.
377. Alves, L.; Ballesteros, B.; Boronat, M.; Cabrero-Antonino, J.R.; Concepción, P.; Corma, A.; Correa-Duarte, M.A.; Mendoza, E. *J. Am. Chem. Soc.* **2011**, *133*, 10251–10261.
378. Boronat, M.; Corma, A. *J. Catal.* **2011**, *284*, 138–147.
379. Jiang, J.; Oxford, S.M.; Fu, B.; Kung, M.C.; Kung, H.H.; Ma, J. *Chem. Commun.* **2010**, *46*, 3791–3793.
380. Jiang, J.; Kung, H.H.; Kung, M.C.; Ma, J. *Gold Bull.* **2009**, *42*, 280–287.
381. Uphade, B.S.; Tsubota, S.; Hayashi, T.; Haruta, M. *Chem. Lett.* **1998**, *27*, 1277–1278.
382. Uphade, B.S.; Akita, T.; Nakamura, T.; Haruta, M. *J. Catal.* **2002**, *209*, 331–340.
383. Woodham, A.P.; Meijer, G.; Fielicke, A. *Angew. Chem. Int. Ed. Engl.* **2012**, *51*, 4444–4447.
384. Lang, S.M.; Bernhardt, T.M.; Barnett, R.N.; Yoon, B.; Landman, U. *J. Am. Chem. Soc.* **2009**, *131*, 8939–8951.
385. Lyalin, A.; Taketsugu, T. *J. Phys. Chem. Lett.* **2010**, *1*, 1752–1757.
386. Kalvachev, Y.A.; Hayashi, T.; Tsubota, S.; Haruta, M. *J. Catal.* **1999**, *186*, 228–233.
387. Brávo-Suárez, J.J.; Bando, K.K.; Akita, T.; Fujitani, T.; Fuhrer, T.J.; Oyama, S.T. *Chem. Commun.* **2008**, 3272–3274.

388. Brávo-Suarez, J.J.; Bando, K.K.; Fujitani, T.; Oyama, S.T. *J. Catal.* **2008**, *257*, 32–42.
389. Brávo-Suárez, J.J.; Bando, K.K.; Lu, J.; Fujitani, T.; Oyama, S.T. *J. Catal.* **2008**, *255*, 114–126.
390. Lang, S.M.; Bernhardt, T.M.; Barnett, R.N.; Landman, U. *Angew. Chem. Int. Ed. Engl.* **2010**, *49*, 980–983.
391. Lang, S.M.; Bernhardt, T.M. *Faraday Discuss.* **2011**, *152*, 337–351.
392. Huang, J.; Haruta, M. *Res. Chem. Intermed.* **2012**, *38*, 1–24.
393. Ishino, M.; Yamamoto, J. *Shokubai* **2006**, *48*, 511–515.
394. Tullo, A. *Chem. Eng. News* **2004**, *82*(36), 15.
395. Nijhuis, T.A.; Makkee, M.; Moulijn, J.A.; Weckhuysen, B.M. *Ind. Eng. Chem. Res.* **2006**, *45*, 3447–3459.
396. Hughes, M.D.; Xu, Y.; Jenkins, P.; McMorn, P.; Landon, P.; Enache, D.I.; Carley, A.F.; Attard, G.A.; Hutchings, G.J.; King, F.; Stitt, E.H.; Johnston, P.; Griffin, K.; Kiely, C.J. *Nature* **2005**, *437*, 1132–1135.
397. Lignier, P.; Morfin, F.; Mangematin, S.; Massin, L.; Rousset, J.L.; Caps, V. *Chem. Commun.* **2007**, 186–188.
398. Aprile, C.; Corma, A.; Domine, M.E.; Garcia, H.; Mitchell, C. *J. Catal.* **2009**, *264*, 44–53.
399. Stangland, E.E.; Taylor, B.; Andres, R.P.; Delgass, W.N. *J. Phys. Chem. B* **2005**, *109*, 2321–2330.
400. Stangland, E.E.; Stavens, K.B.; Andres, R.P.; Delgass, W.N. *J. Catal.* **2000**, *191*, 332–347.
401. Nijhuis, T.A.; Weckhuysen, B.M. *Chem. Commun.* **2005**, 6002–6004.
402. Nijhuis, T.A.; Weckhuysen, B.M. *Catal. Today* **2006**, *117*, 84–89.
403. Nijhuis, T.A.; Gardner, T.Q.; Weckhuysen, B.M. *J. Catal.* **2005**, *236*, 153–163.
404. Nijhuis, T.A.; Visser, T.; Weckhuysen, B.M. *Angew. Chem. Int. Ed. Engl.* **2005**, *44*, 1115–1118.
405. Nijhuis, T.A.; Visser, T.; Weckhuysen, B.M. *J. Phys. Chem. B* **2005**, *109*, 19309–19319.
406. Chowdhury, B.; Brávo-Suárez, J.J.; Daté, M.; Tsubota, S.; Haruta, M. *Angew. Chem. Int. Ed. Engl.* **2006**, *45*, 412–415.
407. Bravo-Suárez, J.J.; Bando, K.K.; Lu, J.; Haruta, M.; Fujitani, T.; Oyama, S.T. *J. Phys. Chem. C* **2008**, *112*, 1115–1123.
408. Sinha, A.K.; Seelan, S.; Tsubota, S.; Haruta, M. *Angew. Chem. Int. Ed. Engl.* **2004**, *43*, 1546–1548.
409. Sinha, A.K.; Seelan, S.; Okumura, M.; Akita, T.; Tsubota, S.; Haruta, M. *J. Phys. Chem. B* **2005**, *109*, 3956–3965.
410. Sinha, A.K.; Seelan, S.; Tsubota, S.; Haruta, M. *Top. Catal.* **2004**, *29*(3–4), 95–102.
411. Qi, C.; Akita, T.; Okumura, M.; Kuraoka, K.; Haruta, M. *Appl. Catal. A* **2003**, *253*, 75–89.
412. Qi, C.; Akita, T.; Okumura, M.; Haruta, M. *Appl. Catal. A* **2001**, *218*, 81–89.
413. Chowdhury, B.; Bravo-Suárez, J.J.; Mimura, N.; Lu, J.; Bando, K.K.; Tsubota, S.; Haruta, M. *J. Phys. Chem. B* **2006**, *110*, 22995–22999.
414. Kapoor, M.P.; Sinha, A.K.; Seelan, S.; Inagaki, S.; Tsubota, S.; Yoshida, H.; Haruta, M. *Chem. Commun.* **2002**, 2902–2903.
415. Bravo-Suárez, J.J.; Lu, J.; Dallos, C.G.; Fujitani, T.; Oyama, S.T. *J. Phys. Chem. C* **2007**, *111*, 17427–17436.
416. Lu, J.; Zhang, X.; Bravo- Suárez, J.J.; Tsubota, S.; Gaudet, J.; Oyama, S.T. *Catal. Today* **2007**, *123*, 189–197.
417. Lu, J.; Zhang, Z.; Bravo-Suárez, J.J.; Bando, K.K.; Fujitani, T.; Oyama, S.T. *J. Catal.* **2007**, *250*, 350–359.

418. Sacaliuc-Parvulescu, E.; Friedrich, H.; Palkovits, R.; Weckhuysen, B.M.; Nijhuis, T.A. *J. Catal.* **2008**, *259*, 43–53.
419. Sacaliuc, E.; Beale, A.M.; Weckhuysen, B.M.; Nijhuis, T.A. *J. Catal.* **2007**, *248*, 235–248.
420. Yang, H.; Tang, D.; Lu, X.; Yuan, Y. *J. Phys. Chem. C* **2009**, *113*, 8186–8293.
421. Cumaranatunge, L.; Delgass, W.N. *J. Catal.* **2005**, *232*, 38–42.
422. Huang, J.; Takei, T.; Akita, T.; Ohashi, H.; Haruta, M. *Appl. Catal. B* **2010**, *95*, 430–438.
423. Lu, J.; Zhang, X.; Bravo-Suárez, J.J.; Fujitani, T.; Oyama, S.T. *Catal. Today* **2009**, *147*, 186–195.
424. Oyama, S.T.; Zhang, X.; Lu, J.; Gu, Y.; Fujitani, T. *J. Catal.* **2008**, *257*, 1–4.
425. Nijhuis, T.A.; Huizinga, B.J.; Makkee, M.; Moulijn, J.A. *Ind. Eng. Chem. Res.* **1999**, *38*, 884–891.
426. Yap, N.; Andres, R.P.; Delgass, W.N. *J. Catal.* **2004**, *226*, 156–170.
427. Taylor, B.; Lauterbach, J.; Delgass, W.N. *Appl. Catal. A Gen.* **2005**, *291*, 188–198.
428. Taylor, B.; Lauterbach, J.; Blau, G.E.; Delgass, W.N. *J. Catal.* **2006**, *242*, 142–152.
429. Taylor, B.; Lauterbach, J.; Delgass, W.N. *Catal. Today* **2007**, *123*, 50–58.
430. Lee, W.S.; Akatay, M.C.; Stach, E.A.; Ribeiro, F.H.; Delgass, W.N. *J. Catal.* **2012**, *287*, 178–189.
431. Du, M.; Zhan, G.; Yang, X.; Wang, H.; Lin, W.; Zhou, Y.; Zhu, J.; Lin, L.; Huang, J.; Sun, D.; Jia, L.; Li, Q. *J. Catal.* **2011**, *283*, 192–201.
432. Wang, F.; Qi, C.; Ma, J. *Catal. Commun.* **2007**, *8*, 1947–1952.
433. Chen, J.; Halin, S.J.A.; Perez Ferrandez, D.M.; Schouten, J.C.; Nijhuis, T.A. *J. Catal.* **2012**, *285*, 324–327.
434. Qi, C.; Huang, J.; Bao, S.; Su, H.; Akita, T.; Haruta, M. *J. Catal.* **2011**, *281*, 12–20.
435. Joshi, A.M.; Delgass, W.N.; Thomson, K.T. *J. Phys. Chem. C* **2007**, *111*, 7841–7844.
436. Joshi, A.M.; Delgass, W.N.; Thomson, K.T. *J. Phys. Chem. B* **2006**, *110*, 2572–2581.
437. Huang, J.; Lima, E.; Akita, T.; Guzmán, A.; Qi, C.; Takei, T.; Haruta, M. *J. Catal.* **2011**, *278*, 8–15.
438. Ojeda, M.; Iglesia, E. *Chem. Commun.* **2009**, 352–354.
439. Chang, C.; Wang, Y.; Li, J. *Nano Res.* **2011**, *4*(1), 131–142.
440. Biella, S.; Prati, L.; Rossi, M. *IV World Congress on Oxidation Catalysis*, *Berlin*, 2001; Vol. I, p 371.
441. Biella, S.; Rossi, M. *Chem. Commun.* **2003**, 378–379.
442. Zheng, N.; Stucky, G.D. *J. Am. Chem. Soc.* **2006**, *128*, 14278–14280.
443. Takei, T.; Iguchi, N.; Haruta, M. *New J. Chem.* **2011**, *35*, 2227–2233.
444. Wittstock, A.; Zielasek, V.; Biener, J.; Friend, C.M.; Baümer, M. *Science* **2010**, *327*, 319–322.
445. Han, Q.; Xu, T.; Su, X.; Xu, H.; Ding, Y. *ChemCatChem* **2010**, *2*, 383–386.
446. Zhao, F.; Hu, Y.; Deng, M.; Ling, M.; Lu, Y. *Green Chem.* **2011**, *13*, 55–58.
447. Zhao, F.; Hu, Y.; Deng, M.; Lu, Y. *Chem. Commun.* **2011**, *47*, 9642–9644.
448. Armor, J.N. *Appl. Catal. B* **1992**, *1*, 221–256.
449. Crump, D.R. In *Volatile Organic Compounds in Indoor Air, in Volatile Organic Compounds in the Atmosphere*; Hester, R.E., Harrison, R.M., Eds.; The Royal Society of Chemistry: London, 1995; p 118.
450. Prasad, R.; Kennedy, L.A.; Ruckenstein, E. *Catal. Rev. Sci. Eng.* **1984**, *26*, 1–58.
451. Zwinkels, M.F.M.; Jaras, S.G.; Menon, P.G.; Griffin, T.A. *Catal. Rev. Sci. Eng.* **1993**, *35*, 319–358.
452. Dalla Betta, R.A. *Catal. Today* **1997**, *35*, 129–135.
453. Alifanti, M.; Kirchnerova, J.; Delmon, B.; Klvana, D. *Appl. Catal. A Gen.* **2004**, *262*, 167–176.

454. Haruta, M.; Ueda, A.; Tsubota, S.; Torres Sanchez, R.M. *Catal. Today* **1996**, *29*, 443–447.
455. Li, C.; Shen, Y.; Jia, M.; Sheng, S.; Adebajo, M.O.; Zhu, H. *Catal. Commun.* **2008**, *9*, 355–361.
456. Jia, M.; Shen, N.; Li, Y.; Bao, R.; Sheng, S. *Catal. Lett.* **2005**, *99*, 235–239.
457. Zhang, J.; Jin, Y.; Li, C.; Shen, Y.; Han, L.; Hua, Z.; Di, X.; Liu, Z. *Appl. Catal. B* **2009**, *91*, 11–20.
458. Li, H.; Zhang, N.; Chen, P.; Luo, M.; Lu, J. *Appl. Catal. B* **2011**, *110*, 279–285.
459. Chen, H.; Tong, X.; Li, Y. *Appl. Catal. A* **2009**, *370*, 59–65.
460. Ahn, H.G.; Choi, B.M.; Lee, D.J. *J. Nanosci. Nanotechnol.* **2006**, *6*, 3599–3603.
461. Li, J.; Ma, C.; Xu, X.; Yu, J.; Hao, Z.; Qiao, S. *Environ. Sci. Technol.* **2008**, *42*, 8947–8951.
462. Ma, C.; Mu, Z.; Li, J.; Jin, Y.; Cheng, J.; Lu, G.; Hao, Z.; Qiao, S. *J. Am. Chem. Soc.* **2010**, *132*, 2608–2613.
463. Xue, W.; Wang, Y.; Li, P.; Liu, Z.; Hao, Z.; Ma, C. *Catal. Commun.* **2011**, *12*, 1265–1268.
464. Sekine, Y. *Atmos. Environ.* **2002**, *36*, 5543–5547.
465. Shen, Y.; Yang, X.; Wang, Y.; Zhang, Y.; Zhu, H.; Gao, L.; Jia, M. *Appl. Catal. B* **2008**, *79*, 142–148.
466. Chen, X.; Zhu, H.; Zhao, J.; Zheng, Z.; Gao, X. *Angew. Chem. Int. Ed. Engl.* **2008**, *47*, 5353–5356.
467. Gluhoi, A.C.; Nieuwenhuys, B.E. *Catal. Today* **2007**, *119*, 305–310.
468. Delannoy, L.; Fajerwerg, K.; Lakshmanan, P.; Potvin, C.; Méthivier, C.; Louis, C. *Appl. Catal. B* **2010**, *94*, 117–124.
469. Lakshmanan, P.; Delannoy, L.; Richard, V.; Méthivier, C.; Potvin, C.; Louis, C. *Appl. Catal. B* **2010**, *96*, 117–125.
470. Gluhoi, A.C.; Bogdanchikova, N.; Nieuwenhuys, B.E. *J. Catal.* **2005**, *229*, 154–162.
471. Gluhoi, A.C.; Bogdanchikova, N.; Nieuwenhuys, B.E. *Catal. Today* **2006**, *113*, 178–181.
472. Solsona, B.; Pérez-Cabero, M.; Vázqueza, I.; Dejoz, A.; García, T.; Álvarez-Rodríguez, J.; El-Haskouri, J.; Beltrán, D.; Amorós, P. *Chem. Eng. J.* **2012**, *187*, 391–400.
473. Gluhoi, A.C.; Bogdanchikova, N.; Nieuwenhuys, B.E. *J. Catal.* **2005**, *232*, 96–101.
474. Ousmanea, M.; Liotta, L.F.; Pantaleo, G.; Venezia, A.M.; Di Carlo, G.; Aouine, M.; Retailleau, L.; Giroir-Fendler, A. *Catal. Today* **2011**, *176*, 7–13.
475. Centeno, M.A.; Paulis, M.; Montes, M.; Odriozola, J.A. *Appl. Catal. B* **2005**, *61*, 177–183.
476. Lai, S.Y.; Qiu, Y.; Wang, S. *J. Catal.* **2006**, *237*, 303–313.
477. Domínguez, M.I.; Sánchez, M.; Centeno, M.A.; Montes, M.; Odriozola, J.A. *J. Mol. Catal. A* **2007**, *277*, 145–154.
478. Della Pina, C.; Falletta, E.; Prati, L.; Rossi, M. *Chem. Soc. Rev.* **2008**, *37*, 2077–2095.
479. Arcadi, A. *Chem. Rev.* **2008**, *108*, 3266–3325.
480. Dimitratos, N.; Lopez-Sanchez, J.A.; Hutchings, G.J. *Chem. Sci.* **2012**, *3*, 20–44.
481. Corma, A.; García, H. *Chem. Soc. Rev.* **2008**, *37*, 2096–2126.
482. Abad, A.; Almela, C.; Corma, A.; García, H. *Tetrahedron* **2006**, *62*, 6666–6672.
483. Abad, A.; Corma, A.; García, H. *Pure Appl. Chem.* **2007**, *79*, 1847–1854.
484. Abad, A.; Almela, C.; Corma, A.; García, H. *Chem. Commun.* **2006**, 3178–3180.
485. Nielsen, I.S.; Taarning, E.; Egeblad, K.; Madsen, R.; Christensen, C.H. *Catal. Lett.* **2007**, *116*, 35–40.
486. Su, F.-Z.; Liu, Y.-M.; Wang, L.-C.; Cao, Y.; He, H.-Y.; Fan, K.-N. *Angew. Chem. Int. Ed. Engl.* **2008**, *47*, 334–337.
487. Kimmerle, B.; Grunwaldt, J.-D.; Baiker, A. *Top. Catal.* **2007**, *44*, 285–292.

488. Zheng, N.; Stucky, G.D. *Chem. Commun.* **2007**, 3862–3864.
489. Haider, P.; Baiker, A. *J. Catal.* **2007**, *248*, 175–187.
490. Choudhary, V.R.; Dumbre, D.K. *Catal. Commun.* **2011**, *13*, 82–86.
491. Biella, S.; Castiglioni, G.L.; Fumagalli, C.; Prati, L.; Rossi, M. *Catal. Today* **2002**, *72*, 43–49.
492. Villa, A.; Janjic, N.; Spontoni, P.; Wang, D.; Su, D.S.; Prati, L. *Appl. Catal. A Gen.* **2009**, *364*, 221–228.
493. Miyamura, H.; Matsubara, R.; Miyazaki, Y.; Kobayashi, S. *Angew. Chem. Int. Ed. Engl.* **2007**, *46*, 4151–4154.
494. Kanaoka, S.; Yagi, N.; Fukuyama, Y.; Aoshima, S.; Tsunoyama, H.; Tsukuda, T.; Sakurai, H. *J. Am. Chem. Soc.* **2007**, *129*, 12060–12061.
495. Biffis, A.; Cunial, S.; Spontoni, P.; Prati, L. *J. Catal.* **2007**, *251*, 1–6.
496. Liu, H.; Liu, Y.; Li, Y.; Tang, Z.; Jian, H. *J. Phys. Chem. C* **2010**, *114*, 13362–13369.
497. Esken, D.; Turner, S.; Lebedev, O.I.; Van Tendeloo, G.; Fischer, R.A. *Chem. Mater.* **2010**, *22*, 6393–6401.
498. Mitsudome, T.; Noujima, A.; Mizugaki, T.; Jitsukawa, K.; Kaneda, K. *Adv. Synth. Catal.* **2009**, *351*, 1890–1896.
499. Liu, P.; Guan, Y.; Van Santen, R.A.; Li, C.; Hensen, E.J.M. *Chem. Commun.* **2011**, *47*, 11540–11542.
500. Ni, J.; Yu, W.-J.; He, L.; Sun, H.; Cao, Y.; He, H.-Y.; Fan, K.-N. *Green Chem.* **2009**, *11*, 756–759.
501. Christensen, C.H.; Jørgensen, B.; Rass-Hansen, J.; Egeblad, K.; Madsen, R.; Klitgaard, S.K.; Hansen, S.M.; Hansen, M.R.; Andersen, H.C.; Riisager, A. *Angew. Chem. Int. Ed. Engl.* **2006**, *45*, 4648–4651.
502. Jørgensen, B.; Christensen, S.E.; Thomsen, M.L.D.; Christensen, C.H. *J. Catal.* **2007**, *251*, 332–337.
503. Villa, A.; Chan-Thaw, C.E.; Veith, G.M.; More, K.L.; Ferri, D.; Prati, L. *ChemCatChem* **2011**, *3*, 1612–1618.
504. Ishida, T.; Ogihara, Y.; Ohashi, H.; Akita, T.; Honma, T.; Oji, H.; Haruta, M. *ChemSusChem* **2012**, *11*, 2243–2248.
505. Huang, J.; Dai, W.-L.; Li, H.; Fan, K. *J. Catal.* **2007**, *252*, 69–76.
506. Brett, G.L.; Miedziak, P.J.; Dimitratos, N.; Lopez-Sanchez, J.A.; Dummer, N.F.; Tiruvalam, R.; Kiely, C.J.; Knight, D.W.; Taylor, S.H.; Morgan, D.J.; Carley, A.F.; Hutchings, G.J. *Catal. Sci. Technol.* **2012**, *2*, 97–104.
507. Dimitratos, N.; Lopez-Sanchez, J.A.; Meenakshisundaram, S.; Anthonykutty, J.M.; Brett, G.; Carley, A.F.; Taylor, S.H.; Knight, D.W.; Hutchings, G.J. *Green Chem.* **2009**, *11*, 1209–1216.
508. Abad, A.; Corma, A.; García, H. *Chem. Eur. J.* **2008**, *14*, 212–222.
509. Conte, M.; Miyamura, H.; Kobayashi, S.; Chechik, V. *J. Am. Chem. Soc.* **2009**, *131*, 7189–7196.
510. Fristrup, P.; Johansen, L.B.; Christensen, C.H. *Catal. Lett.* **2008**, *120*, 184–190.
511. Fristrup, P.; Johansen, L.B.; Christensen, C.H. *Chem. Commun.* **2008**, 2750–2752.
512. Tsunoyama, H.; Ichikuni, N.; Sakurai, H.; Tsukuda, T.J. *J. Am. Chem. Soc.* **2009**, *131*, 7086–7093.
513. Juárez, R.; Parker, S.F.; Concepción, P.; Corma, A.; García, H. *Chem. Sci.* **2010**, *1*, 731–738.
514. Su, F.-Z.; He, L.; Ni, J.; Cao, Y.; He, H.-Y.; Fan, K.-N. *Chem. Commun.* **2008**, 3531–3533.
515. Fang, W.; Chen, J.; Zhang, Q.; Deng, W.; Wang, Y. *Chem. Eur. J.* **2011**, *17*, 1247–1256.
516. Ishida, T.; Takamura, R.; Akita, T.; Haruta, M. *Appl. Catal. A Gen.* **2011**, *413–414*, 261–266.

517. Zhu, B.; Angelici, R.J. *Chem. Commun.* **2007**, 2157–2159.
518. Zhu, B.; Lazar, M.; Trewyn, B.G.; Angelici, R.J. *J. Catal.* **2008**, *260*, 1–6.
519. Grirrane, A.; Corma, A.; García, H. *J. Catal.* **2009**, *264*, 138–144.
520. Aschwanden, L.; Mallat, T.; Grunwaldt, J.-D.; Krumeich, F.; Baiker, A. *J. Mol. Catal. A Chem.* **2009**, *300*, 111–115.
521. Aschwanden, L.; Mallat, T.; Krumeich, F.; Baiker, A. *J. Mol. Catal. A Chem.* **2009**, *309*, 57–62.
522. So, M.-H.; Liu, Y.; Ho, C.-M.; Che, C.-M. *Chem. Asian J.* **2009**, *4*, 1551–1561.
523. Miyamura, H.; Morita, M.; Inasaki, T.; Kobayashi, S. *Bull. Chem. Soc. Jpn.* **2011**, *84*, 588–599.
524. Ishida, T.; Kawakita, N.; Akita, T.; Haruta, M. *Gold Bull.* **2009**, *42*, 267–274.
525. Grirrane, A.; Corma, A.; García, H. *Science* **2008**, *322*, 1661–1664.
526. Lignier, P.; Morfin, F.; Piccolo, L.; Rousset, J.-L.; Caps, V. *Catal. Today* **2007**, *122*, 284–291.
527. Mendez, V.; Guillois, K.; Daniele, S.; Tuel, A.; Caps, V. *Dalton Trans.* **2010**, *39*, 8457–8463.
528. Gajan, D.; Guillois, K.; Delichére, P.; Basset, J.-M.; Candy, J.-P.; Caps, V.; Copéret, C.; Lesage, A.; Emsley, L. *J. Am. Chem. Soc.* **2009**, *131*, 14667–14669.
529. Wang, L.; Wang, H.; Hapala, P.; Zhu, L.; Ren, L.; Meng, X.; Lewis, J.P.; Xiao, F.-S. *J. Catal.* **2011**, *281*, 30–39.
530. Zhu, Y.; Qian, H.; Zhu, M.; Jin, R. *Adv. Mater.* **2010**, *22*, 1915–1920.
531. Zhao, R.; Ji, D.; Lv, G.; Qian, G.; Yan, L.; Wang, X.; Suo, J. *Chem. Commun.* **2004**, 904–905.
532. Lu, G.; Zhao, R.; Qian, G. *Catal. Lett.* **2004**, *97*, 115–118.
533. Li, L.; Jin, C.; Wang, X.; Ji, W.; Pan, Y.; van der Knaap, T.; van der Stoel, R.; Au, C.T. *Catal. Lett.* **2009**, *129*, 303–311.
534. Wu, P.; Bai, P.; Loh, K.P.; Zhao, X.S. *Catal. Today* **2010**, *158*, 220–227.
535. Wu, P.; Xiong, Z.; Loh, K.P.; Zhao, X.S. *Catal. Sci. Technol.* **2011**, *1*, 285–294.
536. Wu, P.; Bai, P.; Lei, Z.; Loh, K.P.; Zhao, X.S. *Microporous Mesoporous Mater.* **2011**, *141*, 222–230.
537. Chen, L.; Hu, J.; Richards, R. *J. Am. Chem. Soc.* **2009**, *131*, 914–915.
538. Wu, J.C.S.; Cheng, T.-S.; Lai, C.-L. *Appl. Catal. A Gen.* **2006**, *314*, 233–239.
539. Mertens, P.G.N.; Wahlen, J.; Ye, X.; Poelman, H.; De Vos, D.E. *Catal. Lett.* **2007**, *118*, 15–21.
540. Zhu, Y.; Tian, L.; Jiang, Z.; Pei, Y.; Xie, S.; Qiao, M.; Fan, K. *J. Catal.* **2011**, *281*, 106–118.
541. Wang, M.-M.; He, L.; Liu, Y.-M.; Cao, Y.; He, H.-Y.; Fan, K.-N. *Green Chem.* **2011**, *13*, 602–607.
542. Liu, L.; Quia, B.; Ma, Y.; Zhang, J.; Deng, Y. *Dalton Trans.* **2008**, 2542–2548.
543. Milone, C.; Ingoglia, R.; Tropeano, M.L.; Neri, G.; Galvagno, S. *Chem. Commun.* **2003**, 868–869.
544. Zhu, Y.; Qian, H.; Drake, B.A.; Jin, R. *Angew. Chem. Int. Ed. Engl.* **2010**, *49*, 1295–1298.
545. Milone, C.; Ingoglia, R.; Tropeano, M.L.; Neri, G.; Galvagno, S. *Chem. Commun.* **2002**, 868–869.
546. Lenz, J.; Campo, B.C.; Alvarez, M.; Volpe, M.A. *J. Catal.* **2009**, *267*, 50–56.
547. Claus, P. *Appl. Catal. A Gen.* **2005**, *291*, 222–229.
548. Kitahara, H.; Sakurai, H. *J. Organomet. Chem.* **2011**, *696*, 442–449.
549. Blaser, H.-U.; Steiner, H.; Studer, M. *ChemCatChem* **2009**, *1*, 210–221.
550. Chen, Y.; Qiu, J.; Wang, X.; Xiu, J. *J. Catal.* **2006**, *242*, 227–230.
551. He, D.; Shi, H.; Wu, Y.; Xu, B.-Q. *Green Chem.* **2007**, *9*, 849–851.

552. Corma, A.; Concepción, P.; Serna, P. *Angew. Chem. Int. Ed. Engl.* **2007**, *46*, 7266–7269.
553. Boronat, M.; Concepción, P.; Corma, A.; González, S.; Illas, F.; Serna, P. *J. Am. Chem. Soc.* **2007**, *129*, 16230–16237.
554. Shimizu, K.; Miyamoto, Y.; Kawasaki, T.; Tanji, T.; Tai, Y.; Satsuma, A. *J. Phys. Chem. C* **2009**, *113*, 17803–17810.
555. Corma, A.; Serna, P.; García, H. *J. Am. Chem. Soc.* **2007**, *129*, 6358–6359.
556. Serna, P.; López-Haro, M.; Calvino, J.J.; Corma, A. *J. Catal.* **2009**, *263*, 328–334.
557. Shimizu, K.; Yamamoto, T.; Tai, Y.; Satsuma, A. *J. Mol. Catal. A Chem.* **2011**, *345*, 54–59.
558. Mitsudome, T.; Noujima, A.; Mikami, Y.; Mizugaki, T.; Jitsukawa, K.; Kaneda, K. *Angew. Chem. Int. Ed. Engl.* **2010**, *49*, 5545–5548.
559. Mitsudome, T.; Noujima, A.; Mikami, Y.; Mizugaki, T.; Jitsukawa, K.; Kaneda, K. *Chem. Eur. J.* **2010**, *16*, 11818–11821.
560. Noujima, A.; Mitsudome, T.; Mizugaki, T.; Jitsukawa, K.; Kaneda, K. *Angew. Chem. Int. Ed. Engl.* **2011**, *50*, 2986–2989.
561. Yin, L.; Liebscher, J. *Chem. Rev.* **2007**, *107*, 133–173.
562. Miyaura, N.; Suzuki, A. *Chem. Rev.* **1995**, *95*, 2457–2483.
563. Tsunoyama, H.; Sakurai, H.; Ichikuni, N.; Negishi, Y.; Tsukuda, T. *Langmuir* **2004**, *20*, 11293–11296.
564. Sakurai, H.; Tsunoyama, H.; Tsukuda, T. *J. Organomet. Chem.* **2007**, *692*, 368–374.
565. Chaicharoenwimolkul, L.; Munmai, A.; Chairam, S.; Tewasekson, U.; Sapudom, S.; Lakliang, Y.; Somsook, E. *Tetrahedron Lett.* **2008**, *49*, 7299–7302.
566. Carrettin, S.; Guzman, J.; Corma, A. *Angew. Chem. Int. Ed. Engl.* **2005**, *44*, 2242–2245.
567. Willis, N.G.; Guzman, J. *Appl. Catal. A Gen.* **2008**, *339*, 68–75.
568. Han, J.; Liu, Y.; Guo, R. *J. Am. Chem. Soc.* **2009**, *131*, 2060–2061.
569. de Souza, R.O.M.A.; Bittar, M.S.; Mendes, L.V.P.; da Silva, C.M.F.; da Silva, V.T.; Antunes, O.A.C. *Synlett* **2008**, 1777–1780.
570. Primo, A.; Quignard, F. *Chem. Commun.* **2010**, *46*, 5593–5595.
571. Kanuru, V.K.; Kyriakou, G.; Beaumont, S.K.; Papageorgiou, A.C.; Watson, D.J.; Lambert, R.M. *J. Am. Chem. Soc.* **2010**, *132*, 8081–8086.
572. Kyriakou, G.; Beaumont, S.K.; Humphrey, S.M.; Antonetti, C.; Lambert, R.M. *ChemCatChem* **2010**, *2*, 1444–1449.
573. Beaumont, S.K.; Kyriakou, G.; Lambert, R.M. *J. Am. Chem. Soc.* **2010**, *132*, 12246–12248.
574. M. Boronat, D. Combita, P. Concepción, A. Corma, H. Garciá, R. Juárez, S. Laursen, J. de Dios López-Castro, *J. Phys. Chem. C*. http://dx.doi.org/doi: 10.1021/jp3071585.
575. Corma, A.; Juárez, R.; Boronat, M.; Sánchez, F.; Iglesias, M.; García, H. *Chem. Commun.* **2011**, *47*, 1446–1448.
576. Zhang, X.; Corma, A. *Angew. Chem. Int. Ed. Engl.* **2008**, *47*, 4358–4361.
577. Kantam, M.L.; Prakash, B.V.; Reddy, C.; Reddy, V.; Sreedhar, B. *Synlett* **2005**, 2329–2332.
578. Zhu, F.-X.; Wang, W.; Li, H.-X. *J. Am. Chem. Soc.* **2011**, *133*, 11632–11640.
579. Ito, H.; Yajima, T.; Tateiwa, J.-I.; Hosomi, A. *Chem. Commun.* **2000**, 981–982.
580. Caporusso, A.M.; Aronica, L.A.; Schiavi, E.; Martra, G.; Vitulli, G.; Salvadori, P. *J. Organomet. Chem.* **2005**, *690*, 1063–1066.
581. Aronica, L.A.; Schiavi, E.; Evangelisti, C.; Caporusso, A.M.; Salvadori, P.; Vitulli, G.; Bertinetti, L.; Martra, G. *J. Catal.* **2009**, *266*, 250–257.
582. Corma, A.; González-Arellano, C.; Iglesias, M.; Sánchez, F. *Angew. Chem. Int. Ed. Engl.* **2007**, *46*, 7820–7822.

583. Corma, A.; González-Arellano, C.; Iglesias, M.; Navarro, M.T.; Sánchez, F. *Chem. Commun.* **2008**, 6218–6220.
584. Miyazaki, Y.; Kobayashi, S. *J. Comb. Chem.* **2008**, *10*, 355–357.
585. Kitahara, H.; Sakurai, H. *Chem. Lett.* **2010**, *39*, 46–48.
586. Yamane, Y.; Liu, X.; Hamasaki, A.; Ishida, T.; Haruta, M.; Yokoyama, T.; Tokunaga, M. *Org. Lett.* **2009**, *11*, 5162–5165.
587. Corma, A.; Concepción, P.; Domínguez, I.; Fornés, V.; Sabater, M.J. *J. Catal.* **2007**, *251*, 39–47.
588. Kamiya, I.; Tsunoyama, H.; Tsukuda, T.; Sakurai, H. *Chem. Lett.* **2007**, *36*, 646–647.
589. Biella, S.; Prati, L.; Rossi, M. *J. Catal.* **2002**, *206*, 242–247.
590. Comotti, M.; Della Pina, C.; Matarrese, R.; Rossi, M. *Angew. Chem. Int. Ed. Engl.* **2004**, *43*, 5812–5815.
591. Comotti, M.; Della Pina, C.; Falletta, E.; Rossi, M. *J. Catal.* **2006**, *244*, 122–125.
592. Okatsu, H.; Kinoshita, N.; Akita, T.; Ishida, T.; Haruta, M. *Appl. Catal. A Gen.* **2009**, *369*, 8–14.
593. Comotti, M.; Della Pina, C.; Rossi, M. *J. Mol. Catal. A Chem.* **2006**, *251*, 89–92.
594. Comotti, M.; Della Pina, C.; Falletta, E.; Rossi, M. *Adv. Synth. Catal.* **2006**, *348*, 313–316.
595. Beltrame, P.; Comotti, M.; Della Pina, C.; Rossi, M. *Appl. Catal. A Gen.* **2006**, *297*, 1–7.
596. Mirescu, A.; Berndt, H.; Martin, A.; Prüsse, U. *Appl. Catal. A Gen.* **2007**, *317*, 204–209.
597. Tan, X.; Deng, W.; Liu, M.; Zhang, Q.; Wang, Y. *Chem. Commun.* **2009**, 7179–7181.
598. Zhang, J.; Liu, X.; Hedhili, M.N.; Zhu, Y.; Han, Y. *ChemCatChem* **2011**, *3*, 1294–1298.
599. An, D.; Ye, A.; Deng, W.; Zhang, Q.; Wang, Y. *Chem. Eur. J.* **2012**, *18*, 2938–2947.
600. Kuusisto, J.; Tokarev, A.V.; Murzina, E.V.; Roslund, M.U.; Mikkola, J.-P.; Murzin, D.Y.; Salmi, T. *Catal. Today* **2007**, *121*, 92–99.
601. Murzina, E.V.; Tokarev, A.V.; Kordás, K.; Karhu, H.; Mikkola, J.-P.; Murzin, D.Y. *Catal. Today* **2008**, *131*, 385–392.
602. Carrettin, S.; McMorn, P.; Johnston, P.; Griffin, K.; Hutchings, G.J. *Chem. Commun.* **2002**, 696–697.
603. Carrettin, S.; McMorn, P.; Johnston, P.; Griffin, K.; Kiely, C.J.; Attard, G.A.; Hutchings, G.J. *Top. Catal.* **2004**, *27*, 131–136.
604. Carrettin, S.; McMorn, P.; Johnston, P.; Griffin, K.; Kiely, C.J.; Hutchings, G.J. *Phys. Chem. Chem. Phys.* **2003**, *5*, 1329–1336.
605. Hutchings, G.J.; Sarrettin, S.; Landon, P.; Edwards, J.K.; Enache, D.; Knight, D.W.; Xu, Y.-J.; Carley, A.F. *Top. Catal.* **2006**, *38*, 223–230.
606. Damirel, S.; Kern, P.; Lucas, M.; Claus, P. *Catal. Today* **2007**, *122*, 292–300.
607. Prati, L.; Porta, F. *Appl. Catal. A Gen.* **2005**, *291*, 199–203.
608. Dimitratos, N.; Lopez-Sanchez, J.A.; Lennon, D.; Porta, F.; Prati, L.; Villa, A. *Catal. Lett.* **2006**, *108*, 147–153.
609. Ketchie, W.C.; Fang, Y.; Wong, M.S.; Murayama, M.; Davis, R.J. *J. Catal.* **2007**, *250*, 94–101.
610. Porta, F.; Prati, L. *J. Catal.* **2004**, *224*, 397–403.
611. Bianchi, C.L.; Canton, P.; Dimitratos, N.; Porta, F.; Prati, L. *Catal. Today* **2005**, *102–103*, 203–212.
612. Damirel, S.; Lehnert, K.; Lucas, M.; Claus, P. *Appl. Catal. B Environ.* **2007**, *70*, 637–643.
613. Rodrigues, E.G.; Pareira, M.F.R.; Chen, X.; Delgado, J.J.; Órfão, J.J.M. *J. Catal.* **2011**, *281*, 119–127.

614. Demirel-Gülen, S.; Lucas, M.; Claus, P. *Catal. Today* **2005**, *102–103*, 166–172.
615. Tsuji, A.; Rao, K.T.V.; Nishimura, S.; Takagaki, A.; Ebitani, K. *ChemSusChem* **2011**, *4*, 542–548.
616. Takagaki, A.; Tsuji, A.; Nishimura, S.; Ebitani, K. *Chem. Lett.* **2011**, *40*, 150–152.
617. Villa, A.; Veith, G.M.; Prati, L. *Angew. Chem. Int. Ed. Engl.* **2010**, *49*, 4499–4502.
618. Brett, G.L.; He, Q.; Hammond, C.; Miedziak, P.J.; Dimitratos, N.; Sankar, M.; Herzing, A.A.; Conte, M.; Lopez-Sanchez, J.A.; Kiely, C.J.; Knight, D.W.; Taylor, S.H.; Hutchings, G.J. *Angew. Chem. Int. Ed. Engl.* **2011**, *50*, 10136–10139.
619. Dimitratos, N.; Wagland, A.; Hutchings, G.J.; Stitt, E.H. *Catal. Today* **2009**, *145*, 169–175.
620. Kimura, H. *Polym. Adv. Technol.* **2001**, *12*, 697–710.
621. Taarning, E.; Madsen, A.T.; Marchetti, J.M.; Egeblad, K.; Christensen, C.H. *Green Chem.* **2008**, *10*, 408–414.
622. Shen, Y.; Zhang, S.; Li, H.; Ren, Y.; Liu, H. *Chem. Eur. J.* **2010**, *16*, 7368–7371.
623. Taarning, E.; Nielsen, I.S.; Egeblad, K.; Madsen, R.; Christensen, C.H. *ChemSusChem* **2008**, *1*, 75–78.
624. Gorbanev, Y.Y.; Klitgaard, S.K.; Woodley, J.M.; Christensen, C.H.; Riisager, A. *ChemSusChem* **2009**, *2*, 672–675.
625. Casanova, O.; Iborra, S.; Corma, A. *J. Catal.* **2009**, *265*, 109–116.
626. Casanova, O.; Iborra, S.; Corma, A. *ChemSusChem* **2009**, *2*, 1138–1145.
627. Davis, S.E.; Houk, L.R.; Tamargo, E.C.; Datye, A.K.; Davis, R.J. *Catal. Today* **2011**, *160*, 55–60.
628. Pasini, T.; Piccinini, M.; Blosi, M.; Bonelli, R.; Albonetti, S.; Dimitratos, N.; Lopez-Sanchez, J.A.; Sankar, M.; He, Q.; Kiely, C.J.; Hutchings, G.J.; Cavani, F. *Green Chem.* **2011**, *13*, 2091–2099.
629. Gupta, N.K.; Nishimura, S.; Tagagaki, A.; Ebitani, K. *Green Chem.* **2011**, *13*, 824–827.
630. Du, X.-L.; He, L.; Zhao, S.; Liu, Y.-M.; Cao, Y.; He, H.-Y.; Fan, K.-N. *Angew. Chem. Int. Ed. Engl.* **2011**, *50*, 7815–7819.
631. Budroni, G.; Corma, A. *J. Catal.* **2008**, *257*, 403–408.
632. Kegnæs, S.; Mielby, J.; Mentzel, U.V.; Christensen, C.H.; Riisager, A. *Green Chem.* **2011**, *12*, 1437–1441.
633. Santos, L.L.; Serna, P.; Corma, A. *Chem. Eur. J.* **2009**, *15*, 8196–8203.
634. Sun, H.; Su, F.-Z.; Ni, J.; Cao, Y.; He, H.-Y.; Fan, K.-N. *Angew. Chem. Int. Ed. Engl.* **2009**, *48*, 4390–4393.
635. Shimizu, K.-I.; Nishimura, M.; Satsuma, A. *ChemCatChem* **2009**, *1*, 497–503.
636. Peng, Q.; Zhang, Y.; Shi, F.; Deng, Y. *Chem. Commun.* **2011**, *47*, 6476–6478.
637. He, L.; Lou, X.-B.; Ni, J.; Liu, Y.-M.; Cao, Y.; He, H.-Y.; Fan, K.-N. *Chem. Eur. J.* **2010**, *16*, 13965–13969.
638. Klitgaard, S.K.; Egeblad, K.; Mentzel, U.V.; Popov, A.G.; Jensen, T.; Taarning, E.; Nielsen, I.S.; Christensen, C.H. *Green Chem.* **2008**, *10*, 421–423.
639. Wang, Y.; Zhu, D.; Tang, L.; Wang, S.; Wang, Z. *Angew. Chem. Int. Ed. Engl.* **2011**, *50*, 8917–8921.
640. Soulé, J.-F.; Miyamura, H.; Kobayashi, S. *J. Am. Chem. Soc.* **2011**, *133*, 18550–18553.
641. Ishida, T.; Haruta, M. *ChemSusChem* **2009**, *2*, 538–541.
642. Preedasuriyachai, P.; Kitahara, H.; Chavasiri, W.; Sakurai, H. *Chem. Lett.* **2010**, *39*, 1174–1176.
643. Preedasuriyachai, P.; Chavasiri, W.; Sakurai, H. *Synlett* **2011**, 1121–1124.
644. Klobukowski, E.R.; Mueleer, M.L.; Angelici, R.J.; Woo, L.K. *ACS Catal.* **2011**, *1*, 703–708.
645. Juárez, R.; Concepción, P.; Corma, A.; Fornés, V.; García, H. *Angew. Chem. Int. Ed. Engl.* **2010**, *49*, 1286–1290.
646. Tsunoyama, H.; Tsukuda, T. *Hyomen Kagaku (J. Surf. Sci. Soc. Jpn.)* **2012**, *33*, 399–403.

647. Liu, Y.; Tsunoyama, H.; Akita, T.; Xie, S.; Tsukuda, T. *ACS Catal.* **2011**, *1*, 2–6.
648. Woehrle, G.H.; Warner, M.G.; Hutchison, J.E. *J. Phys. Chem. B* **2002**, *106*, 9979–9981.
649. Schmid, G.; Pfeil, R.; Boese, R.; Brandermann, F.; Meyer, S.; Calis, G.H.M.; van der Velden, J.W.A. *Chem. Ber.* **1981**, *114*, 3634–3642.
650. Weare, W.W.; Reed, S.M.; Warner, M.G.; Hutchison, J.E. *J. Am. Chem. Soc.* **2000**, *122*, 12890–12891.
651. Zheng, N.; Fan, J.; Stucky, G.D. *J. Am. Chem. Soc.* **2006**, *128*, 6550–6551.
652. Liu, X.; Mou, C.-Y.; Lee, S.; Li, Y.; Secrest, J.; Jang, B.W.-L. *J. Catal.* **2012**, *285*, 152–159.
653. Haruta, M; Yu, Y.; Huang, J.; Taketoshi, A.; Ishida, T.; Akita, T.; Ogata, A.; Kim, H. Gold cluster catalysts and their production methods. Japan Patent Application 2012-133329, 12 June, 2012.
654. Lu, J.; Aydin, C.; Browning, N.D.; Gates, B.C. *Angew. Chem. Int. Ed. Engl.* **2012**, *51*, 5842–5846.
655. Laursen, A.B.; Hojholt, K.T.; Lundegaard, L.F.; Simonsen, S.B.; Helveg, S.; Schüth, F.; Paul, M.; Grunwalt, J.-D.; Kegnoes, S.; Christensen, C.H.; Egeblad, K. *Angew. Chem. Int. Ed. Engl.* **2010**, *49*, 3504–3507.
656. Xie, X.; Li, Y.; Liu, Z.-Q.; Haruta, M.; Shen, W. *Nature* **2009**, *458*, 746–749.
657. van Bokhoven, J.A. *ChemCatChem* **2009**, *1*, 363–364.
658. Castro, T.; Reifenberger, R.; Choi, E.; Andres, R.P. *Phys. Rev. B* **1990**, *42*, 8548–8556.
659. Zope, B.N.; Hibbitts, D.D.; Neurock, M.; Davis, R.J. *Science* **2010**, *330*, 74–78.